Geophysical interpretation of Proterozoic mafic-ultramafic intrusions in the Arunta Region, central Australia

GEOSCIENCE AUSTRALIA RECORD 2003/29

by

Meixner, A.J. & Hoatson, D.M.

Geoscience Australia
GPO Box 378
Canberra ACT 2601

Department of Industry, Tourism and Resources
Minister for Industry, Tourism and Resources: The Hon. Ian Macfarlane, MP
Parliamentary Secretary: The Hon. Warren Entsch, MP
Secretary: Mark Paterson

Geoscience Australia
Chief Executive Officer: Dr Neil Williams

ISSN 1448-2177
ISBN 0 642 46790 0

GeoCat No. 47806

Bibliographic reference: Meixner, A.J. and Hoatson, D., 2004. Geophysical interpretation of Proterozoic mafic-ultramafic intrusions in the Arunta Region, central Australia. Geoscience Australia Record 2003/29.

Contents

Abstract

This geophysical study follows on from previous work by Hoatson & Stewart (2001), who summarised the field relationships and mineralisation features of 16 Proterozoic mafic-ultramafic intrusions in the Arunta Region of central Australia. The major aims of this study were to investigate geophysical datasets to define the total areal and sub-cropping extent of the outcropping intrusions, and to identify other previously unknown mafic-ultramafic intrusions concealed beneath alluvial cover.

Various data and image enhancement techniques were applied to grids of the magnetic, gravity and gamma-ray spectrometric data, and 2-D computer modelling was carried out on the magnetic data. From these manipulations it was possible to define various features of the outcropping intrusions, including: total sub-cropping extent; depth of burial beneath alluvial cover; internal structure; spatial association with faults and; the orientation of the intrusions.

The larger outcropping intrusions exhibited a high gravity response, but the internal structure of the intrusions could not be determined due to the sparse gravity station spacing, generally 11 km. The magnetic responses of the intrusions were variable and more sensitive to composition, metamorphic grade and post-emplacement deformation. Generally the lower the metamorphic grade, the easier it was to determine magnetic signatures originating from primary igneous features such as macroscopic layering and contrasting rock compositions. The high-grade, intensely deformed intrusions exhibit more complex magnetic signatures and are less readily differentiated from country rock. The majority of the 14 outcropping intrusions investigated have sub-cropping extents far exceeding the outcropping component. The depth of burial for the sub-cropping intrusions was less than 120 m.

A number of previously unknown mafic-ultramafic intrusions concealed under cover, were identified based on their gravity and magnetic signatures. A series of bodies were identified on a prominent east-west trending gravity ridge on which the Andrew Young Hills mafic intrusion outcrops. These bodies have similar magnetic character to the Andrew Young Hills intrusion and are probably related. A series of ovoid shaped magnetic highs, located east of the Mount Hay Granulite, were also identified as possible plug-like mafic intrusions.

The study highlighted the deficiency of the existing gravity data, which does not allow the determination of internal composition based on density variations for the larger bodies, while smaller bodies are generally not imaged at all.

Introduction

This study follows on from previous work by Hoatson & Stewart (2001) who summarised the field relationships and mineralisation of 16 Proterozoic mafic-ultramafic intrusions in the Arunta Region of central Australia (Fig. 1). A summary of the outcropping mafic-ultramafic intrusions is shown in Table 1. The geophysical data indicated that for many of these intrusions, the total horizontal extents of the bodies are obscured by shallow (generally < 120 m) alluvial cover. In this study magnetic and gravity datasets are used to determine the overall dimensions of the intrusions, the intrusion type and orientation, as well as defining any internal structures and relationships with surrounding regional structures. Due to the large areas of alluvial cover it is highly probable that more mafic-ultramafic intrusive bodies exist beneath the cover. By defining the geophysical characteristics of outcropping intrusions, it is possible to use these characteristics as a framework for identifying concealed intrusions.

The dimensions and geometry of the body are important elements when assessing the prospectivity of intrusions. Laterally extensive stratabound PGE-enriched layers, such as the Merensky Reef in the Bushveld Complex of South Africa and in the Munni Munni Complex of the west Pilbara Craton, Western Australia, typically occur in large layered mafic-ultramafic intrusions, whereas massive Ni-Cu-Co sulphides are concentrated in depressions and/or embayments in the basal contacts, or feeder conduits of relatively smaller mafic intrusions (Hoatson & Sun, 2002).

Table 1. Mafic and mafic-ultramafic intrusions investigated in the Arunta Region (modified after Hoatson & Stewart, 2001).

Intrusion	*Outcrop extent (km)*	*Approximate thickness (km)*	*Total extent (km)*	*Form*	*Major rock types*	*Metamorphic grade*	*Magnetic Susceptibility SI (10^{-6})*
Andrew Young Hills	6.5 x 4.5	> 5	22 x 13	Plunging synform	Gabn, MtGabn, BiotGabn, Gab, Ton, Dior	Sub-amphibolite	16 000-45 000 (Gab)
Papunya gabbro	3 x 0.5	0.4	3 x 0.5	Dipping sill	Gab, MtGab, Gabn, Amph, PlPx	Upper amphibolite to granulite	1150-71 600 (Gab)
Papunya ultramafic	1.8 x 0.8	?1	1.8 x 0.8	Ultramafic ?plug	PlWeb, Web, Gabn, Gab	?Amphibolite	280-480 (Px)
South Papunya gabbro	3.8 x 1	?0.5	3.8 x 1	Shallow-dipping ?sill	Gab, BiotGab, QtzGab, BiotTon	Granulite	260-340 (Gab)
West Papunya gabbro	0.3 x 0.4	?0.2	0.3 x 0.4	Dipping sill	Gabn, Gab	?Amphibolite	380-3400 (Gab)
Anburla Anorthosite	10 x 1	< 1	18 x 35[1]	Folded sheet	An, AnGab, LGab, Gab, PlPx	Upper amphibolite to granulite	60-2100 (An)
Enbra Granulite	15 x 8	?	28 x 11	Dipping ?folded sheet	MGran, LGab, AnGab, An	Granulite	80-16 800 (MGran)
Harry Anorthositic Gabbro	6 x 2	?1	7 x 3	Elongated bodies	AnGab, An, QtzAn, LGab, Px	Granulite	160-3400 (AnGab & An)
Johannsen Metagabbro	6 x 5	< 0.3	7 x 6	Dyke swarm	MGran, Gab	Granulite	4120-29 500 (MGran)
Mount Chapple Metamorphics	62 x 7	?	85 x 22	Folded sheets	MGran, Gab, Char	Granulite	470-48 000 (MGran)
Mount Hay Granulite	35 x 9	3	39 x 16	Antiformal sheath fold	MGran, Gab, Char, LGab, An	Granulite	350-58 000 (MGran)
Mount Stafford dolerite	6 x 7	0.2	6 x 7	Folded dykes and sills	Dol, Gab, Gabn	Amphibolite	510-17 000 (Gab)
Attutra Metagabbro	4 x 6	?	4 x 7	Dipping sheets	Gab, MtGab, Mt, LGab, Px, Amph	Amphibolite	180-5030 (Gab)
Kanandra Granulite	15 x 15	?	100 x 25	Fault-bounded sheets	MGran, Px	Upper amphibolite to granulite	340-32 700 (MGran)
Mordor Igneous Complex	6 x 6	< 1.2	6 x 6	Alkaline ultramafic plugs	Syen, Monz, Shon, Wehr, OlCpx, Lherz, Dun	Sub-amphibolite	1530-23 500 (Px & Per)
Riddock Amphibolite	70 x 6	< 2	70 x 6	Concordant folded sheets	Amph, Ton, AnGab, An, Per	Upper amphibolite to granulite	150-610 (Amph)

[1] Total outcrop and interpreted subcrop extent of 4 separate bodies.

Major rock types are arranged in approximate order of decreasing abundance. The prefix 'meta' has been deleted from all metamorphosed rock types. Amph = amphibolite; An = anorthosite; AnGab = anorthositic gabbro; BiotGab = Biotite gabbro; BiotGabn = biotite gabbronorite; BiotTon = biotite tonalite; Char = charnockite; Dior = diorite; Dol = dolerite; Dun = dunite; Gab = Gabbro; Gabn = gabbronorite; LGab = leucogabbro; Lherz = lherzolite; MGran =mafic granulite; Monz = monzonite; Mt = magnetitite; MtGab = magnetite gabbro; MtGabn = magnetite gabbronorite; OlCpx = olivine clinopyroxenite; Per = peridotite; PlPx = plagioclase pyroxenite; PlWeb = plagioclase websterite; Px = pyroxenite; QtzGab = quartz gabbro; Shon = shonkinite; Syen = syenite; Ton = tonalite; Web = websterite; Wehr = wehrlite.

Datasets

Airborne Magnetics

The majority of the Arunta Region is covered by regional airborne magnetic surveys with flight line spacings better than 500 m (Richardson, 2001). Grids of the individual surveys were merged to form a seamless grid of the region (Minty et al., 2003). Various technical enhancements were applied to the merged grid data to aid intrusion identification, as detailed below.

Greyscale images of the total magnetic intensity, reduced to pole dataset are shown in Figures 2 and 3. The reduction to the pole process was carried out to remove magnetic polarity effects due to the non-vertical inclination of the magnetic field in this region. Gradient-enhanced images with a north easterly illumination are shown in Figures 4 and 5. Figures 6 and 7 show images of the vertical gradient of the total magnetic intensity, reduced to pole.

The various images of the magnetic field enhance different characteristics. The greyscale images of the total magnetic intensity (Figs 2 & 3) enhance the relative intensities of the magnetic field, allowing for the differentiation of the relative magnetic properties of the source rocks. The gradient enhanced colour images of the same dataset (Figs 4 & 5), are useful for identifying structures within the source rock, while still retaining a feel for the relative magnetic intensities. The addition of the sun angle, although enhancing structural detail, may also create a distorted perception of the structure orientation, due to the preferential alignment of anomalies in the direction perpendicular to the applied sun angle. Applying a vertical gradient to the total magnetic intensity, while suppressing the long wavelength amplitude anomalies, enhances the higher frequency anomalies. These images (Figs 6 & 7) are therefore ideal for defining source rock structure.

Gravity

Gradient-enhanced images of the Bouguer gravity field using values from the Australian National Gravity Database (Murray, 1999), are shown in Figures 8 and 9. Gravity stations in the study area are typically spaced 11 km apart resulting in an under sampled dataset and the loss of the high frequency component of the gravity field. Also, the resulting data will be aliased i.e. a gravity field with a wavelength of 11 km will not show any variation if sampled every 11 km.

Vertical gradient images of the Bouguer gravity field are shown in Figures 10 and 11. The vertical gradient process enhances the higher frequency component of the field, while suppressing the long wavelength component. Therefore, deeply source anomalies are suppressed, while the shallow-sourced anomalies are enhanced. The process also separates overlapping anomalies allowing for the identification of individual source bodies. Unfortunately the sparse gravity stations do not resolve fine detail and are therefore, only an indication of the existence of large areas of contrasting dense material.

The vertical gradient of the gravity field allows a better comparison with total magnetic intensity data, as the fall-off rates of the fields for equivalent source configurations are the same.

Magnetic Susceptibility

Magnetic susceptibility measurements of rock samples are shown in Appendix 1 of Hoatson & Stewart (2001) and summarised in Table 1.

Methodology

The geophysical images were combined with digital versions of published 1:250 000 geology maps in ArcMap, a component of the ArcGIS package. Superimposing the geology with the magnetic and gravity images allows for the geophysical character of the outcropping bodies to be determined. By extrapolating from the mapped outcrop outwards beneath the cover, the interpreted sub-cropping extents of the bodies were determined. Using the various magnetic images, the bodies were subdivided according to their magnetic character. These subdivisions were based on the amplitude information (i.e. the relative magnetic intensities of the source body), and the texture of the magnetic field. Different source body types produce differing textures in the magnetic field. For example: a layered intrusion will result in coherent linear anomalies, due to the variation in the magnetic properties of the layers; a large intrusion with no apparent internal variation in composition, will produce a random 'massive' pattern of highs and lows due to minor variations in the susceptibility; an intrusion devoid of magnetic minerals will result in no magnetic anomaly. The orientation of the intrusion for the above scenarios will also result in different magnetic signatures.

Computer modelling of selected bodies were undertaken to determine the orientation of the intrusions, as well as the depth of burial by alluvium. The modelling was conducted using ModelVision, a forward modelling package that incorporates an inversion routine. Only bodies exhibiting strong coherent linear anomalies were modelled using a dipping tabular body as the source model. The assumption is that the tabular bodies simulate macroscopic cyclic layering within the intrusions. All modelling was performed assuming induced magnetisation only. No obvious remanent magnetisation was encountered and if present, is only a minor component of the magnetic anomaly. Modelled sections were chosen to cut through the centre and perpendicular to a linear anomaly, while the strike lengths of the tabular bodies were constrained by the strike length of the anomaly. Once an initial tabular body was generated, the inversion function of the application was used to finetune the model. Only model properties where the observed and calculated fields closely matched were retained. The depth estimates are an indication of the depth of alluvial cover as well as the extent of weathering. Magnetite destruction due to weathering may result in depth estimates that are larger than the true depth of alluvial cover. A further limitation to the depth estimate modelling is the ratio of height of the instrument above the source body to the data spacing. Reliable modelling is possible only where sample spacing is less than or equal to one-half of the height above source the body (Reid, 1980). The modelling was performed by extracting profiles from the magnetic grid, with the exception of the Andrew Young Hills modelling which was performed on over sampled line data. The grid cell spacing is 100 m giving a minimum detectable depth for acquisition of 200 m. As most of the surveys were flown with a mean flying height of 80 m above topography, then it is impossible to accurately model source bodies with depths below the surface of less than 120 m.

Outcropping mafic-ultramafic intrusions

Andrew Young Hills intrusion (Figures 12a to 12e)

The Andrew Young Hills intrusion consists of a homogeneous mafic sequence of fine- to medium-grained gabbronorite, magnetite gabbronorite, biotite gabbronorite, gabbro, hornblende tonalite and diorite (Hoatson & Stewart, 2001), with a total outcrop area of ~ 6.5 by 4.5 km. The rocks contain well-preserved igneous features, are not strongly recrystallised and are of ?sub-amphibolite metamorphic facies. The outcropping body corresponds with a well defined anomaly in the vertical gradient gravity. The magnetic signature of the intrusion comprises coherent linear anomalies that generally strike east-west. The interpreted sub-surface extent exceeds its outcrop extent and measures approximately 22 km east-west by 13 km north-south. The structure is interpreted as a broad inclined synform, with the fold axis plunging to the south. Southerly dips of the magnetic units range through steep to vertical on the western side of the intrusion, shallowing to approximately 30^{o} in the centre, then steepening again to approximately 80^{o} on the eastern side of the body. The internal coherent arcuate magnetic texture is interpreted as macroscopic cyclic layering. Only a portion of the body outcrops, the rest is buried by surficial sediments with thicknesses of 100 m or less.

Three smaller magnetic anomalies are situated to the south and southeast of the main outcropping mafic intrusion. These anomalies have similar magnetic character to the main body and are probably of similar composition. A moderate intensity anomaly with a sub-linear texture is situated to the northwest and adjacent to the main intrusion. Prior to tilting this body would have been sub-vertical and situated beneath the main intrusion, and may be a feeder conduit for the intrusion.

West Papunya gabbro (Figures 13a to 13d & 14)

The West Papunya gabbro is a small (260 by 400 m) north trending ovoid mafic body of gabbronorite, gabbro and magnetite gabbro (Hoatson & Stewart, 2001). A body of this size (260 m east-west) may not be detected by the airborne survey (400 m north-south line spacing), and may explain why there is no corresponding anomalies in the gamma-ray spectrometric and magnetic images.

Papunya gabbro (Figures 13a to 13d & 15)

The Papunya gabbro is an east-trending elongated mafic body with outcropping dimensions of 3 by 0.5 km (Hoatson & Stewart, 2001). It comprises a homogeneous mafic sequence of fine-grained recrystallised gabbro, magnetite gabbro, gabbronorite, amphibolite and rare plagioclase pyroxenite. The gabbros are not compositionally layered, generally foliated and of ?upper amphibolite to granulite metamorphic facies.

Outcropping Papunya gabbro corresponds with a magnetic low and low concentrations of potassium, uranium and thorium. Two faults are interpreted adjacent, and to the south and west of the intrusion. On the geophysical images these faults appear to truncate the intrusion. However, on the mapped geology the southern

fault runs a short distance to the south of the intrusion. This disparity is due to the resolution of the magnetic data, which is not high enough to resolve to this finer detail.

Papunya ultramafic intrusion (Figures 13a to 13d & 15)

The Papunya ultramafic intrusion is a poorly exposed ovoid plagioclase pyroxenite body that outcrops over an area of 1.8 by 0.8 km. The margins of the intrusion appear to be concordant with the foliated felsic gneissic country rocks and the intrusion has a similar ovoid geometry to the nearby West Papunya gabbro body. Dominant rocks are weakly recrystallised fine- to medium-grained massive plagioclase websterite and websterite with minor gabbronorite and gabbro (Hoatson & Stewart 2001). The Papunya ultramafic intrusion corresponds with a magnetic low as well as low concentrations of potassium, uranium and thorium.

South Papunya gabbro (Figures 13a to 13d & 16)

The South Papunya gabbro is a northeast trending elongated metagabbroic body with outcrop dimensions of 3.8 by 1 km. It is composed of a homogeneous sequence of fine- to medium-grained gabbros of ?granulite metamorphic facies (Hoatson & Stewart).

The intrusion corresponds to region of low and flat magnetic character. As the surrounding stratigraphy has a similar magnetic character, the intrusion cannot be differentiated by the magnetic data. The intrusion stands out on the gamma-ray spectrometric image with low concentrations of potassium, uranium and thorium, contrasting to the surrounding stratigraphy, which has high concentrations of the three elements. The southeastern contact is obscured by alluvium and is interpreted to be fault bounded.

North Papunya gabbro (informal name, Figures 13a to 13d)

Five kilometres to the north of the Papunya gabbro is a high intensity magnetic anomaly. The majority of the source body is under alluvial cover except for the extreme eastern end, which corresponds to outcropping quartz-bearing gabbro and mafic granulite (Close et al., 2002b). The body has dimensions of ~ 4 by 2 km and appears to be truncated by faults to the north and west. This intrusion differs in character from the nearby Papunya intrusions by its positive magnetic signature.

Mount Chapple Metamorphics (Figures 17a to 17b)

The Mount Chapple Metamorphics is a large composite mafic-intermediate-felsic granulite body (Hoatson & Stewart, 2001). The body forms a component of the regionally extensive Narwietooma Metamorphic Complex (Shaw & Warren 1995). The central part of Mount Chapple is dominated by mafic granulite, whereas the western and eastern parts contain large bodies of quartzofeldspathic gneiss, felsic granulite, intermediate gneiss, orthopyroxene-bearing gneissic granite (charnockite) and various migmatitic metasediments.

Outcropping Mount Chapple Metamorphics correspond to an east-west trending anomaly in the vertical gradient gravity image. Interpreted sub-cropping dimensions

are defined by similar magnetic characteristics to regions of outcrop and the overall size of this large body is approximately 85 km east-west by 22 km north-south. There are two regions of coherent linear, high magnetic intensity anomalies, situated on the western and eastern ends of the body. These magnetically intensive regions are surrounded by areas of low and flat magnetics as well as areas of moderate intensity and a massive, featureless texture. There is no discernible correlation of magnetic intensity or texture with the mapped geology. The body is structurally complex with numerous internal faults, while the majority of the body is fault bounded with the country rocks. Modelling of selected magnetic anomalies has defined south dipping source bodies. Three out of the four dips are generated from anomalies adjacent to faults, and as such are more likely to be defining the dips of fault planes, rather than internal lithological layering or metamorphic fabrics.

Mount Hay Granulite and Anburla Anorthosite intrusions (Figures 18a to 18e)

The Mount Hay Granulite comprises dominantly mafic granulite (~60%), felsic and intermediate granulite (~25%), while the remainder consists of anorthosite, migmatitic metasediments and various felsic rocks (Hoatson & Stewart, 2001). Hoatson & Stewart (2001) describe the body as a sheath fold that is interpreted as a large sub-horizontal elongate balloon-like body. The present ground level cuts up-section from the lower, synformal portion of the balloon in the west to the upper, antiformal portion in the east. The Mount Hay Granulite in the northeast appears to be faulted against the Anburla Anorthosite intrusion, which consists of monomineralic plagioclase rocks (anorthosite), to more mafic variants containing up to 30 per cent ferromagnesian minerals (two pyroxenes and hornblende: leucogabbro), to plagioclase-bearing mafic granulite (metagabbro). The anorthositic rocks are devoid of sulphide and have a very low magnetite content (Hoatson & Stewart, 2001).

Outcropping granulites and anorthosite intrusions correspond to a gravity high which forms the western portion of an elongated east-west trending high. The magnetic character of the Mount Hay Granulite body is complex, with the western and the southern portions of the body consisting of moderate intensity curvilinear anomalies. The observed magnetic trends and modelled dips of the magnetic units are consistent with the mapped geology and define the synformal western portion of the intrusion. The magnetic character of the central-eastern portion of the body is of high intensity and massive texture, indicating a homogeneous body of high magnetite composition. Adjacent and to the northeast of this unit is a narrow and linear, very high intensity anomaly, which has been broken up by a series of faults. The variation of the magnetic character has not been mapped in outcrop. Interpretation of the magnetics shows the Mount Hay Granulite to be in faulted contact to the north (Harry Creek Deformed Zone) and to the south. A northwest-trending fault, inferred in the mapped geology, is prominent in the magnetics and appears to produce an offset in the portion of the granulite with the complex magnetic signature.

Outcrop of the Anburla Anorthosite corresponds to a low and flat, elongate, northwest trending magnetic anomaly. An identical northwest-trending anomaly, approximately 8 km to the east, may be sourced from a body of similar composition to the Anburla Anorthosite. Two more regions of Anburla Anorthosite outcrop in a

line extending to the southeast of the outcropping elongate body (Shaw et al., 1995). The western body corresponds to an ovoid magnetic low and is enclosed to the east, west and south by the Mount Hay Granulite. The eastern Anburla outcrop is approximately 6 km south of the interpreted southern extent of the Mount Hay Granulite. This body is fault bounded by northwest-trending faults and is within the east-west trending Redbank Thrust Zone. The magnetic response of this body is higher than the low and flat response of the rest of the Anburla Anorthosite.

The continuation to the east of the elongate gravity anomaly corresponds to a parallel sequence of moderate to high intensity, coherent generally east-west trending linear magnetic trends. Outcrop on the eastern end of this sequence is mapped as interlayered mafic granulite and garnet gneiss (Shaw et al., 1983). The magnetic character changes gradually from relatively lower amplitude, continuous linear anomalies in the north, to higher intensity, less coherent anomalies in the south. This change in magnetic character may reflect a change in composition of layering from relatively low proportion mafic layers in a felsic background, to a higher proportion of mafics in the south. Further to the east are a number of ovoid shaped high magnetic intensity bodies, which correspond to a regional circular gravity high. These bodies are interpreted as mafic intrusions and are discussed in more detail later in this report.

Enbra Granulite intrusion (Figures 19a to 19e)

The Enbra Granulite intrusion is a fault-bounded wedge-shaped body consisting of a group of isolated hills that cover an area of 15 by 8 km. It comprises a homogeneous mafic granulite sequence ?overlain by more fractionated felsic rocks in the north. Mafic granulites are the dominant rock type (80%), with irregular felsic granulite, garnet-biotite-feldspar-quartz paragneiss and migmatitic paragneiss (20%) interlayered with the mafic granulites abundant in the central part of the body (Hoatson & Stewart, 2001). The mafic granulites are fine-to medium-grained foliated rocks containing thin segregations (sweats) of felsic granulite.

The magnetic signature of the outcrop region is dominantly of moderate to high magnetic intensity with a massive to sublinear texture. Outcropping felsic segregations correspond to ill defined magnetic lows. The total extent of the body is not well defined. The anomalous gravity high to the west of the outcrop area suggests that dense granulite exists under cover to the west. However, the sparse gravity spacing does not resolve the shape and dimensions of the body. Based on magnetics, the body extends to the northwest beneath alluvial cover (approximately 120 m depth), with a magnetic signature of low to moderate intensity and massive texture. The inferred dimensions of the body are 28 by 11 km, though the northern and western boundaries are not well defined due to the similarity of the magnetic signature with surrounding lithologies. The southern boundary is defined by the Harry Creek Deformed Zone (HCDZ), while a sinistral fault running parallel and to the north of the HCDZ, transects the intrusion. The northeastern boundary is defined by a northwest-trending structure, though there is a small granulite outcrop on the eastern side of this fault.

Harry Anorthositic Gabbro and Johannsen Metagabbro intrusions (Figures 20a to 20e).

The dominant rock type of the Harry Anorthositic gabbro is a medium to coarse-grained uralitised anorthositic gabbro metamorphosed to granulite facies (Hoatson & Stewart, 2001). Associated rocks include minor metamorphosed anorthosite, quartz anorthosite, leucogabbro, gabbro and rare pyroxenite. The intrusion consists of east-trending elongated bodies, that interfinger along strike with elongated bodies of massive brown tonalite and diorite. The Johannsen Metagabbro consists of a mafic granulite ?dyke swarm that radiate outwards from an apparent confluence point 2 km southwest of Johannsen's Phlogopite Mine. Dominant rocks include homogeneous coarse-grained mafic granulite, granoblastic gabbro and felsic granulite. The latter felsic granulites are very homogeneous in composition suggesting that they may be metamorphosed granitic sheets.

The combined outcropping extents of the intrusions are 7 by 7 km, which is too small to be resolved by the available gravity data. The magnetic character of both bodies is of low to moderate intensity, with sublinear texture. The magnetic character of the Harry Anorthositic Gabbro consists of east-west trending sub-linear highs, and are sourced from the elongate intrusions. The Harry Anorthositic Gabbro extends further to the west and south of the outcrop, where it is truncated by the HCDZ to the south and to the west by northwest-trending faults.

Mordor Complex (Figures 21a to 21e)

The Mordor Complex is a composite undeformed plug-like alkaline body that crops out over an area of 6 by 6 km. The intrusion can be broadly subdivided into a western zone of homogeneous syenite and an eastern zone comprising a highly fractionated comagmatic suite of alkaline felsic-mafic rocks spatially associated with phlogopite-bearing ultramafic rocks. Syenite, monzonite, melamonzonite and shonkinite are the dominant felsic-mafic rocks, whereas the ultramafic rocks comprise wehrlite, olivine clinopyroxenite, lherzolite, dunite and pyroxenite. The ultramafic rocks are restricted to the eastern half of the intrusion where they form homogeneous lobate and more irregular bodies with curvilinear contacts (Hoatson & Stewart, 2001).

The vertical gradient of the Bouguer gravity image, highlights the limitations due to the sparse gravity spacing. An anomalously high gravity field is expected over the dense mafic-ultramafic intrusion, and is present. However, the centre of this high, corresponding to the gravity station, is located on the southeast margin of the Mordor Complex, not over the centre. This anomaly offset is directly related to the positioning of the gravity station. A station positioned over the centre of the intrusion would produce an anomaly over the centre of the intrusion. If stations were located some distance from the intrusion, it is possible that an anomaly may not be registered.

The intrusive complex corresponds to a circular region of moderate magnetic intensity, containing four separate anomalies of very high intensity. The large high intensity anomaly in the south east of the complex, corresponds to outcrop of mafic-ultramafic rock, though the data resolution is not high enough to distinguish individual mapped rocks types. The high intensity anomaly located in the north of the complex does not correspond to any mapped mafic-ultramafic rocks. The anomaly may be the result of such rock that are not exposed at the surface. An east-

west trending fault cutting through the centre of the complex, is evident in the vertical gradient image. Modelling of the magnetic field indicate that the source bodies of the three northern anomalies have large depth extents, while the source body to the larger southern anomaly has a limited depth extent (< 1000 m). Modelling also indicates that the intrusions are vertical plug-type bodies.

Kanandra Granulite (Figures 22a to 22e)

The Kanandra Granulite consists of upper amphibolite or hornblende granulite facies, mafic and pelitic rock types (part of Strangways Metamorphic Complex). The largest exposed part of the body northwest of Kanandra Dam (Fig. 22a) covers an area of ~15 by 15 km on ALCOOTA (Shaw et al, 1975), whereas a narrow east-trending fault-bounded corridor is wedged between the Entire Point Fault and the Delny Shear Zone on HUCKITTA (Freeman, 1986).

The outcropping granulite on ALCOOTA, corresponds with a region of highly variable magnetic character, ranging from low and flat to very high with massive to sub-linear texture. The interpreted full extent of the body which is partially covered by alluvial sediments, is delineated by this variable magnetic character, over an east west distance of approximately 100 km. The general trend is for predominantly lower magnetised rocks towards the east into HUCKITTA. The northern section of the body, adjacent to the Delny Shear Zone, is characterised by low and flat magnetisation. This magnetically flat zone may be due to magnetite destruction related to shearing. Alternatively, the magnetic flat zone may correspond to a low magnetite phase of the intrusion. A number of discrete circular highs are scattered throughout the intrusion and maybe sourced from small plug-like intrusions. The body is bounded to the north by the Delny Shear Zone and to the south by the Entire Point Fault and Saint Hill Fault zones. The body is broken up by numerous northwest trending faults, with lesser numbers of easterly and north-easterly trending faults.

The vertical gradient of the Bouguer gravity image shows a high, corresponding to the large outcrop region on ALCOOTA, which does not extend to the narrower eastern portion of the body. This variance may be due to a higher proportion of felsic rocks (quartzofeldspathic gneiss), as labelled on the HUCKITTA sheet (Freeman, 1986).

Attutra Metagabbro intrusion (Figures 23a to 23e).

The Attutra Metagabbro comprises a homogeneous, weakly recrystallised mafic sequence of medium to coarse-grained gabbro, magnetite gabbro, magnetite, with lesser leucogabbro, pyroxenite and amphibolite. Most rock types are generally equigranular, massive and unfoliated, and there is no obvious cyclicity or compositional layering. The general uniformity of rock compositions and abundance of oxide-rich rocks suggest a ?shallow-dipping mafic sequence from the upper part of an evolved tholeiitic intrusion (Hoatson & Stewart, 2001).

The magnetic character of the intrusion is subdued, consisting of a magnetic low surrounded by a variably magnetic terrane corresponding to metasediments of the Bonya Schist. All but the northern section of the body is well defined, either by outcrop geology, or by contrasting magnetic character. Sediments of the Georgina Basin obscure the northern boundary, which also suppresses the magnetic character

due to the increased distance to the magnetic source rocks. Therefore, the northern extent of the intrusion is interpretive and the intrusion may extend further north beneath the Georgina Basin sediments. The total interpreted dimensions of the intrusion are ~5 by 8 km. Two faults are evident, trending northeast and northwest, at a distance of approximately 1 and 4 km respectively on either side of the intrusion. The intrusion corresponds to a vertical gradient gravity high, though the gravity spacing is too low to resolve boundaries of the intrusion.

Mount Stafford dolerite intrusions

The Mount Stafford dolerite intrusions are described by Hoatson & Stewart (2001) as a stacked sequence of hypabyssal sills and associated dykes tightly folded around northwest to north-northeast-trending axes. The sills crop out for distances of up to 3 km along strike, and their thickness range from 10 to 120 m, with a maximum thickness of 200 m. The most common rock types of dolerite, doleritic gabbro, gabbro and gabbronorite are generally fine-grained, massive and weakly recrystallised. These small bodies are not differentiable by their magnetic character, as they are non-magnetic and do not contrast with the surrounding non-magnetic metasediments of the Mount Stafford beds.

Riddock Amphibolite

The Riddock Amphibolite is a composite ?volcano-sedimentary sequence comprising folded concordant mafic sheets within laterally continuous pelitic, calcareous and quartzose schists and gneisses of the Irindina Gneiss (Harts Range Group). The amphibolites are laterally continuous for about 70 km and have a maximum width of 6 to 8 km. Thicknesses of individual bodies range from a few metres up to ?2 km (Hoatson & Stewart, 2001). The amphibolites are non-to very weakly magnetic and are impossible to differentiate based on their magnetic character from the surrounding variably magnetic lithologies. The sparse gravity spacing also precludes the differentiation of the body based on the gravity signature.

Interpreted mafic-ultramafic intrusions

Andrew Young Hills-Type Intrusions

A number of bodies were identified which have similar geophysical characteristics to the Andrew Young Hills intrusion. Two of these bodies lie approximately 30 km to the southeast of Andrew Young Hills, while a string of bodies trend to the west-southwest, over a distance of approximately 120 km. The spatial association, as well as the characteristic gravity high and similar magnetic character, suggest that the bodies are related with similar compositions and emplacement history.

All of these intrusions, with the exception of the small circular intrusion on the eastern end of the trend, reside on large amplitude (700 gravity units), east-west elongate gravity anomaly (Fig. 8) and are interpreted as the main contribution to the anomalously high gravity field.

Western mafic intrusions (Figures 24a to 24d)

On the western end of the elongate east-west trending gravity anomaly (Fig. 8), is a large complex magnetic high. The magnetic character is different between the northern region (high magnetic intensity, massive texture) and the southern region (high magnetic intensity, coherent linear texture). The majority of the body is undercover except for some small outcrops of gabbro, pyroxenite and norite (Close et al., 2002b) which corresponds to a region of moderate magnetic intensity with massive texture. The coherent linear texture is interpreted as magnetite variation due to macroscopic cyclic layering. Modelling of the source bodies to this layering, suggests that the structure is a broad inclined antiform, plunging approximately 45^{o} to the south. Immediately to the southeast is a smaller southwest trending body, also with high magnetic intensity and coherent linear texture. The dip and strike of this source body mirrors the larger body to the north and is probably closely related. There are two dominant fault trends, northeast and northwest. The northwest-trending faults are interpreted to be later structures as they appear to offset the northeasterly trending structures.

Two smaller bodies to the east, correspond to a positive gravity anomaly. The centre of the anomaly is offset with respect to the bodies, due to the location of the nearest gravity station being offset from the body.

Central mafic intrusions (Figures 25a to 25d)

In the central part of the elongated east-west trending gravity anomaly (Fig. 8), are three separate bodies interpreted to be of Andrew Young Hills type. The western body exhibits high magnetic intensity with massive texture, and is separated from the body to the east by a west-northwest trending fault, which also appears to offsets the east-west trending vertical gradient, gravity anomaly.

The southern body, lying in close proximity and to the north of the Desert Bore Shear, consists of two regions of strong coherent linear texture, separated by an east-

west trending fault. The curved coherent linear anomalies of the northern portion, are interpreted to indicate macroscopic cyclic layering. The dip of this layering could not be reliably modelled, due to overlapping anomalies, so it is not possible to determine whether the curved structure is an antiform or synform.

The eastern body is complex, and may be made up of a number of separate intrusions. The structure is complex, with regions of coherent linear and massive textured anomalies separated by a number of faults with predominantly northeasterly and northwesterly trends.

Eastern mafic intrusions (Figure 26)

To the southeast of the Andrew Young Hills mafic intrusion is a region of anomalously high magnetics, corresponding to a gravity high. The source body appears to be made up of at least two separate intrusions. The southern intrusion exhibits coherent curvilinear anomalies, of which the source layering has been modelled as dipping at 45^{o} to the south, indicating that the structure is a broad antiform. Directly to the north of this equidimensional body is a prominent east-west trending anomaly. On either side of this elongate body are two regions of diffuse magnetic anomalies. The source bodies to these anomalies are interpreted to be at some depth beneath the basal surface of the alluvial cover.

Further to the east is a smaller equidimensional magnetic high, of massive texture, which corresponds to a gravity high. The source body is some way off the eastern end of the main gravity trend (Fig. 8), and may not be related to the other interpreted Andrew Young Hills-type intrusions to the west. The high magnetic intensity and density of the source body suggests that it is of mafic composition.

Other interpreted mafic bodies

McEwin Hills mafic intrusion (informal name, Figures 27a to 27d)

South of the McEwin Hills, on the northern boundary of LAKE MACKAY (Close et al., 2002a) is a complex magnetic anomaly and associated gravity high. The body does not outcrop as the region is covered by alluvial sediments and is interpreted as a mafic intrusion based on its geophysical properties. The moderate intensity, massive textured portion of the body is included as a mafic body based on the vertical gradient gravity image. Due to the sparse gravity station spacing, it is impossible to determine whether the anomalous gravity field is due to the interpreted mafic intrusion or to dense lithologies west of the body.

Kakalyl Bore intrusion (informal name, Figures 13a to 13d)

Approximately 3 km west of the West Papunya gabbro is a circular magnetic low with a diameter of approximately 1000 m. The low magnetic character also corresponds to low concentrations of potassium, thorium and uranium, in comparison with the country rocks. Immediately to the north of this anomaly, a southeast-trending passes in close proximity to the West Papunya gabbro. The magnetic and gamma-ray spectrometric characteristics of this body are similar to the Papunya ultramafic body to the east and is interpreted as a mafic-ultramafic intrusion. A further intrusion may exist directly to the north of this body and adjacent to the fault. The wedge shaped region in the gamma-ray spectrometric image has similar low radioelement concentrations, though there is no associated magnetic low.

Joppita Bore mafic intrusions (informal name, Figures 28a to 28d)

Approximately 60 km the east of the Mount Hay Granulite (Fig. 18), are a series of ovoid shaped magnetic anomalies. These anomalies also correspond to a positive regional gravity anomaly and are interpreted as sourced from plug-like mafic intrusions. The bodies do not outcrop as the region is blanketed by alluvium, and are therefore assigned a mafic origin based on their geophysical character. The bodies, which lie approximately 70 km to the west of the Mordor Complex (Fig. 21), have similar shapes and dimensions and may be related.

Most of the intrusions exhibit very high magnetic intensities, except for a single moderately magnetised intrusion, which appears to be truncated by an east-west-trending fault with dextral movement. The smaller bodies to the east may be fragments of a larger body which have been broken up by a southeast-trending shear zone.

The ovoid shaped magnetic anomaly, to the northwest of the intrusions, is not associated with a gravity high and also corresponds to outcropping granite (Shaw et al., 1983).

Conclusions

The major conclusions from this geophysical study of the Arunta intrusions are:

- All of the mafic-ultramafic bodies investigated in this study were covered by airborne magnetic data with flight line spacings of 400 and 500 m. Data at this resolution is more than adequate to identify body size, shape and for the larger bodies, internal structures such as faulting and macroscopic layering. The exception is the West Papunya gabbro intrusion (Fig. 14) which, with a mapped outcrop width of 250 m, was missed by the 400 m line spaced survey and was therefore not imaged by the magnetics.
- Computer modelling of the magnetic signatures was useful in determining the depth of burial of the intrusions under cover. However, due to the limitations imposed by the 100 m grid cell size of the data, the depth of burial of bodies beneath less than 120 m of cover can not be resolved. Computer modelling was also useful in defining the dip and strike of macroscopic layering, allowing the orientation of the larger intrusions (e.g., Andrew Young Hills) to be determined.
- The gravity station spacing (generally 11 km) is too coarse to resolve internal density variations of the intrusive bodies, while small bodies are not be resolvable in the gravity data.
- The subcropping extent of a large proportion of the mapped mafic-ultramafic bodies far exceeds the known outcrop (Table 1).
- The depth of alluvial cover of buried intrusions, with one exception is less then 120 m, the minimum resolvable depth based on magnetic data resolution. The exception is the interpreted mafic intrusion immediately to the southeast of the Andrew Young Hills intrusion (Fig. 26), where the depth of burial beneath cover is up to 210 m.
- The magnetic signatures of the outcropping intrusions are dependant on the metamorphic grade and the post-emplacement deformational history. Low-grade intrusions with minimal deformation, e.g., the Andrew Young Hills intrusion and the Mordor Igneous Complex consist of strong-coherent magnetic anomalies, which are substantially different in character from the country rock, allowing for easy delineation of the overall subcropping extent. These magnetic signatures originate from primary igneous features (Andrew Young Hills - macroscopic layering; Mordor Igneous Complex – contrasting rock compositions). The high-grade, intensely deformed intrusions exhibit variable magnetic signatures and, as such, are less readily differentiated from the country rock. The exception to the above is the high-grade Mount Hay Granulite, which exhibits curvilinear magnetic anomalies, sourced from a compositionally homogeneous body.
- Several newly defined bodies occur on the large east-west trending gravity anomaly (Fig. 8), east and west of the Andrew Young Hills intrusion. The similarity of magnetic properties and the association with the gravity high suggest that the bodies are related with similar compositions and emplacement history. A newly defined body, informally named as the McEwin Hills mafic intrusion (Fig. 27), lies on the northern boundary of Lake Mackay (Close et al., 2002a). This body, defined by its high gravity magnetic signatures, differs from the Andrew Young Hills intrusion by its magnetic signature, which exhibits a massive texture, indicating that there is no internal macroscopic layering. The informally named Kakalyl Bore intrusion (Fig. 13) was defined by its low magnetic character and low concentrations of potassium, uranium and thorium. The magnetic and gamma-ray spectrometric character is similar to the Papunya

ultramafic intrusion, 20 km to the east. A series of ovoid shaped magnetic highs, lying east of the Mount Hay Granulite, were interpreted as mafic intrusions and informally named the Joppita Bore mafic intrusions (Fig. 28). These bodies, associated with a gravity high, have similar shapes and dimensions to the Mordor Complex (Fig. 21), lie approximately 70 km west the Mordor Complex and may be related.

References

Close, D., Scrimgeour, I., Edgoose, C., Cross, A., Clauoe-Long, J., Kinny, P. & Meixner, T., 2003. Redefining the Warumpi Province. in 'Annual Geoscience Exploration Seminar (AGES), 2001. Record of abstracts.' Northern Territory Geological Survey, Record 2003-001.

Close, D.F, Edgoose, C.J. & Scrimgeour, I.R., 2002a. Lake Mackay Second Edition (1:250 000 scale geological map) Northern Territory Geological Survey, Alice Springs.

Close, D.F, Edgoose, C.J. & Scrimgeour, I.R., 2002b. Mount Rennie Second Edition (1:250 000 scale geological map) Northern Territory Geological Survey, Alice Springs.

Freeman, M.J., et al[1]., 1986a. Huckitta, Northern Territory—1:250 000 geological map (sheet SF 53–11). Northern Territory Geological Survey, Darwin (second edition).

Glickson, A.Y., et al[1]., 1983. Bedrock geology of the Glen Helen, Narwietooma and Anburla 1:100 000 sheet areas. Preliminary edition geological map. Bureau of Mineral Resources, Australia.

Hoatson, D.M. & Sun, S-s., 2002. Archean layered mafic-ultramafic intrusions in the west Pilbara Craton, Western Australia: a synthesis of some of the oldest orthomagmatic mineralizing systems in the world. Economic Geology 97, 847-872.

Hoatson, D.M. & Stewart, A.J., 2001. Field investigations of Proterozoic mafic-ultramafic intrusions in the Arunta Province, central Australia. Canberra: Geoscience Australia, Record 2001/39.

Langworthy, A.P. & Black, L.P., 1978. The Mordor Complex: a highly differentiated potassic intrusion with kimberlitic affinities in central Australia. Contributions to Mineralogy and Petrology, 67, 51–62.

Minty, B.R.S., Milligan, P.R., Luyendyk, A.P.J. & Mackey, T., 2003. Merging airborne magnetic surveys into continental-scale compilations. Geophysics, VOL 68 No: 3. In Press.

Murray, A,. 1999. Australian Gravimetry. Australian Geological Survey Organisation, Record 1999/42.

Reid, A.B., 1980. Aeromagnetic Survey Design. Geophysics, 45(5), 973-976.

Richardson, L.M., 2001. Index of Airborne Geophysical Surveys – Fifth Edition. Australian Geological Survey Organisation, Record 2001/14.

Shaw, R.D., et al[1]., 1975. Alcoota, Northern Territory—1:250 000 geological map (sheet SF 53–10). Bureau of Mineral Resources, Australia (first edition).

Shaw, R.D., et al[1]., 1983. Alice Springs, Northern Territory – Australian 1:250 000 geological series ; SF 53-14. Bureau of Mineral Resources, Canberra (second edition).

Shaw, R.D., et al[1]., 1995. Hermannsburg (1:250 000 scale map). Australian Geological Survey Organisation, Canberra.

[1]Only the senior compiler is indicated for preliminary, 1:100 000 and 1:250 000 geological sheets.

Figures

Figure 1. Outcropping mafic-ultramafic intrusions in the Arunta Region (modified from Hoatson & Stewart, 2001).

Figure 2. Greyscale image of the total magnetic intensity – reduced to pole, of the western Arunta region. Solid geology interpretations of the mafic-ultramafic intrusions are superimposed. The locations of subsequent figures are shown.

Figure 3. Greyscale image of the total magnetic intensity – reduced to pole, of the eastern Arunta region. Solid geology interpretations of the mafic-ultramafic intrusions are superimposed. The locations of subsequent figures are shown.

Figure 4. Colour image of the total magnetic intensity – reduced to pole, with a northeasterly illumination of the western Arunta region. Solid geology interpretations of the mafic-ultramafic intrusions are superimposed.

Figure 5. Colour image of the total magnetic intensity – reduced to pole, with a northerly illumination of the eastern Arunta region. Solid geology interpretations of the mafic-ultramafic intrusions are superimposed.

Figure 6. Pseudo colour image of the vertical gradient of the total magnetic intensity – reduced to pole, of the western Arunta region. Solid geology interpretations of the mafic-ultramafic intrusions are superimposed.

Figure 7. Pseudo colour image of the vertical gradient of the total magnetic intensity – reduced to pole, of the eastern Arunta region. Solid geology interpretations of the mafic-ultramafic intrusions are superimposed.

Figure 8. Colour image with a northerly illumination of the Bouguer gravity field, in the western Arunta region. Solid geology interpretations of the mafic-ultramafic intrusions are superimposed. The gravity station locations are also shown.

Figure 9. Colour image with a northerly illumination of the Bouguer gravity field, in the eastern Arunta region. Solid geology interpretations of the mafic-ultramafic intrusions are superimposed. The gravity station locations are also shown.

Figure 10. Colour image of the vertical gradient of the Bouguer gravity field, in the western Arunta region. Solid geology interpretations of the mafic-ultramafic intrusions are superimposed, as are the gravity station locations and the locations of subsequent figures.

Figure 11. Colour image of the vertical gradient of the Bouguer gravity field, in the eastern Arunta region. Solid geology interpretations of the mafic-ultramafic intrusions are superimposed, as are the gravity station locations and the locations of subsequent figures.

Figure 12a. Geological map of the Andrew Young Hills mafic intrusion (from Hoatson & Stewart, 2001).

Figure 12b. Solid geology interpretation of the Andrew Young Hills mafic intrusion. The full subcropping extent of the intrusion is shown, including the results of magnetic modelling defining the depth of alluvial cover and dip and strike of macroscopic layering.

Figure 12c. Vertical gradient image of the Bouguer gravity field, of the Andrew Young Hills mafic intrusion. The locations of the gravity station are shown.

Figure 12d. Grey scale image of the total magnetic intensity – reduced to pole field, of the Andrew Young Hills mafic intrusion.

Figure 12e. Pseudo colour image of the vertical gradient of the total magnetic intensity, of the Andrew Young Hills mafic intrusion.

Figure 13a. Vertical gradient image of the Bouguer gravity field, including gravity station locations of the eastern portion of the Mt Liebig 1:250 000 sheet. The locations of the outcropping and interpreted mafic-ultramafic intrusions are shown. The low density of gravity stations do not resolve bodies of this size.

Figure 13b. Grey scale image of the total magnetic intensity – reduced to pole of the eastern portion of the Mt Liebig 1:250 000 sheet. The locations of the outcropping and interpreted mafic-ultramafic intrusions are shown.

Figure 13c. Pseudocolour image of the vertical gradient of the total magnetic intensity – reduced to pole of the eastern portion of the Mt Liebig 1:250 000 sheet. The locations of the outcropping and interpreted mafic-ultramafic intrusions are shown.

Figure 13d. Ternary gamma-ray spectrometric image (potassium – red, thorium – green, uranium – blue) of the Mt Liebig 1:250 000 sheet. The locations of the outcropping and interpreted mafic-ultramafic intrusions are shown.

Figure 14. Geological map of the West Papunya gabbro intrusion. (from Hoatson & Stewart, 2001).

Figure 15. Geological map of the Papunya gabbro and Papunya ultramafic intrusions. (from Hoatson & Stewart, 2001).

Figure 16. Geological map of the South Papunya gabbro intrusion. (from Hoatson & Stewart, 2001).

Figure 17a. Geological map of the Mount Chapple Metamorphics (from Hoatson & Stewart, 2001).

Figure 17b. Solid geology interpretation showing full extent of the intrusion, including the results of magnetic modelling defining depth of alluvial cover and dip and strike of macroscopic layering.

Figure 17c. Vertical gradient image of the Bouguer gravity field, including gravity station locations.

Figure 17d. Grey scale image of the total magnetic intensity – reduced to pole.

Figure 17e. Pseudo colour image of the vertical gradient applied to the total magnetic intensity (reduced to pole).

Figure 18a. Geological map of the Mount Hay Granulite and Anburla Anorthosite mafic intrusions (modified after Glickson et al., 1983 and Shaw et al., 1995).

Figure 18b. Solid geology interpretation showing the full extent of the Mount Hay Granulite, the extent of mapped and inferred Anburla Anorthosite, and the interpreted eastern extent of the interlayered mafic granulite and garnet gneiss. The results of magnetic modelling defining depth of alluvial cover and dip and strike of macroscopic layering is also shown.

Figure 18c. Vertical gradient image of the Bouguer gravity field, including gravity station locations.

Figure 18d. Grey scale image of the total magnetic intensity – reduced to pole.

Figure 18e. Pseudo colour image of the vertical gradient applied to the total magnetic intensity (reduced to pole).

Figure 19a. Geological map of the Enbra Granulite intrusion (modified after Shaw et al., 1983).

Figure 19b. Solid geology interpretation, showing the full extent of the Enbra Granulite. The results of magnetic modelling, defining depth of alluvial cover and dip and strike of macroscopic layering is also shown.

Figure 19c. Vertical gradient image of the Bouguer gravity field, including gravity station locations.

Figure 19d. Grey scale image of the total magnetic intensity – reduced to pole

Figure 19e. Pseudo colour image of the vertical gradient applied to the total magnetic intensity (reduced to pole).

Figure 20a. Geological map of the Harry Anorthositic Gabbro and Johannsen Metagabbro intrusions (modified after Shaw et al., 1983).

Figure 20b. Solid geology interpretation, showing the full sub-cropping extent of the Harry Anorthositic Gabbro.

Figure 20c. Vertical gradient image of the Bouguer gravity field, including gravity station locations.

Figure 20d. Grey scale image of the total magnetic intensity – reduced to pole.

Figure 20e. Pseudo colour image of the vertical gradient applied to the total magnetic intensity (reduced to pole).

Figure 21a. Geological map of the Mordor Complex (modified after Langworthy & Black, 1978).

Figure 21b. Solid geology interpretation of the Mordor Complex.

Figure 21c. Vertical gradient image of the Bouguer gravity field, including gravity station locations. The offset of the gravity anomaly with respect to the centre of the intrusion is symptomatic of the undersampled gravity field with respect to the intrusion dimensions.

Figure 21d. Grey scale image of the total magnetic intensity – reduced to pole.

Figure 21e. Pseudo colour image of the vertical gradient applied to the total magnetic intensity (reduced to pole).

Figure 22a. Geological map of the Kanandra Granulite (modified after Shaw et al., 1975).

Figure 22b. Solid geology interpretation of the Kanandra Granulite showing the total interpreted sub-cropping extent. The region shown in the geological map (Fig. 22a) is also displayed.

Figure 22c. Vertical gradient image of the Bouguer gravity field, including gravity station locations.

Figure 22d. Grey scale image of the total magnetic intensity – reduced to pole.

Figure 22e. Pseudo colour image of the vertical gradient applied to the total magnetic intensity (reduced to pole)

Figure 23b. Geological map of the Attutra Metagabbro (modified after Freeman, 1986).

Figure 23b. Solid geology interpretation of the Attutra Metagabbro intrusion.

Figure 23c. Vertical gradient image of the Bouguer gravity field, including gravity station locations.

Figure 23d. Grey scale image of the total magnetic intensity – reduced to pole.

Figure 23e. Pseudo colour image of the vertical gradient applied to the total magnetic intensity (reduced to pole).

Figure 24a. Solid geology of the western mafic intrusions, showing the total sub-cropping extent of the interpreted intrusions. The results of magnetic modelling defining depth of alluvial cover and dip and strike of macroscopic layering are also shown.

Figure 24b. Vertical gradient image of the Bouguer gravity field, including gravity station locations.

Figure 24c. Grey scale image of the total magnetic intensity – reduced to pole.

Figure 24d. Pseudo colour image of the vertical gradient applied to the total magnetic intensity (reduced to pole).

Figure 25a. Solid geology interpretation of the central mafic intrusions, showing total sub-cropping extent of the intrusions. The results of magnetic modelling, defining depth of alluvial cover and dip and strike of macroscopic layering are also shown.

Figure 25b. Vertical gradient image of the Bouguer gravity field, including gravity station locations.

Figure 25c. Grey scale image of the total magnetic intensity – reduced to pole.

Figure 25d. Pseudo colour image of the vertical gradient applied to the total magnetic intensity (reduced to pole).

Figure 26a. Solid geology interpretation of the eastern mafic intrusions, showing the total sub-cropping extent and the location of deeply buried intrusions. The results of magnetic modelling defining depth of alluvial cover and dip and strike of macroscopic layering are also shown.

Figure 26b. Vertical gradient image of the Bouguer gravity field, including gravity station locations.

Figure 26c. Grey scale image of the total magnetic intensity – reduced to pole.

Figure 26d. Pseudo colour image of the vertical gradient applied to the total magnetic intensity (reduced to pole).

Figure 27a. Solid geology interpretation of the McEwin Hills mafic body, showing total sub-cropping extent of the intrusion.

Figure 27b. Vertical gradient image of the Bouguer gravity field, including gravity station locations.

Figure 27c. Grey scale image of the total magnetic intensity – reduced to pole.

Figure 27d. Pseudo colour image of the vertical gradient applied to the total magnetic intensity (reduced to pole).

Figure 28a. Solid geology interpretation of the Joppita Bore mafic intrusions, showing the total sub-cropping extent of the intrusions.

Figure 28b. Vertical gradient image of the Bouguer gravity field, including gravity station locations.

Figure 28c. Grey scale image of the total magnetic intensity – reduced to pole.

Figure 28d. Pseudo colour image of the vertical gradient applied to the total magnetic intensity (reduced to pole).

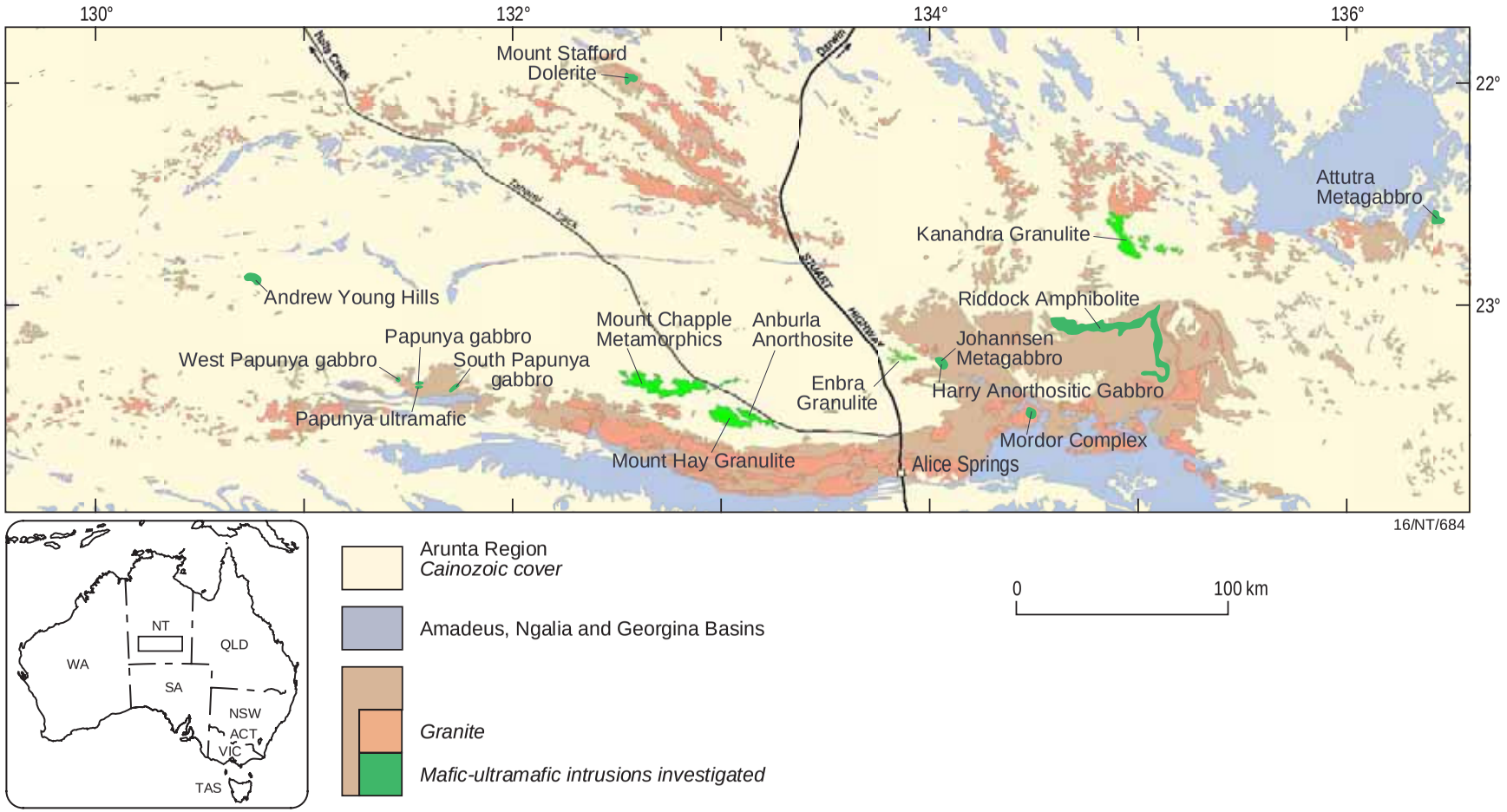

Figure 1. Outcropping mafic-ultramafic intrusions in the Arunta Region (modified from Hoatson & Stewart, 2001).

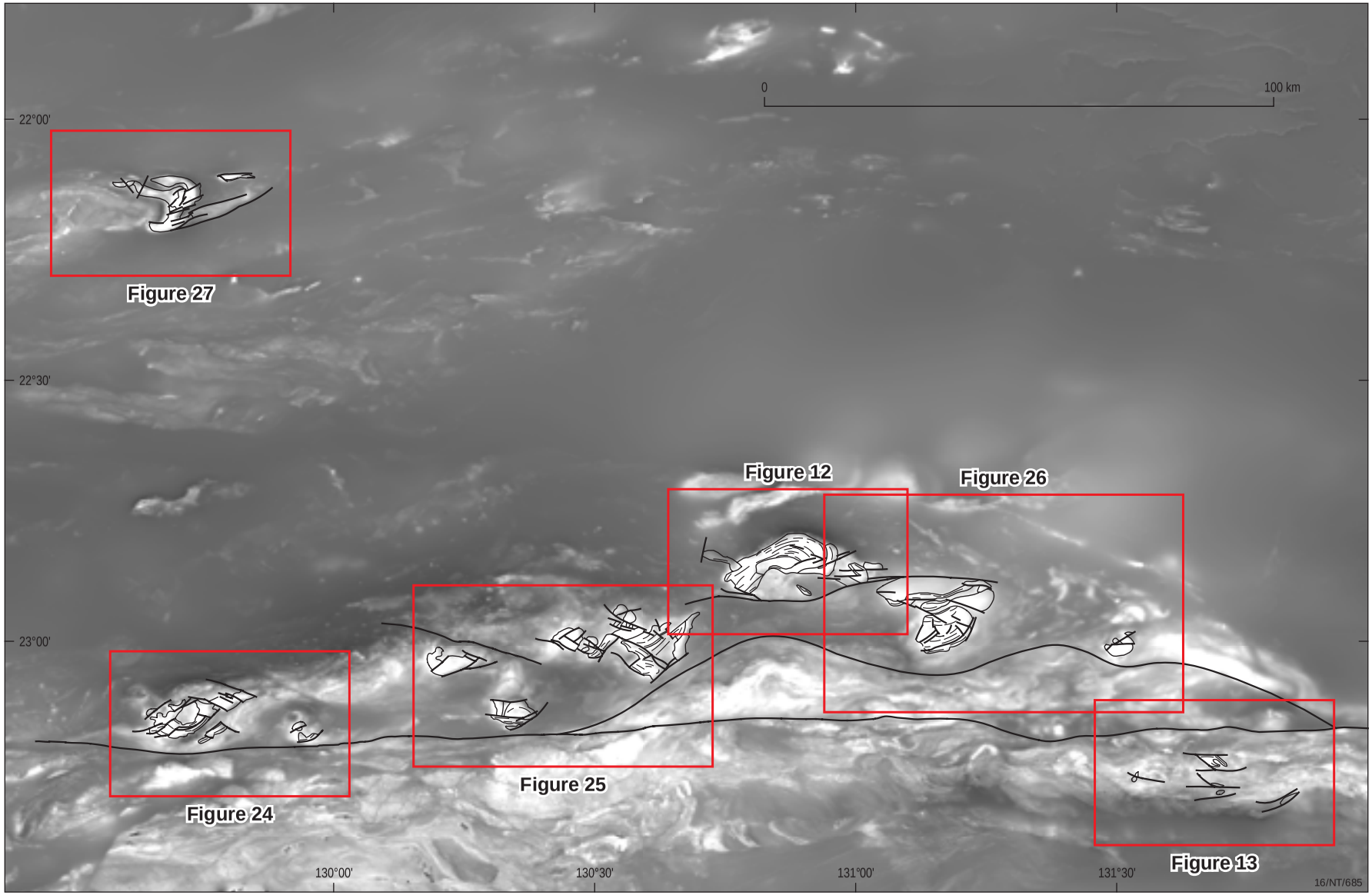

Figure 2. Greyscale image of the total magnetic intensity - reduced to pole, of the western Arunta region. Solid geology interpretations of the mafic-ultramafic intrusions are superimposed. The locations of subsequent figures are shown.

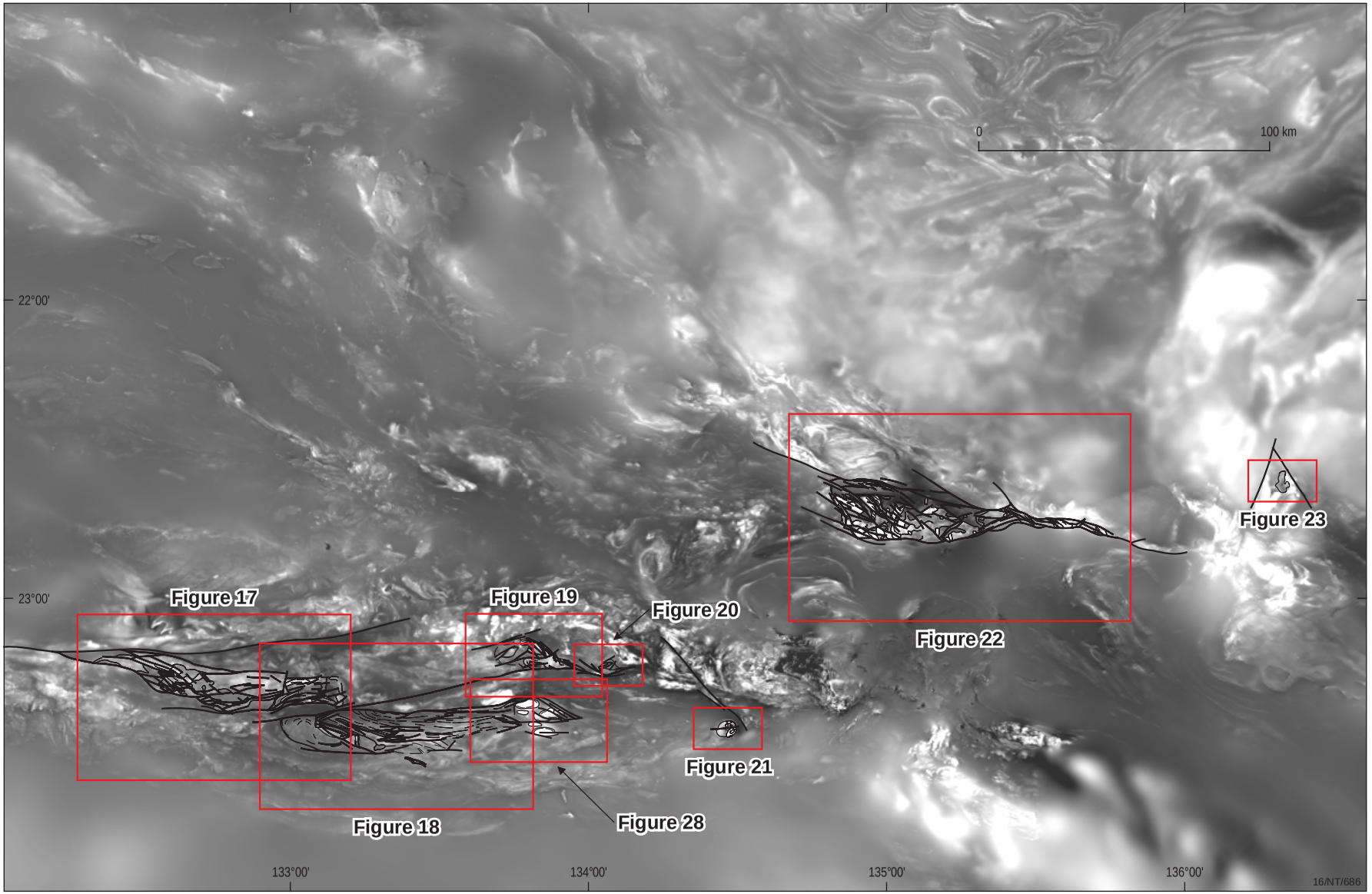

Figure 3. Greyscale image of the total magnetic intensity - reduced to pole, of the eastern Arunta region. Solid geology interpretations of the mafic-ultramafic intrusions are superimposed. The locations of subsequent figures are shown.

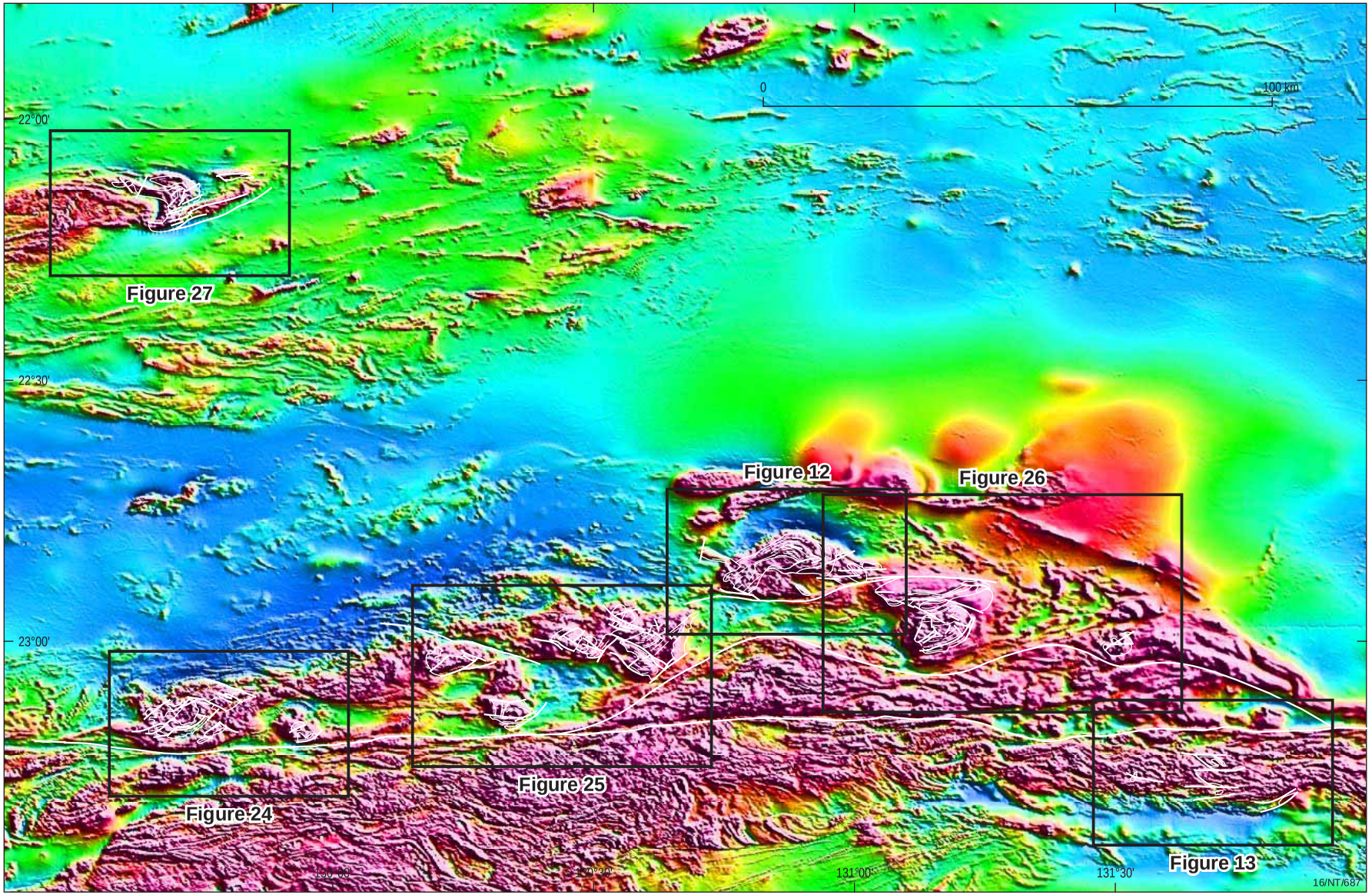

Figure 4. Colour image of the total magnetic intensity - reduced to pole, with a northeasterly illumination of the western Arunta region. Solid geology interpretations of the mafic-ultramafic intrusions are superimposed.

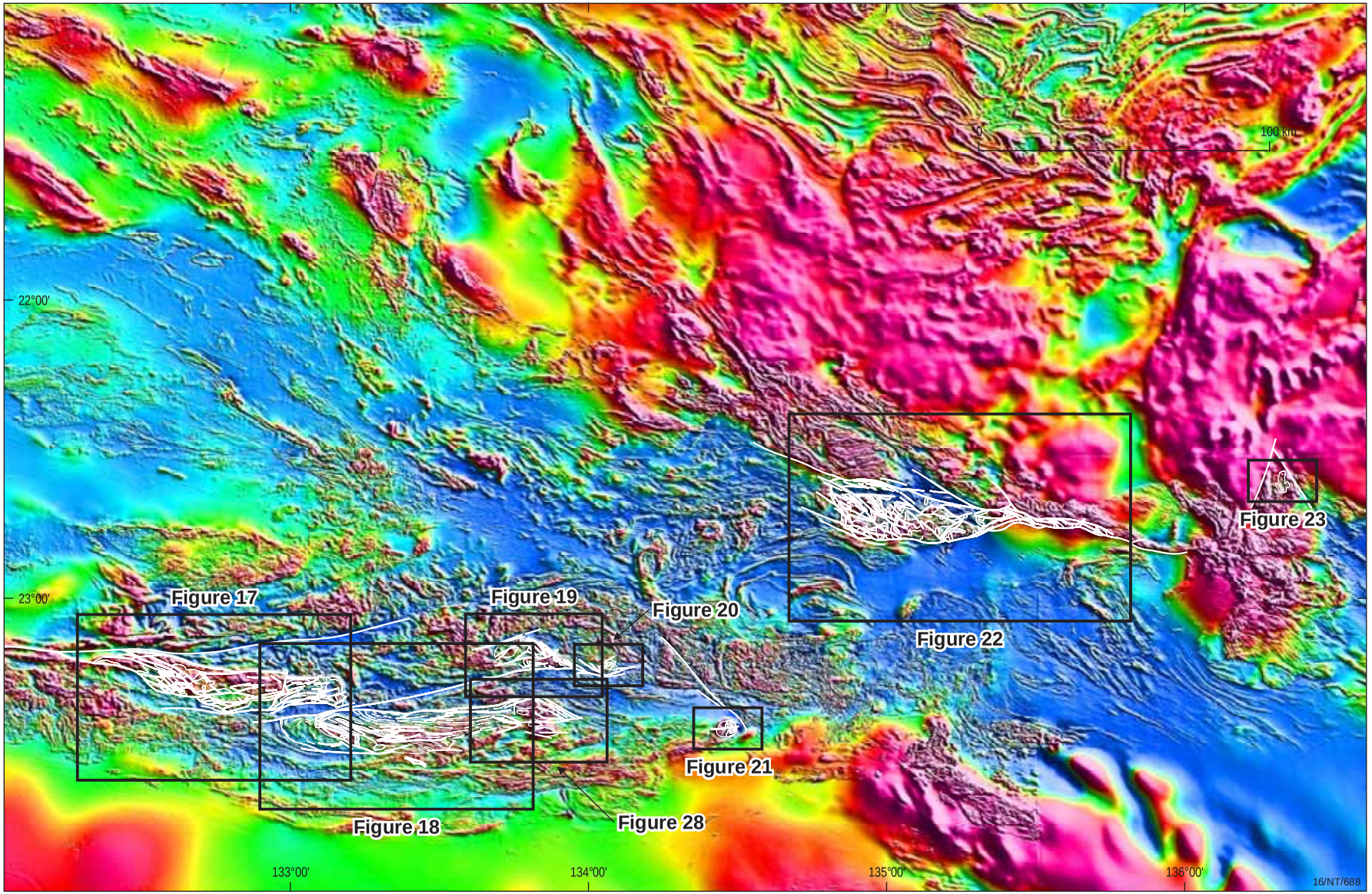

Figure 5. Colour image of the total magnetic intensity - reduced to pole, with a northeasterly illumination of the eastern Arunta region. Solid geology interpretations of the mafic-ultramafic intrusions are superimposed.

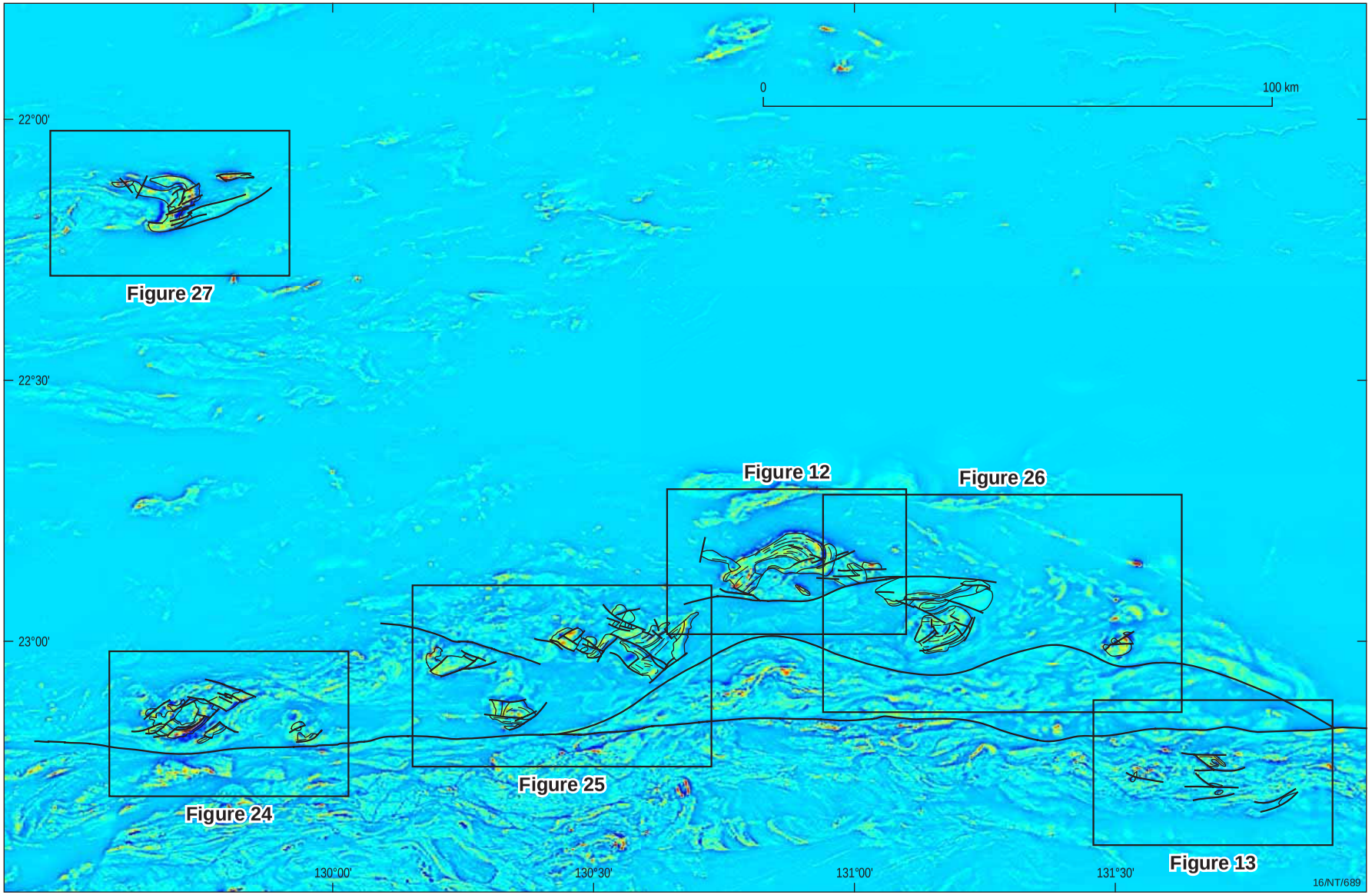

Figure 6. Pseudo colour image of the vertical gradient of the total magnetic intensity - reduced to pole, of the western Arunta region. Solid geology interpretations of the mafic-ultramafic intrusions are superimposed.

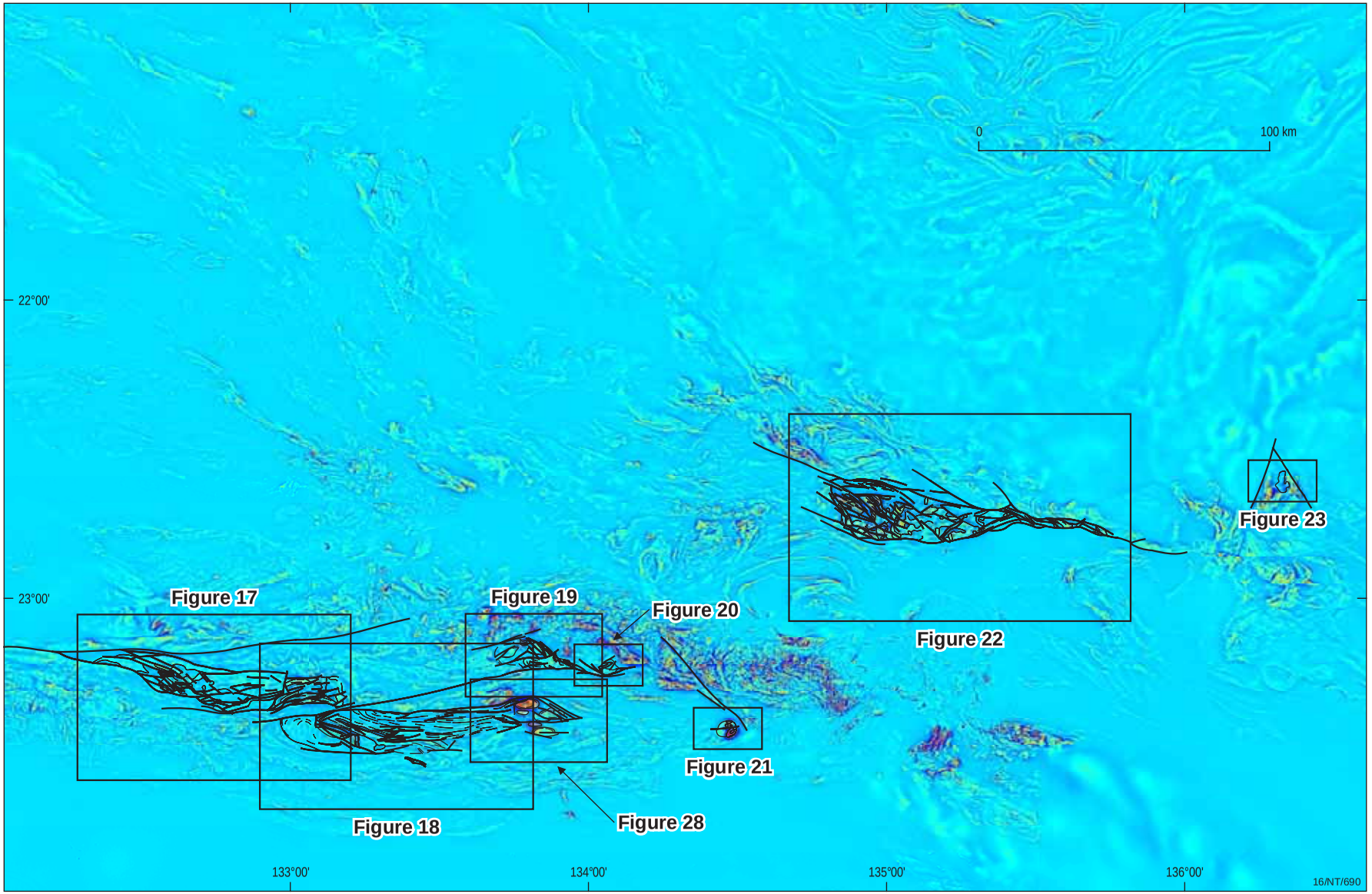

Figure 7. Pseudo colour image of the vertical gradient of the total magnetic intensity - reduced to pole, of the eastern Arunta region. Solid geology interpretations of the mafic-ultramafic intrusions are superimposed.

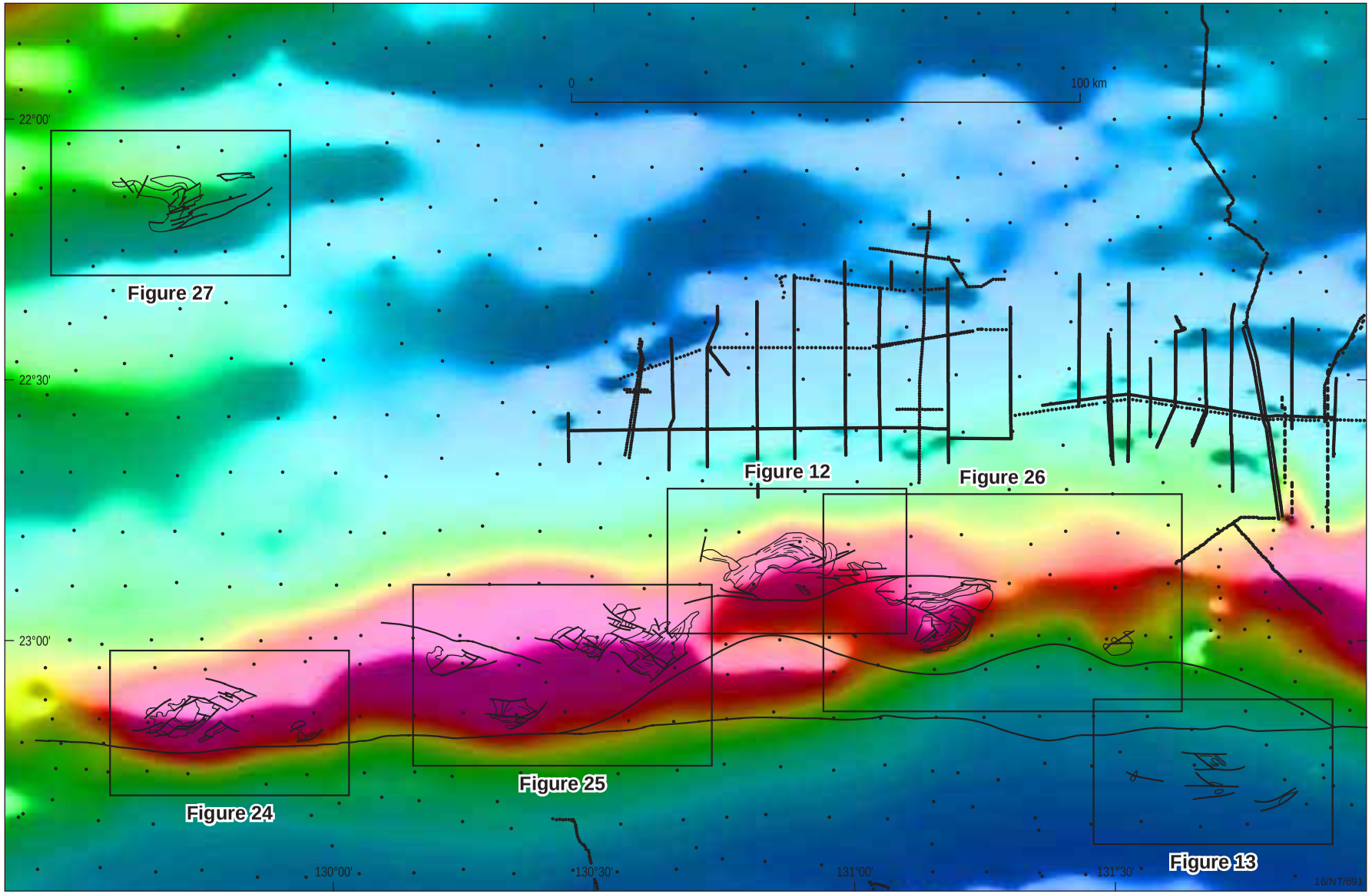

Figure 8. Colour image with a northerly illumination of the Bouguer gravity field, in the western Arunta region. Solid geology interpretations of the mafic-ultramafic intrusions are superimposed. The gravity station locations are also shown.

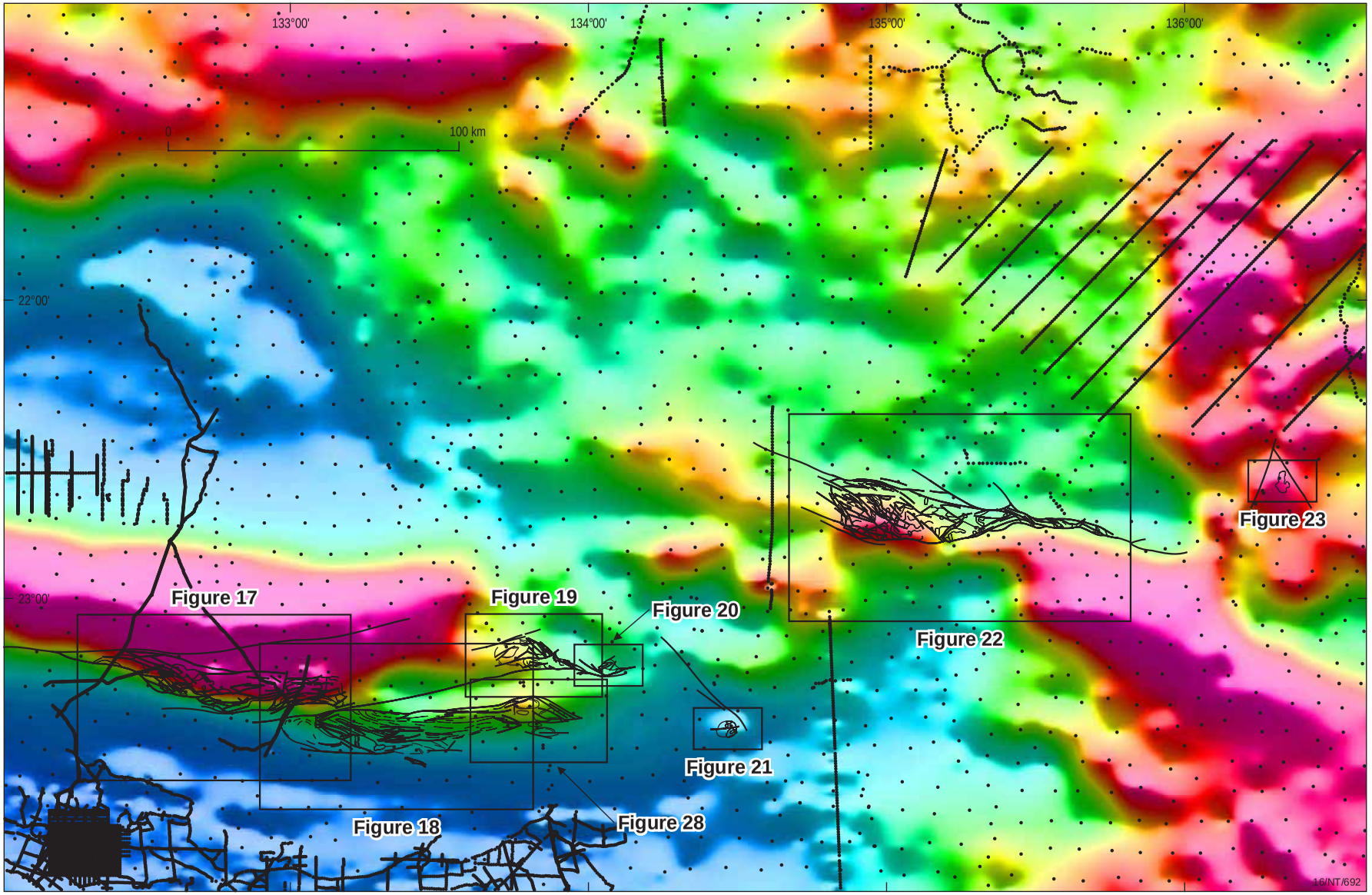

Figure 9. Colour image with a northerly illumination of the Bouguer gravity field, in the eastern Arunta region. Solid geology interpretations of the mafic-ultramafic intrusions are superimposed. The gravity station locations are also shown.

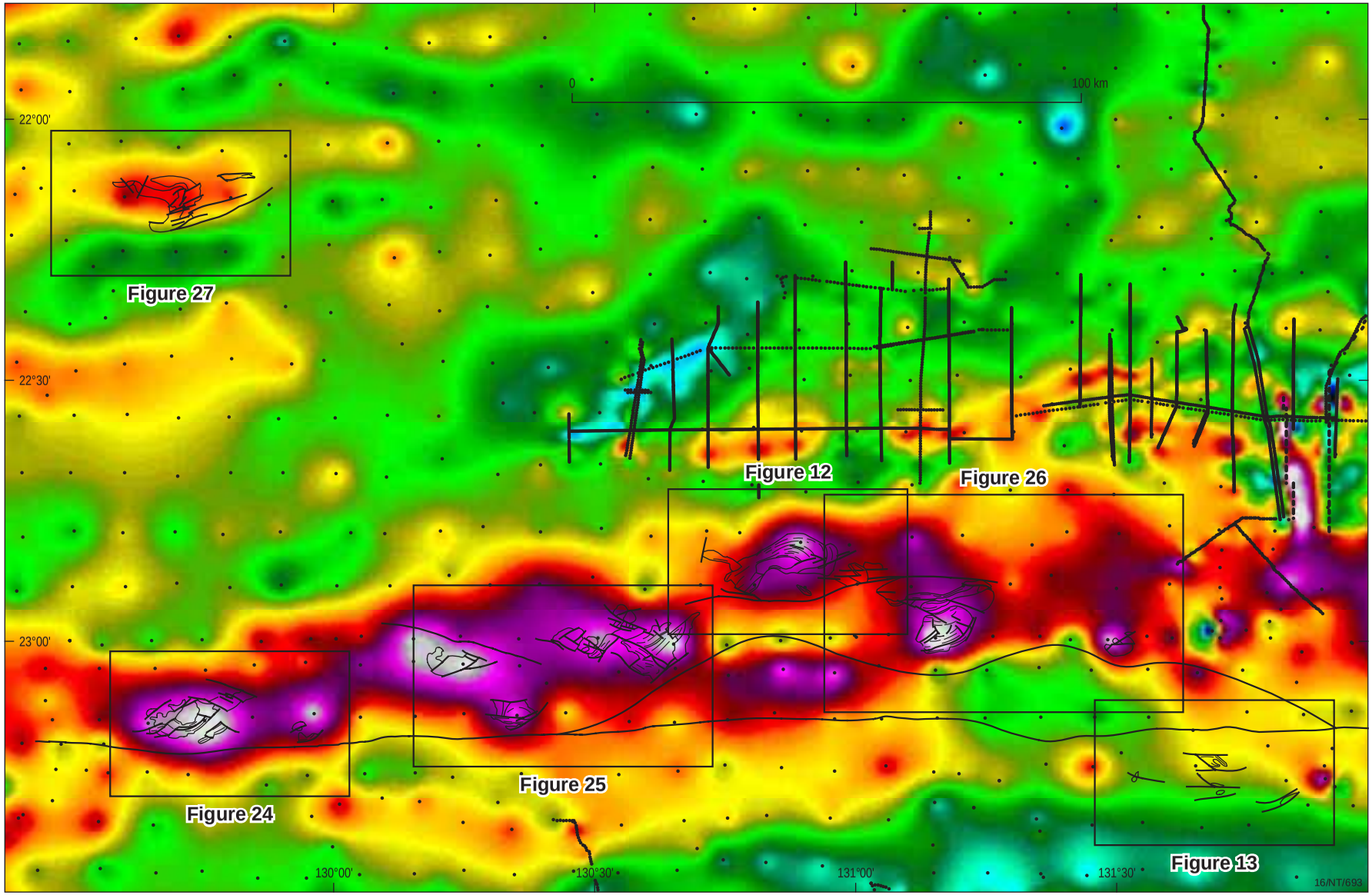

Figure 10. Colour image of the vertical gradient of the Bouguer gravity field, in the western Arunta region. Solid geology interpretations of the mafic-ultramafic intrusions are superimposed, as are the gravity station locations and the locations of subsequent figures.

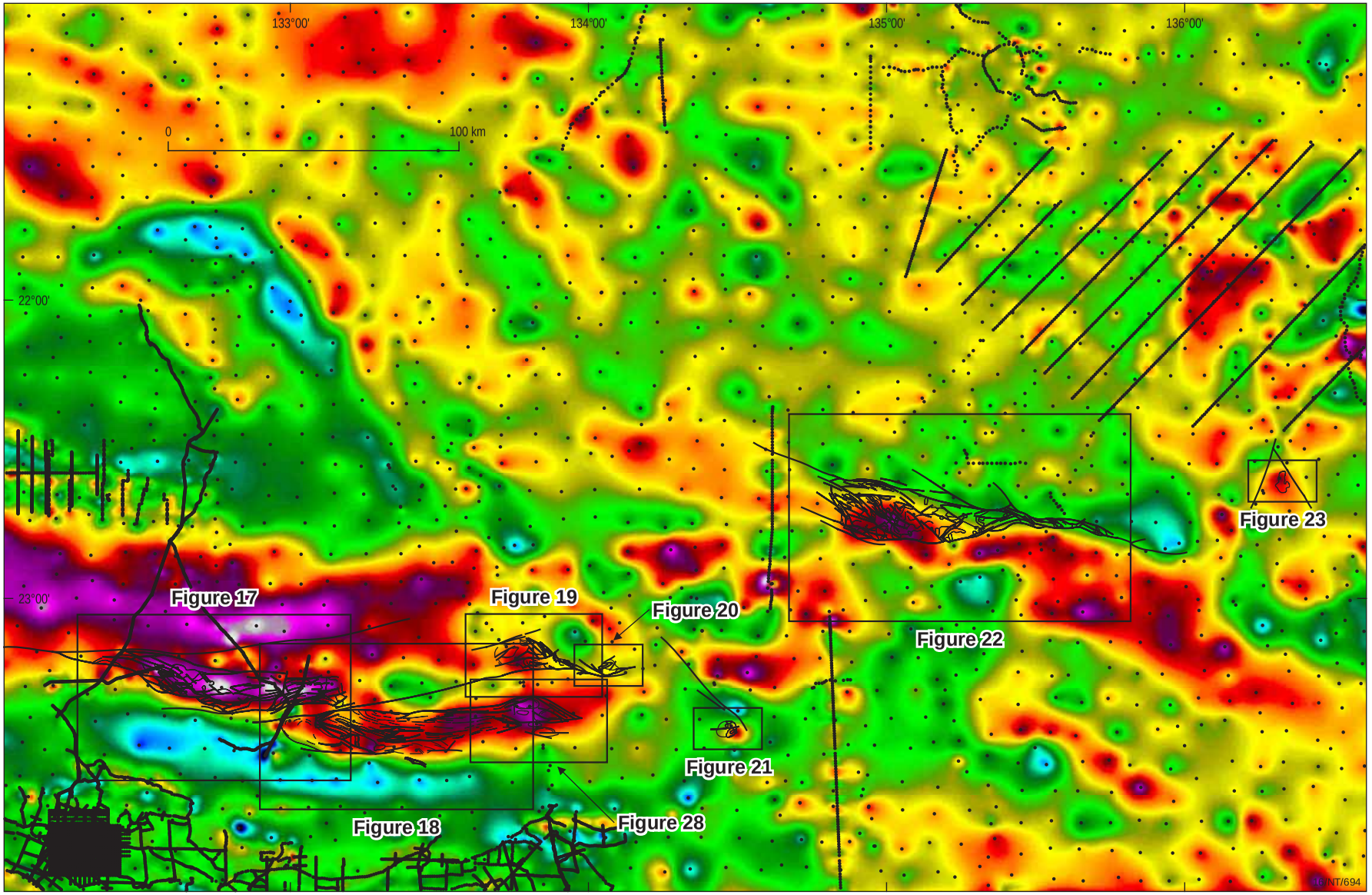

Figure 11. Colour image of the vertical gradient of the Bouguer gravity field, in the eastern Arunta region. Solid geology interpretations of the mafic-ultramafic intrusions are superimposed, as are the gravity station locations and the locations of subsequent figures.

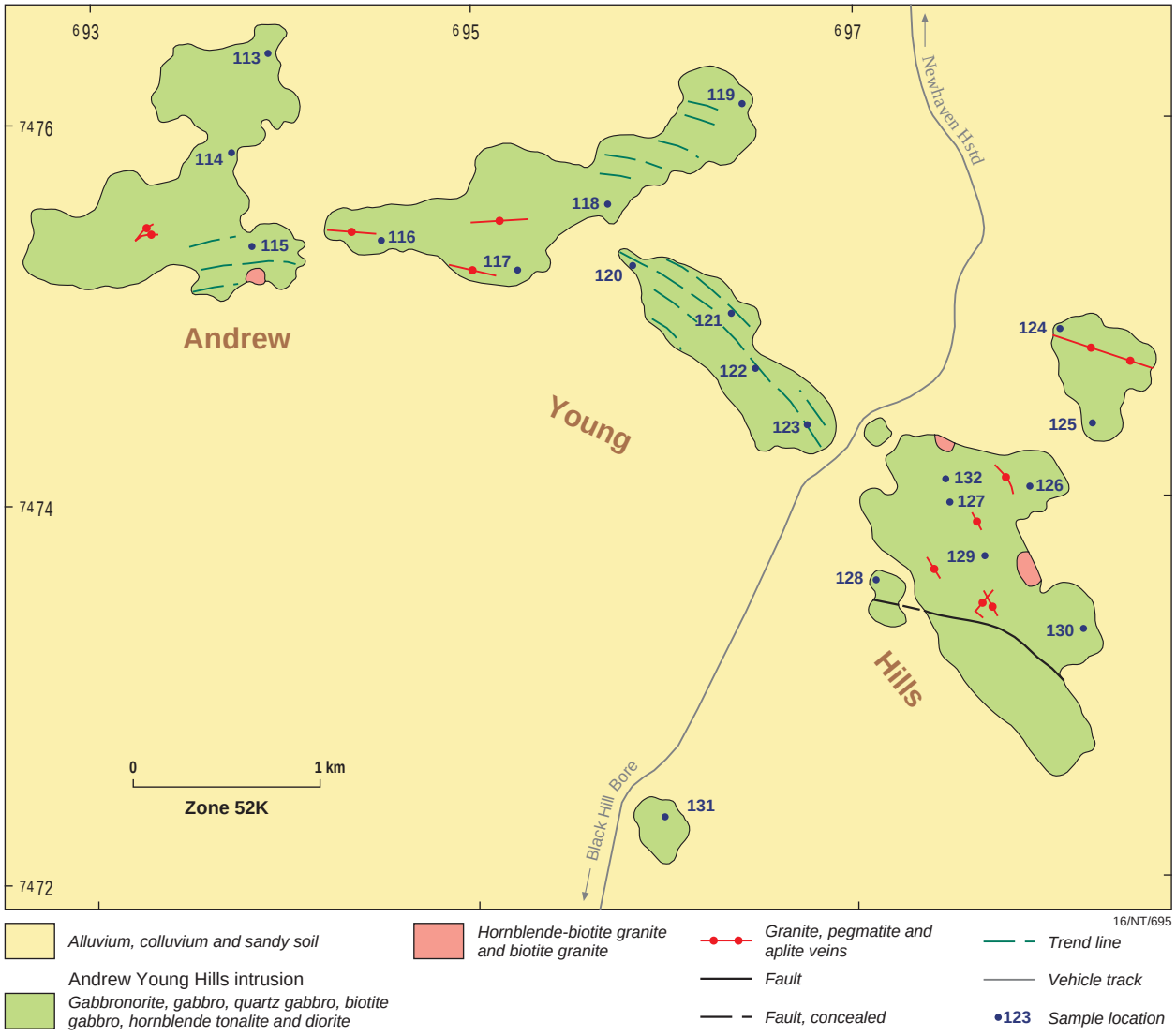

Figure 12a. Geological map of the Andrew Young Hills mafic intrusion (from Hoatson & Stewart, 2001).

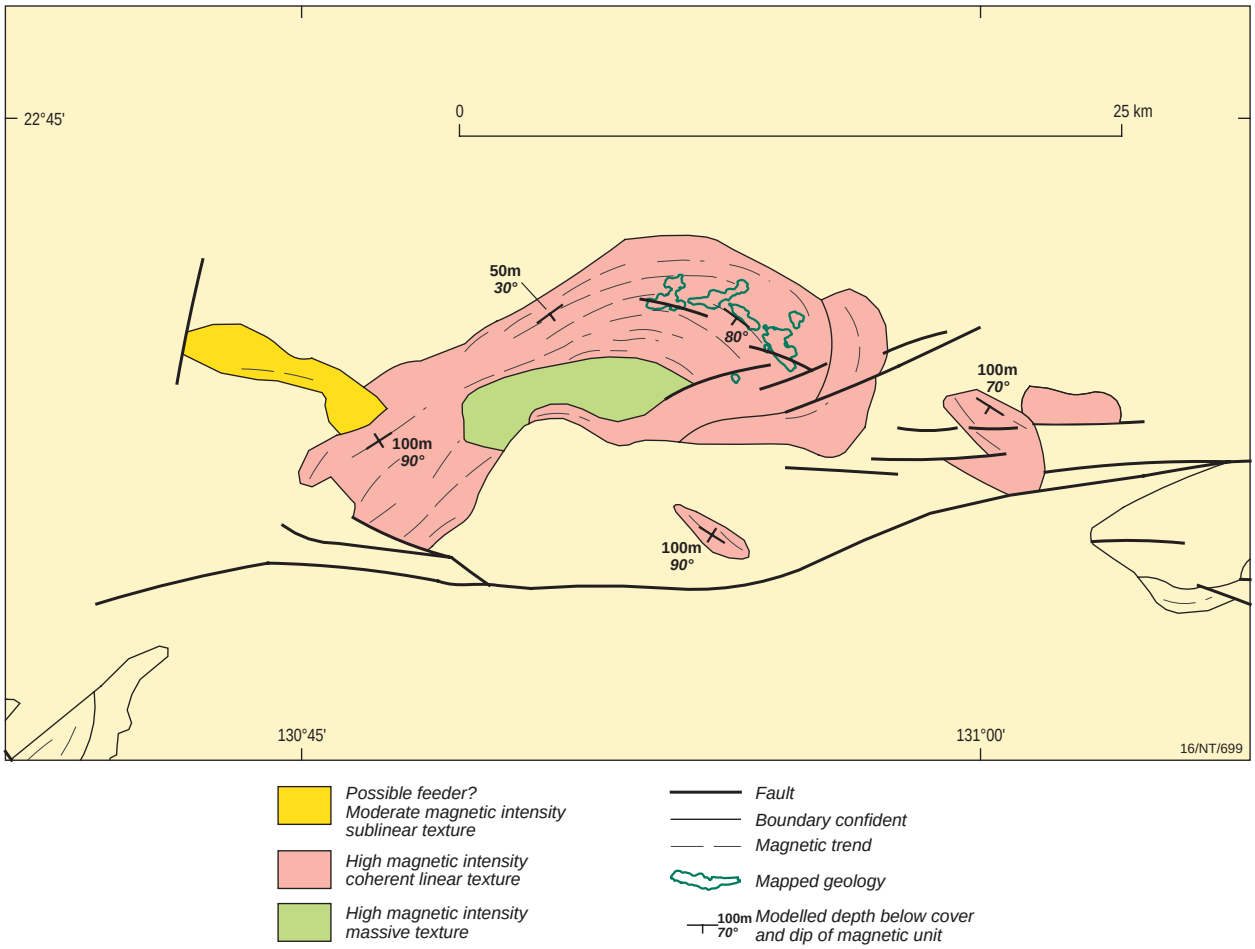

Figure 12b. Solid geology interpretation of the Andrew Young Hills mafic intrusion. The full subcropping extent of the intrusion is shown, including the results of magnetic modelling defining the depth of alluvial cover and dip and strike of macroscopic layering.

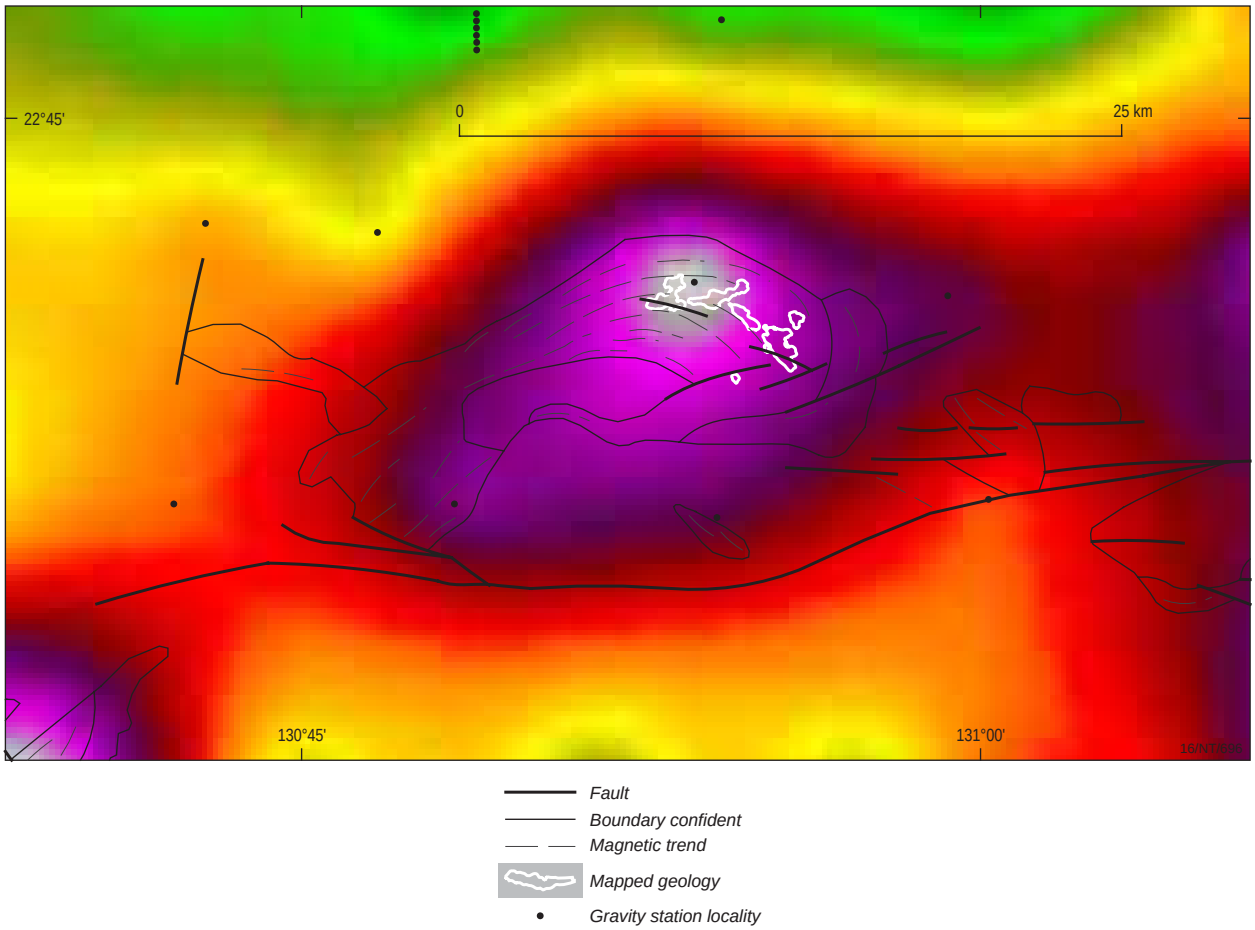

Figure 12c. Vertical gradient image of the Bouguer gravity field, of the Andrew Young Hills mafic intrusion. The locations of the gravity station are shown.

Figure 12d. Grey scale image of the total magnetic intensity - reduced to pole field, of the Andrew Young Hills mafic intrusion.

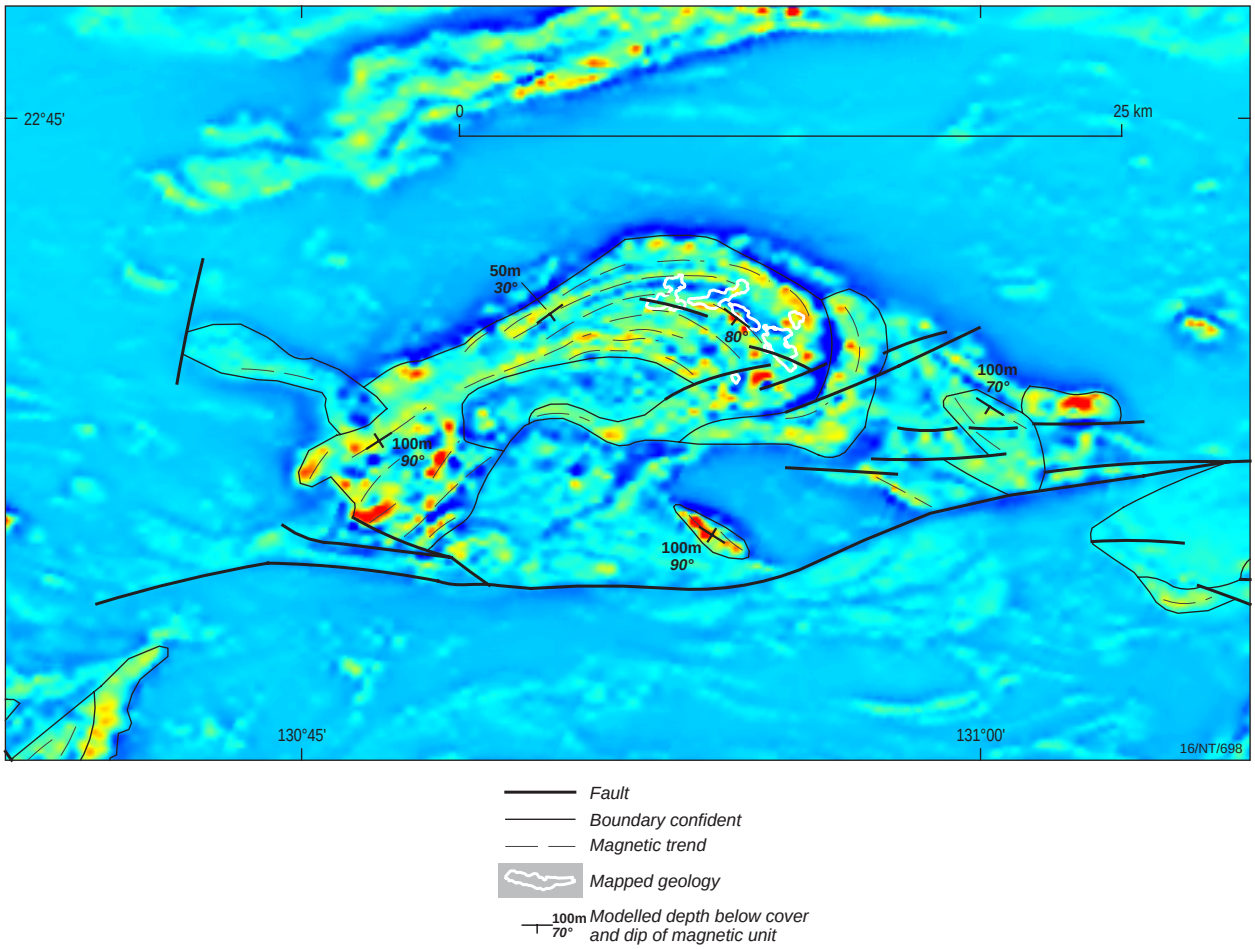

Figure 12e. Pseudo colour image of the vertical gradient of the total magnetic intensity, of the Andrew Young Hills mafic intrusion.

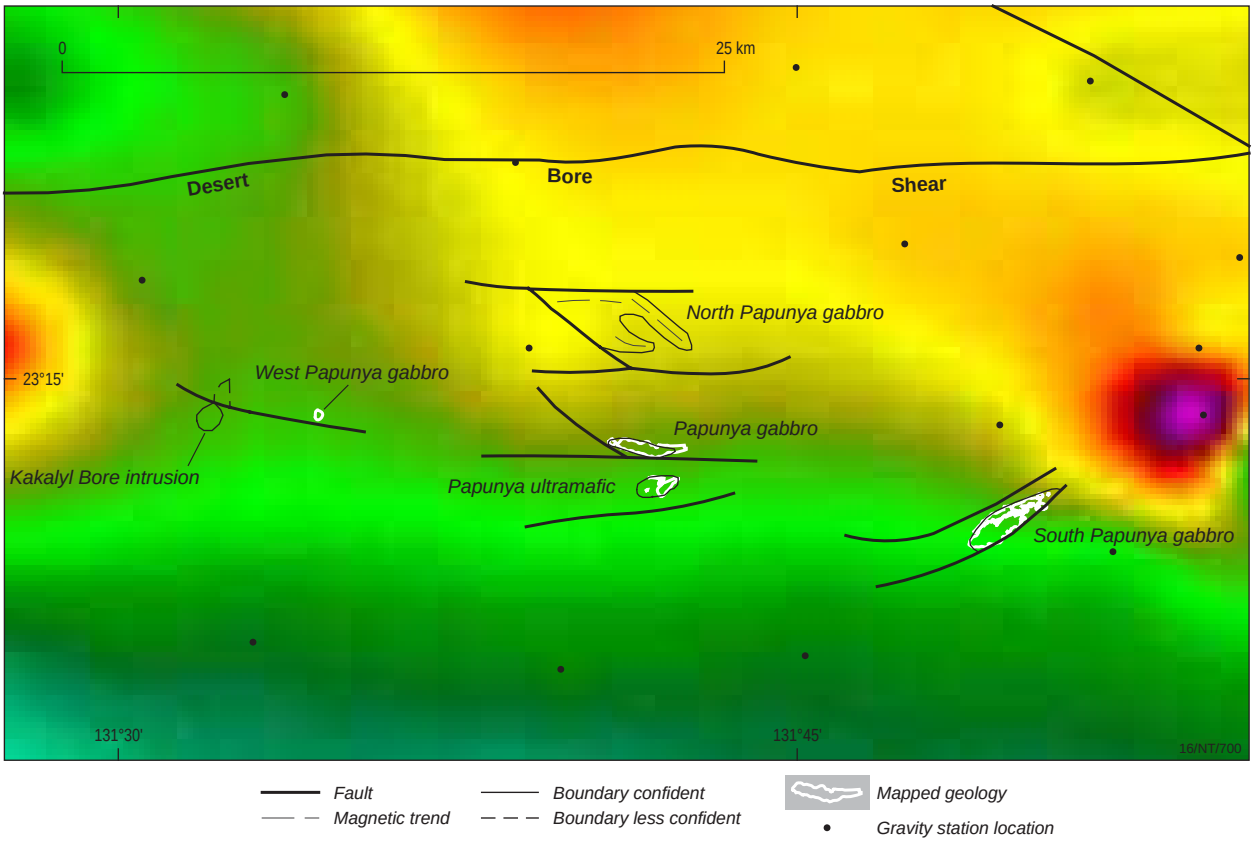

Figure 13a. Verical gradient image of the Bouguer gravity field, including gravity station locations of the eastern portion of the Mt Liebig 1:250 000 sheet. The locations of the outcropping and interpreted mafic-ultramafic intrusions are shown. The low density of gravity stations do not resolve bodies of this size.

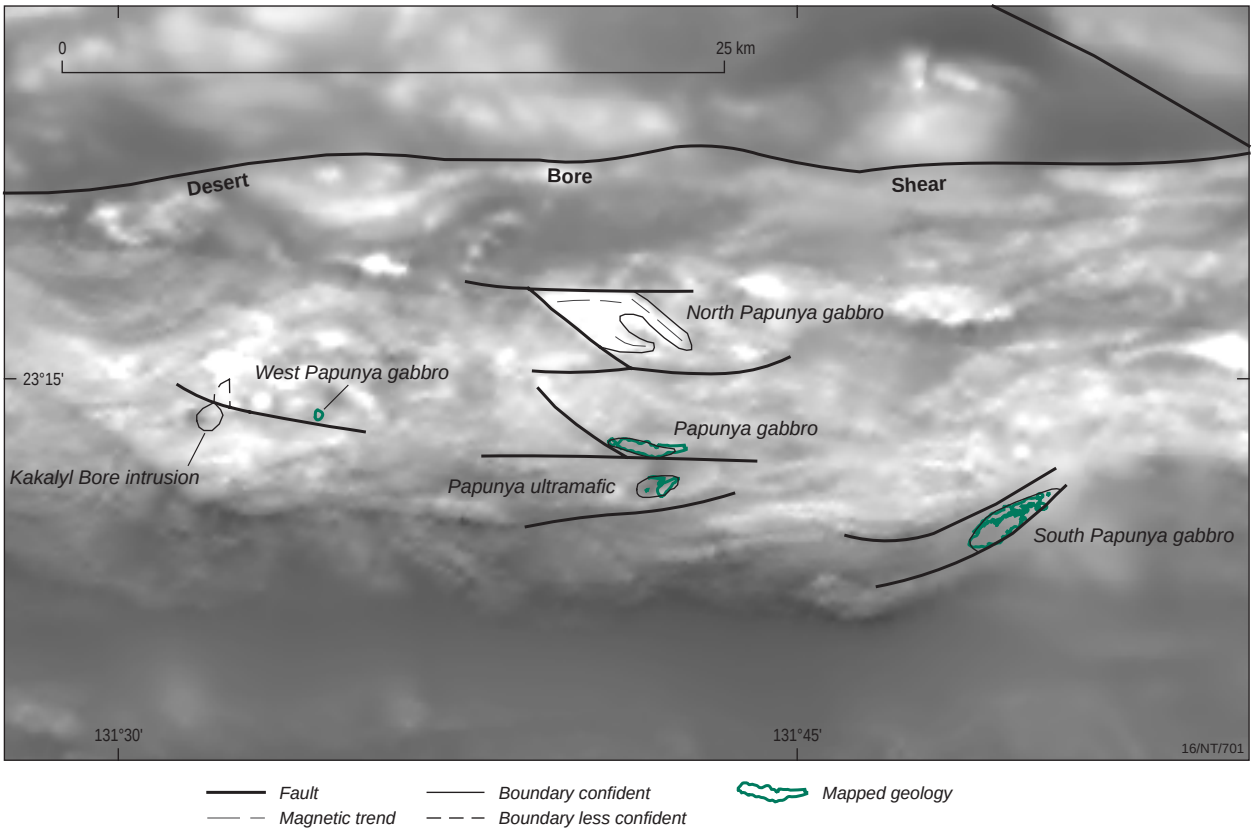

Figure 13b. Grey scale image of the total magnetic intensity - reduced to pole of the eastern portion of the Mt Liebig 1:250 000 sheet. The locations of the outcropping and interpreted mafic-ultramafic intrusions are shown.

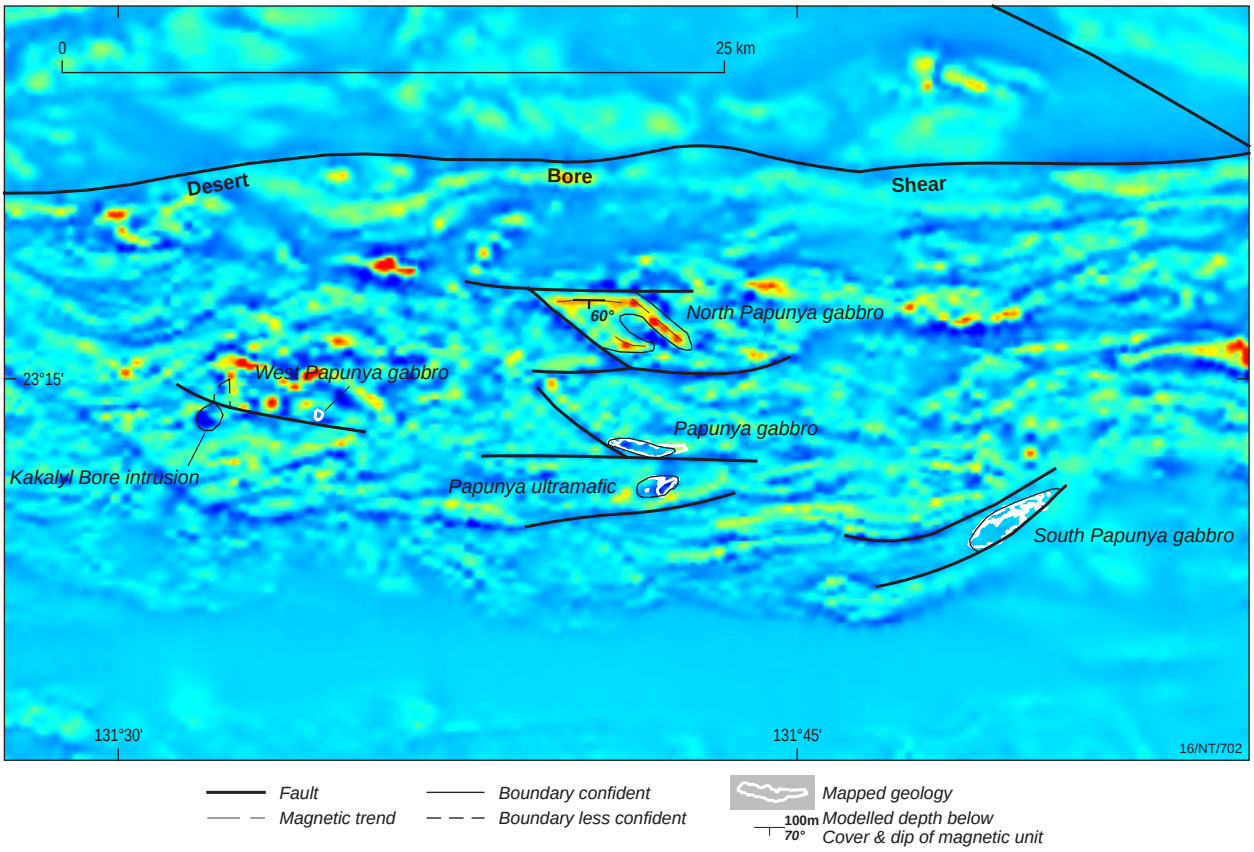

Figure 13c. Pseudocolour image of the vertical gradient of the total magnetic intensity - reduced to pole of the eastern portion of the Mt Liebig 1:250 000 sheet. the locations of the outcropping and interpreted mafic-ultramafic intrusions are shown.

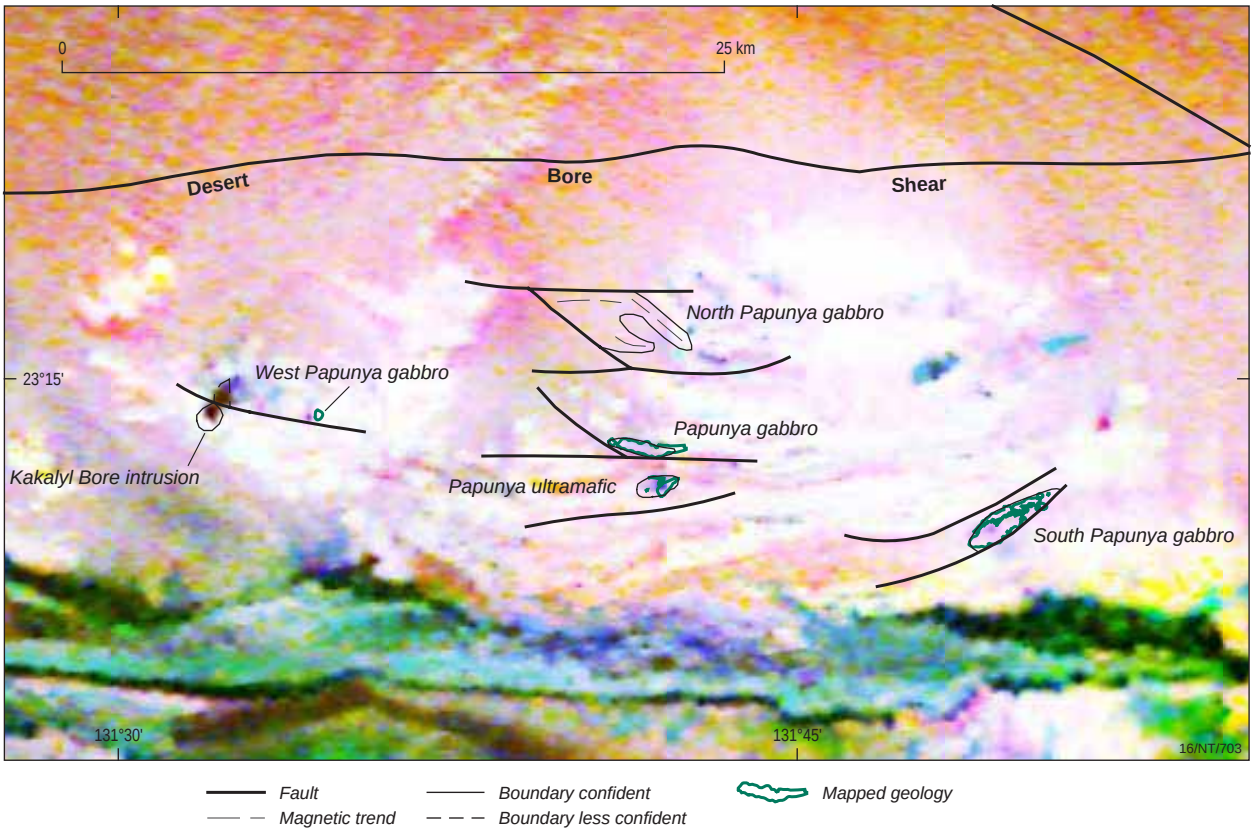

Figure 13d. Ternary radiometric image (potassium - red, thorium - green, uranium - blue) of the Mt Liebig 1:250 000 sheet. The locations of the outcropping and interpreted mafic-ultramafic intrusions are shown.

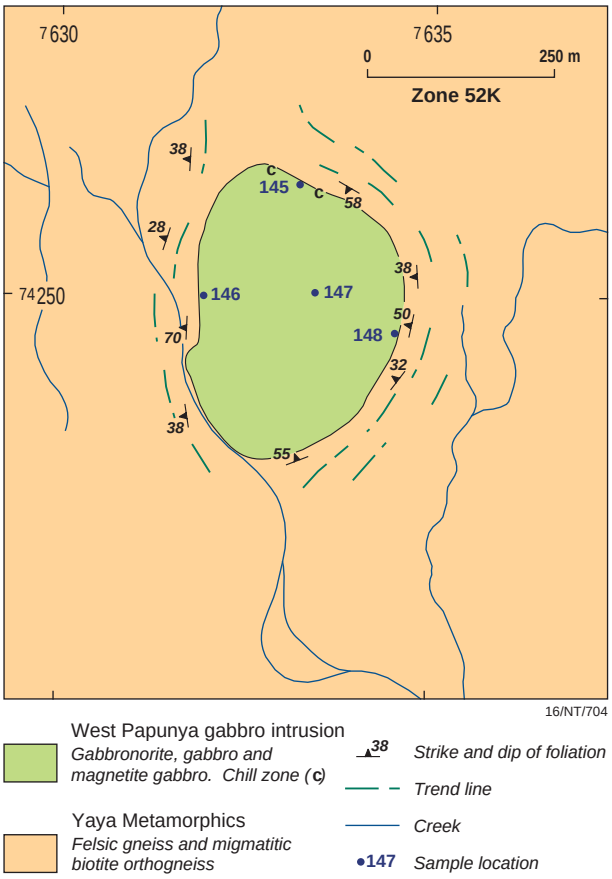

Figure 14. Geological map of the West Papunya gabbro intrusion. (from Hoatson & Stewart, 2001).

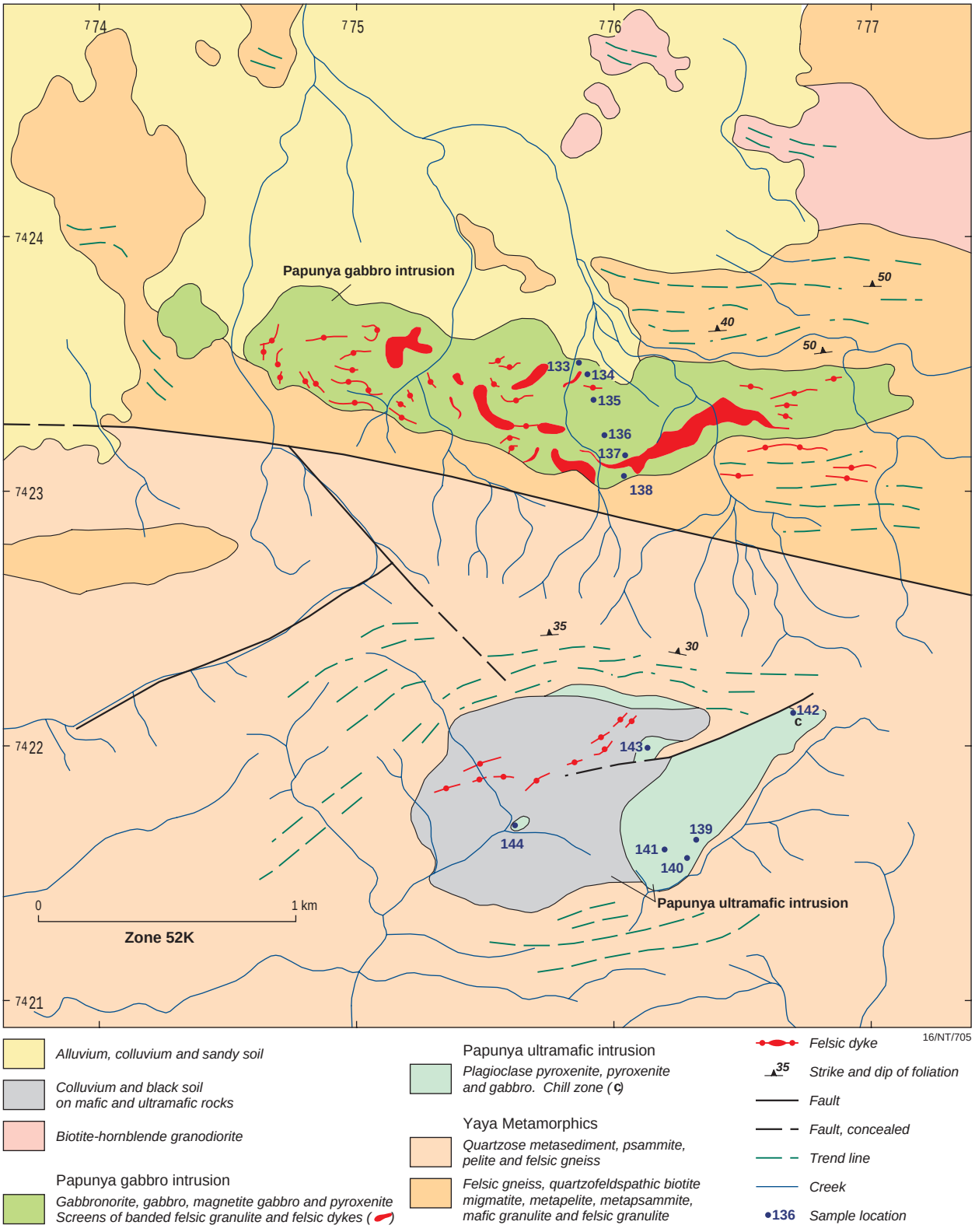

Figure 15. Geological map of the Papunya gabbro and Papunya ultramafic intrusions. (from Hoatson & Stewart, 2001).

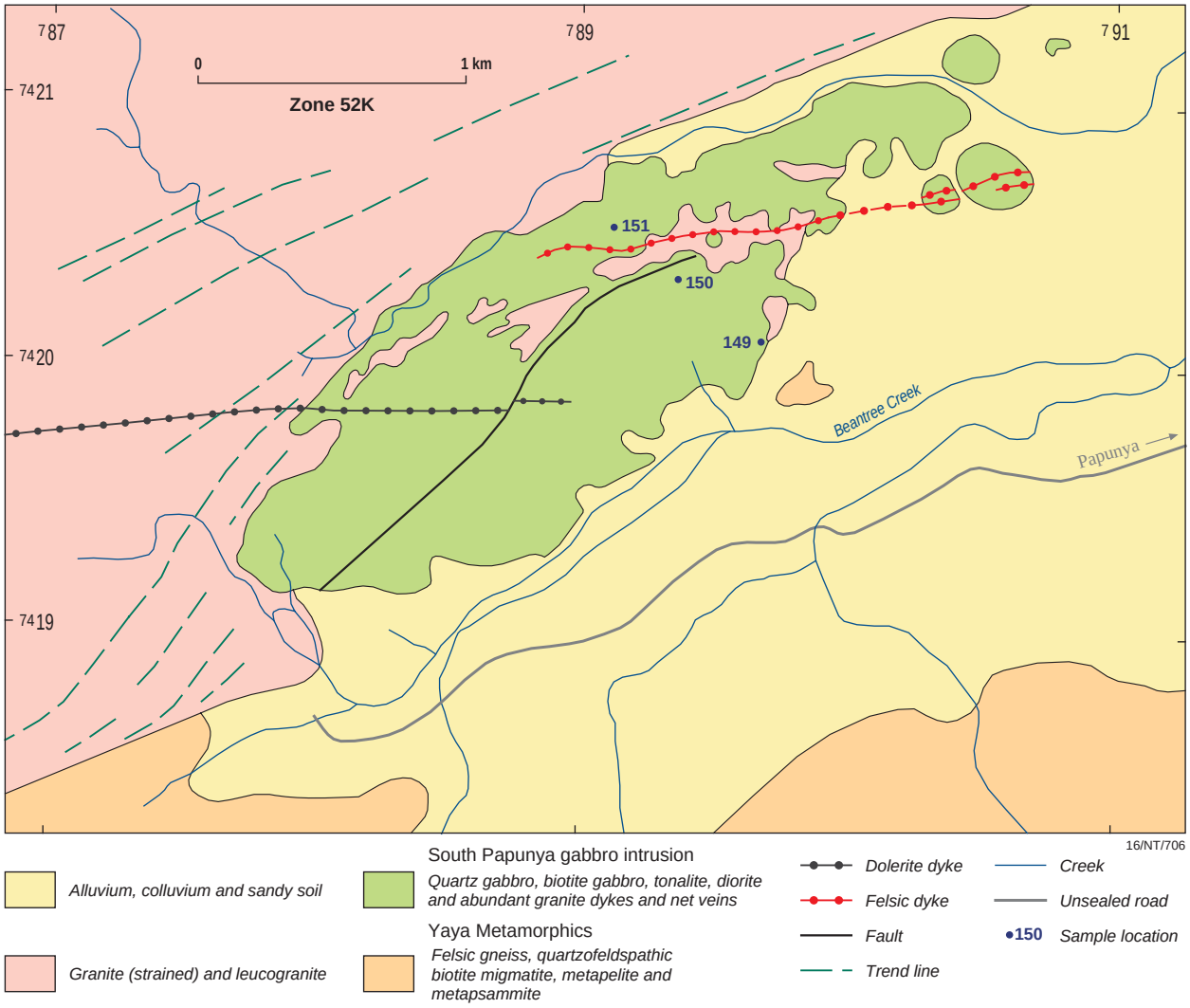

Figure 16. Geological map of the South Papunya gabbro intrusion. (from Houtson & Stewart, 2001).

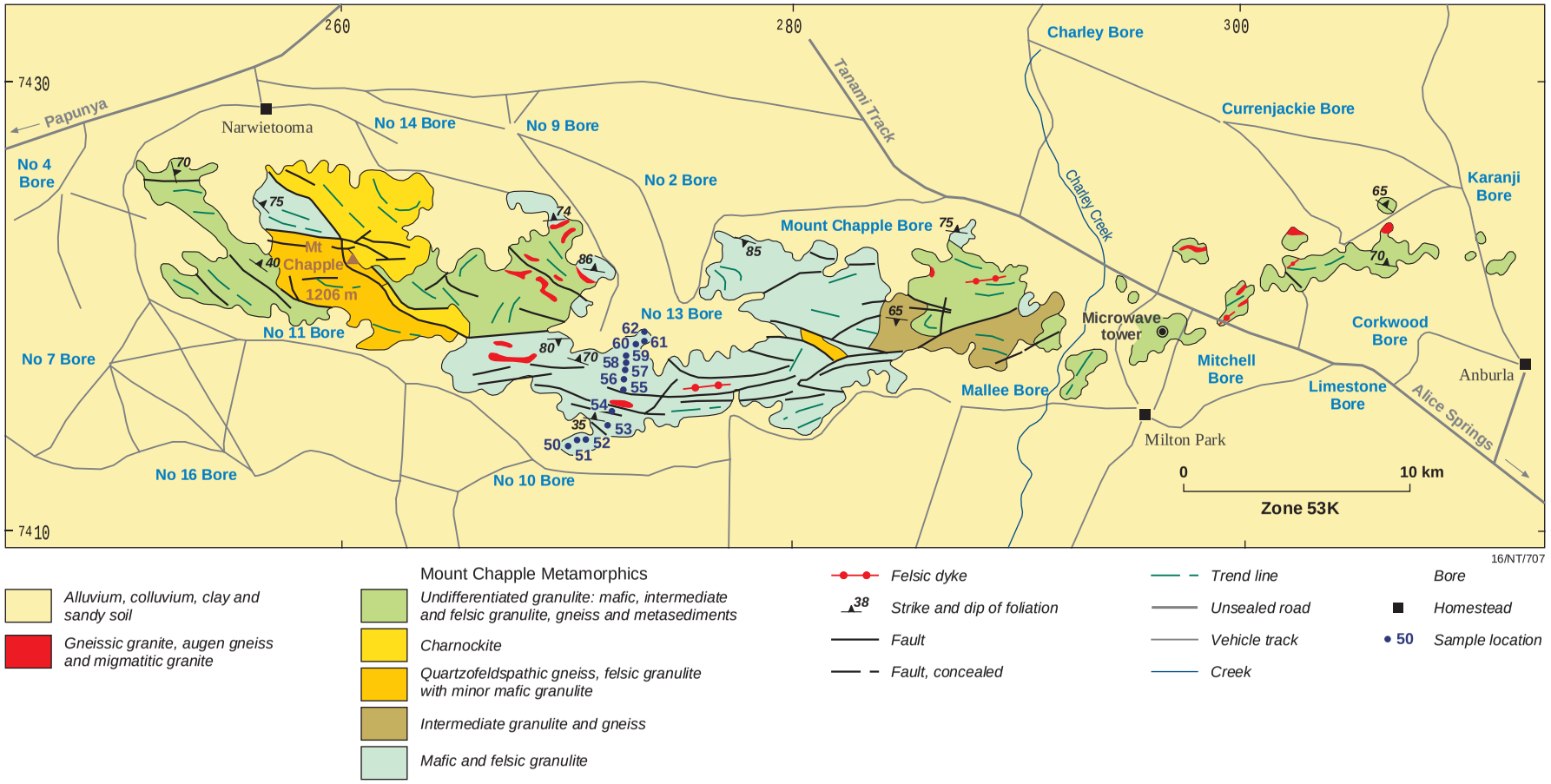

Figure 17a. Geological map of the Mount Chapple Metamorphics. (from Houtson & Stewart, 2001).

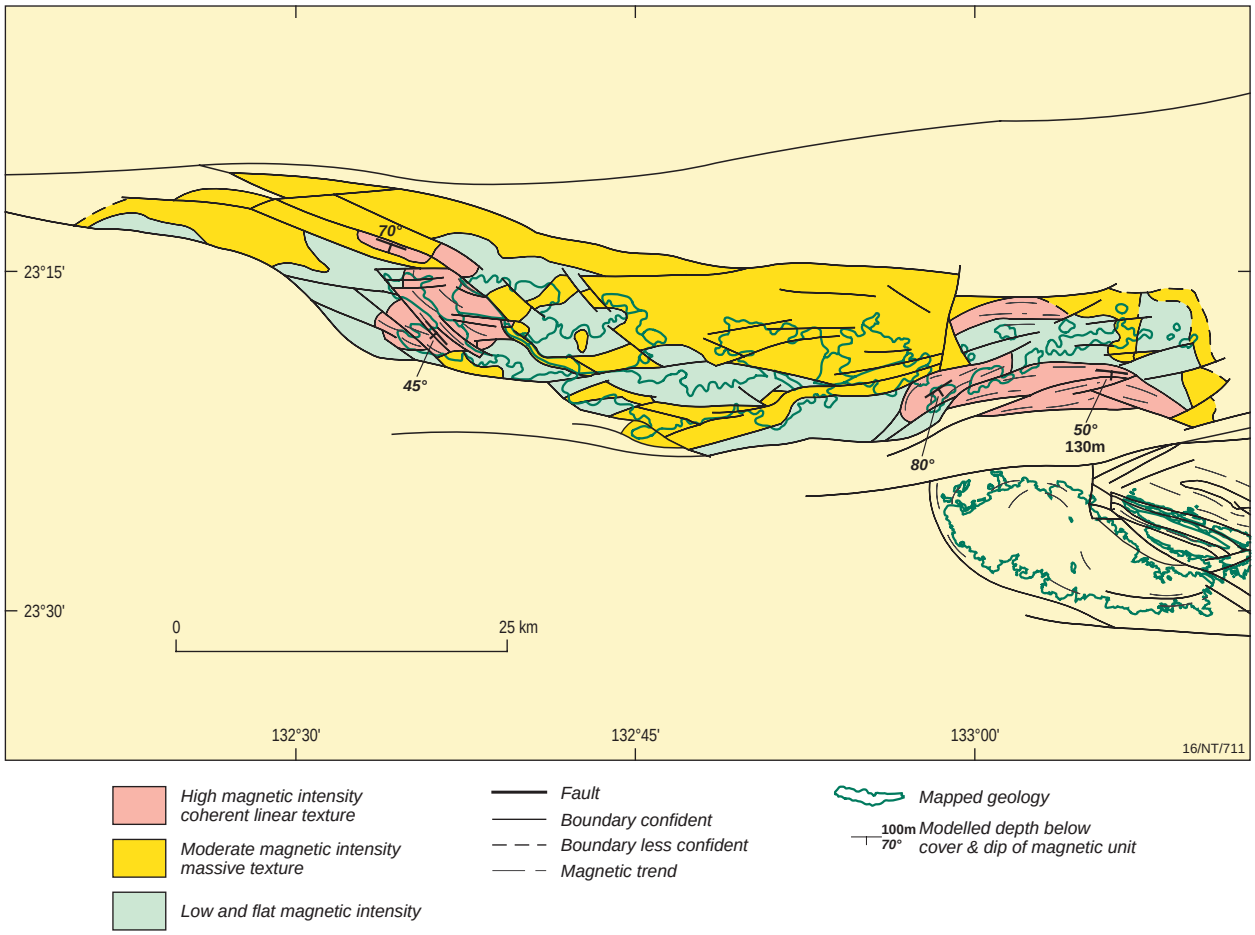

Figure 17b. Solid geology interpretation showing full extent of the intrusion, including the results of magnetic modelling defining depth of alluvial cover and dip and strike of macroscopic layering.

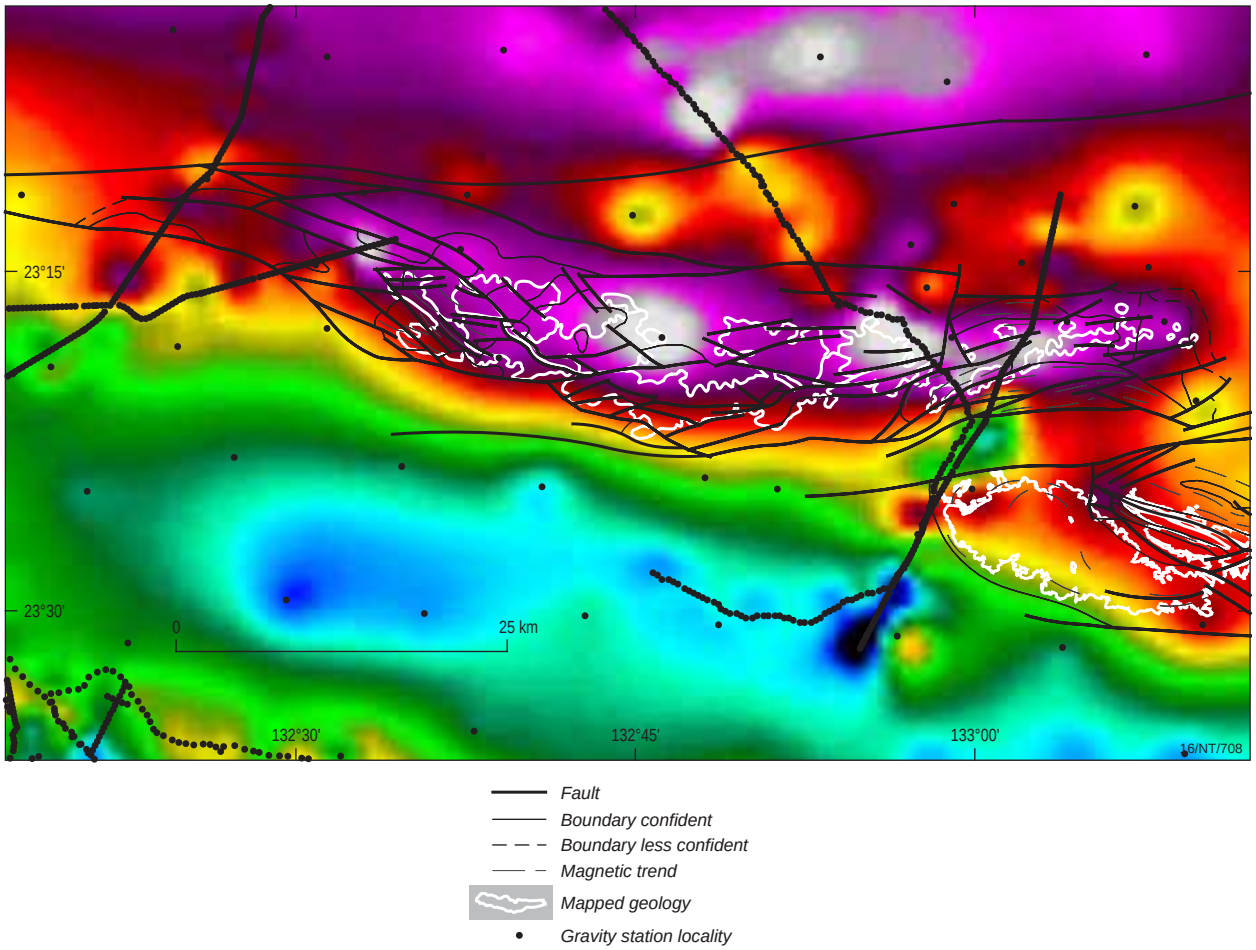

Figure 17c. Vertical gradient image of the Bouguer gravity field, including gravity station locations.

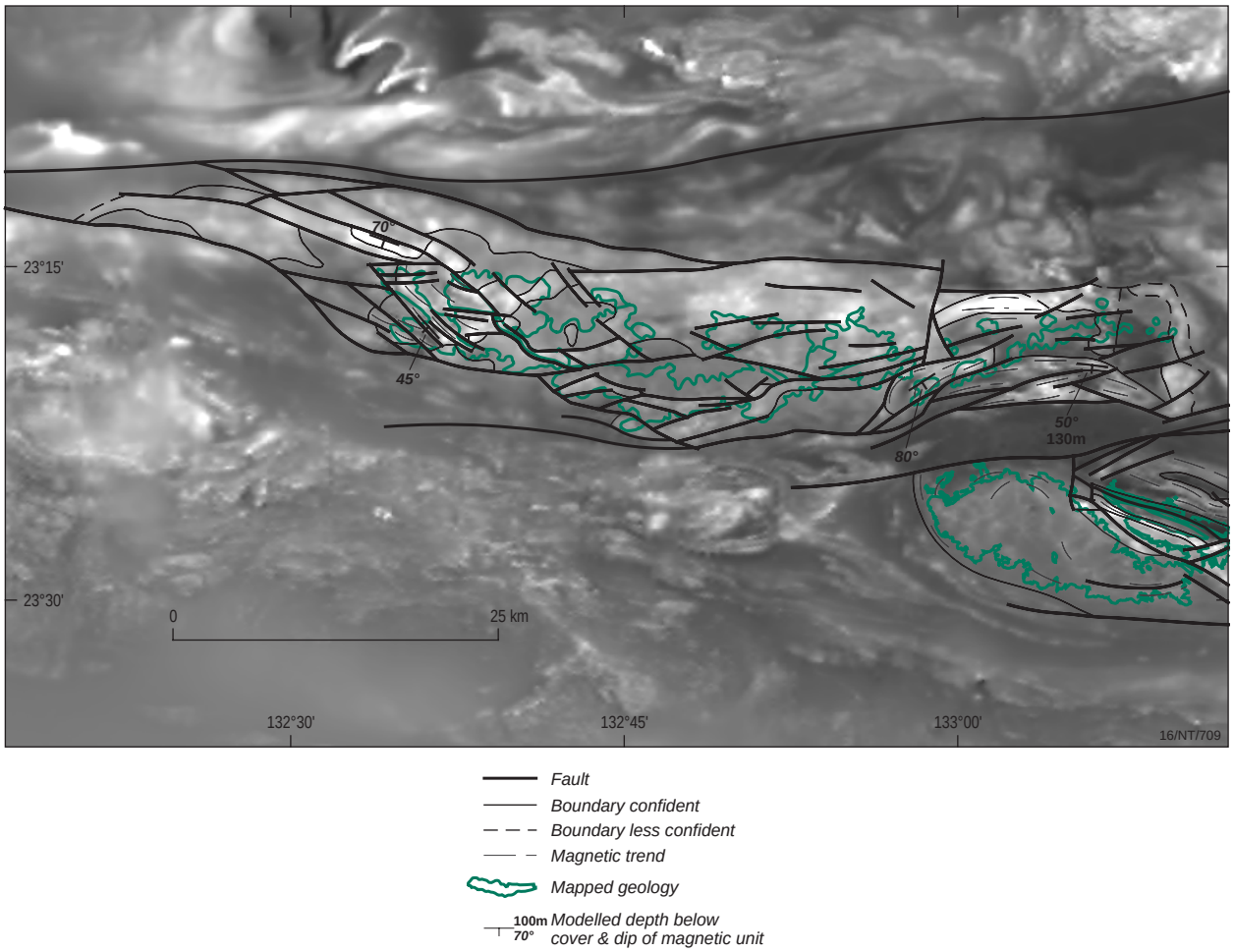

Figure 17d. Grey scale image of the total magnetic intensity - reduced to pole.

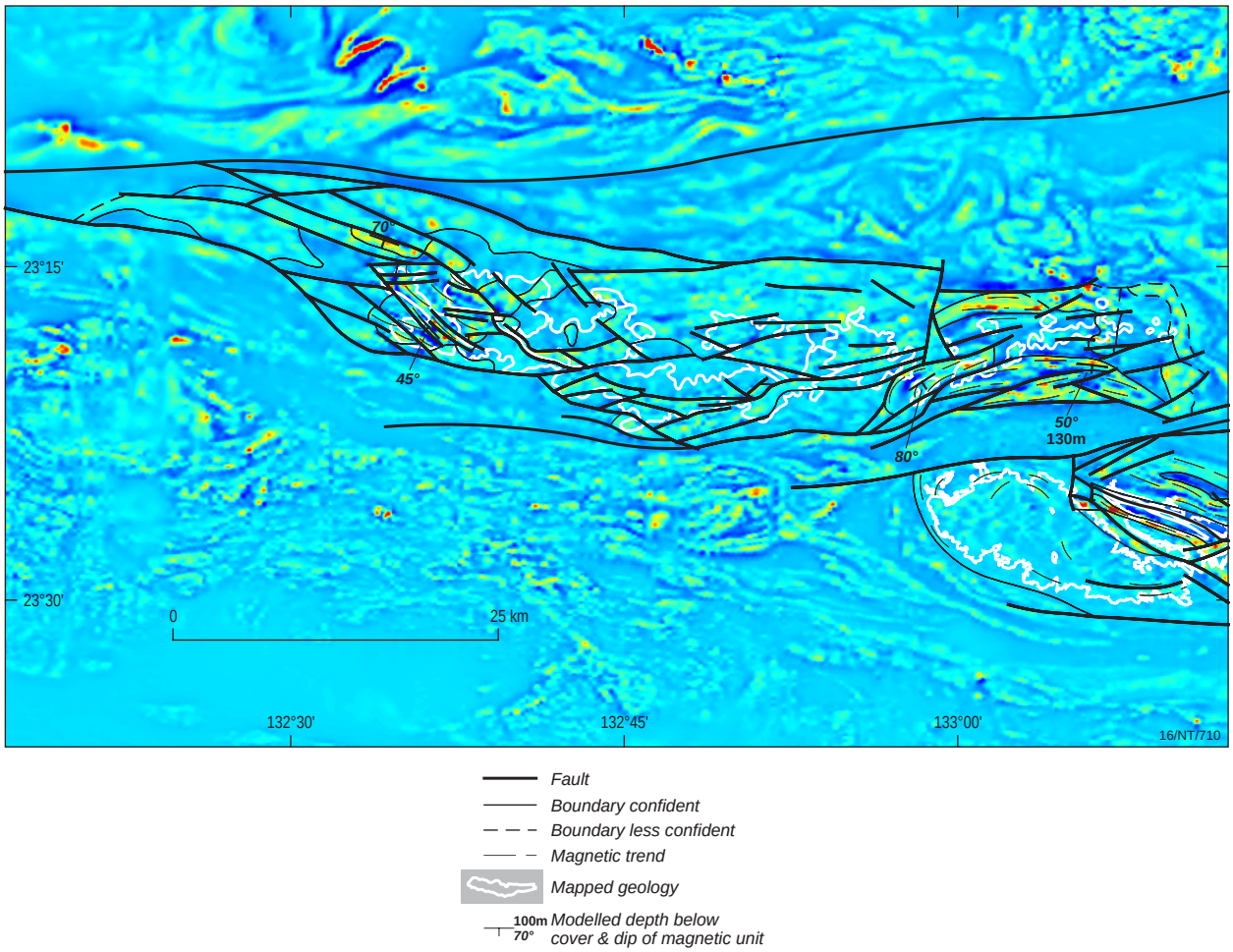

Figure 17e. Pseudo colour image of the vertical gradient applied to the total magnetic intensity (reduced to pole).

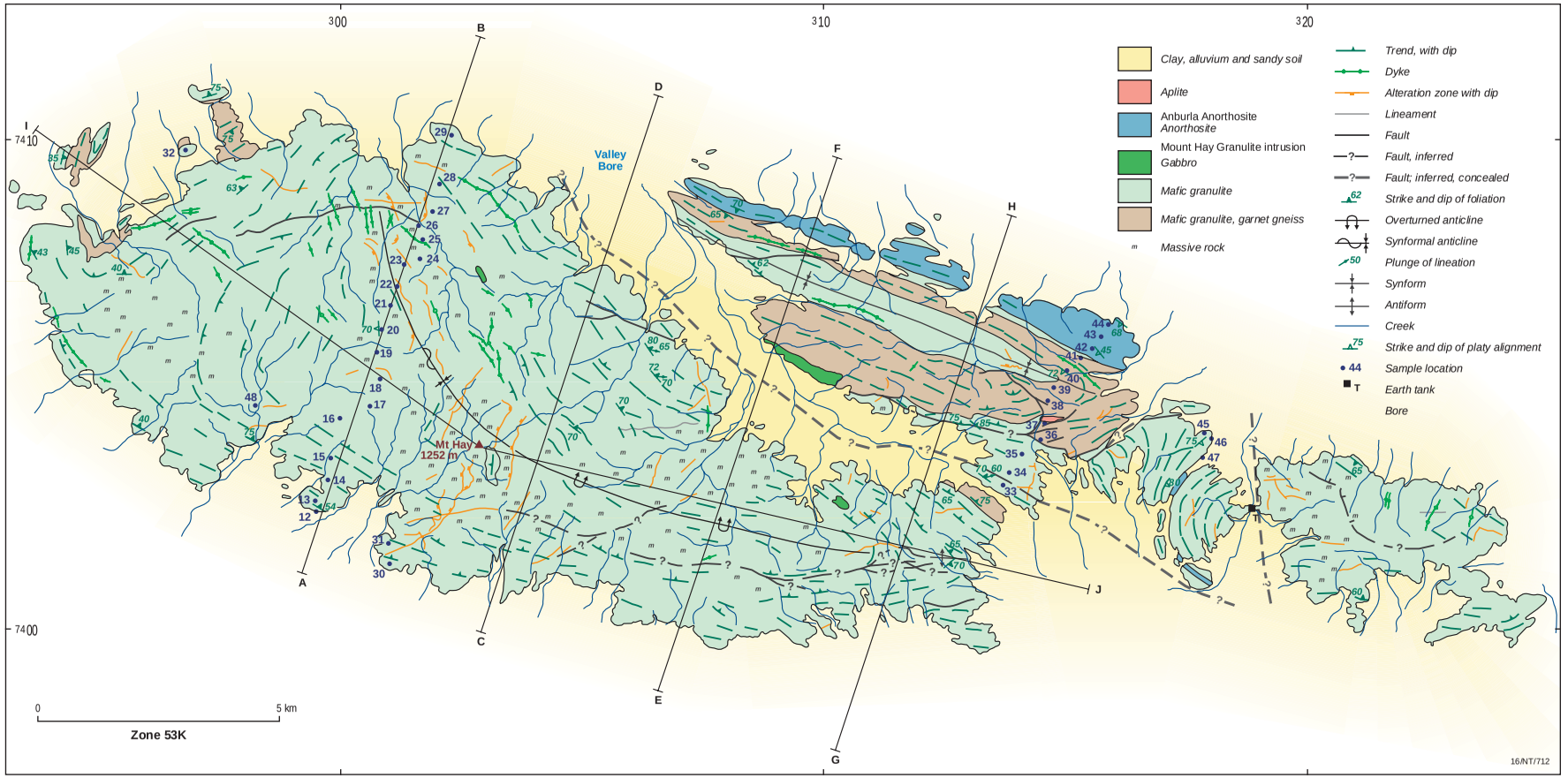

Figure 18a. Geological map of the Mount Hay Granulite and Anburla Anorthosite mafic intrusions (modified after Glikson et al., 1983 and Shaw et al., 1995).

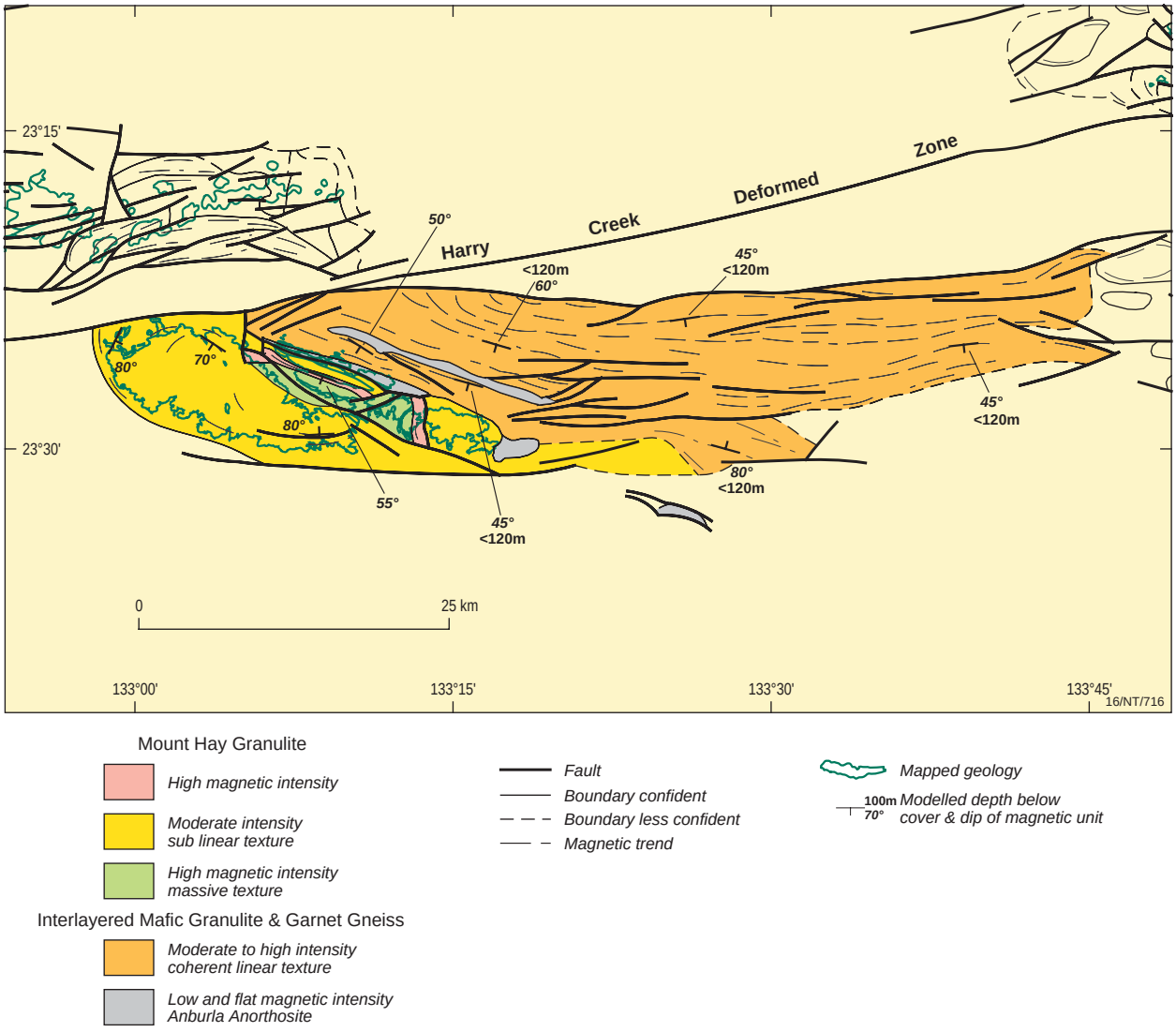

Figure 18b. Solid geology interpretation showing the full extent of the Mount Hay Granulite, the extent of mapped and inferred Anburla Anorthosite, and the interpreted eastern extent of the interlayered mafic granulite and garnet gneiss. The results of magnetic modelling defining depth of alluvial cover and dip and strike of macroscopic layering is also shown.

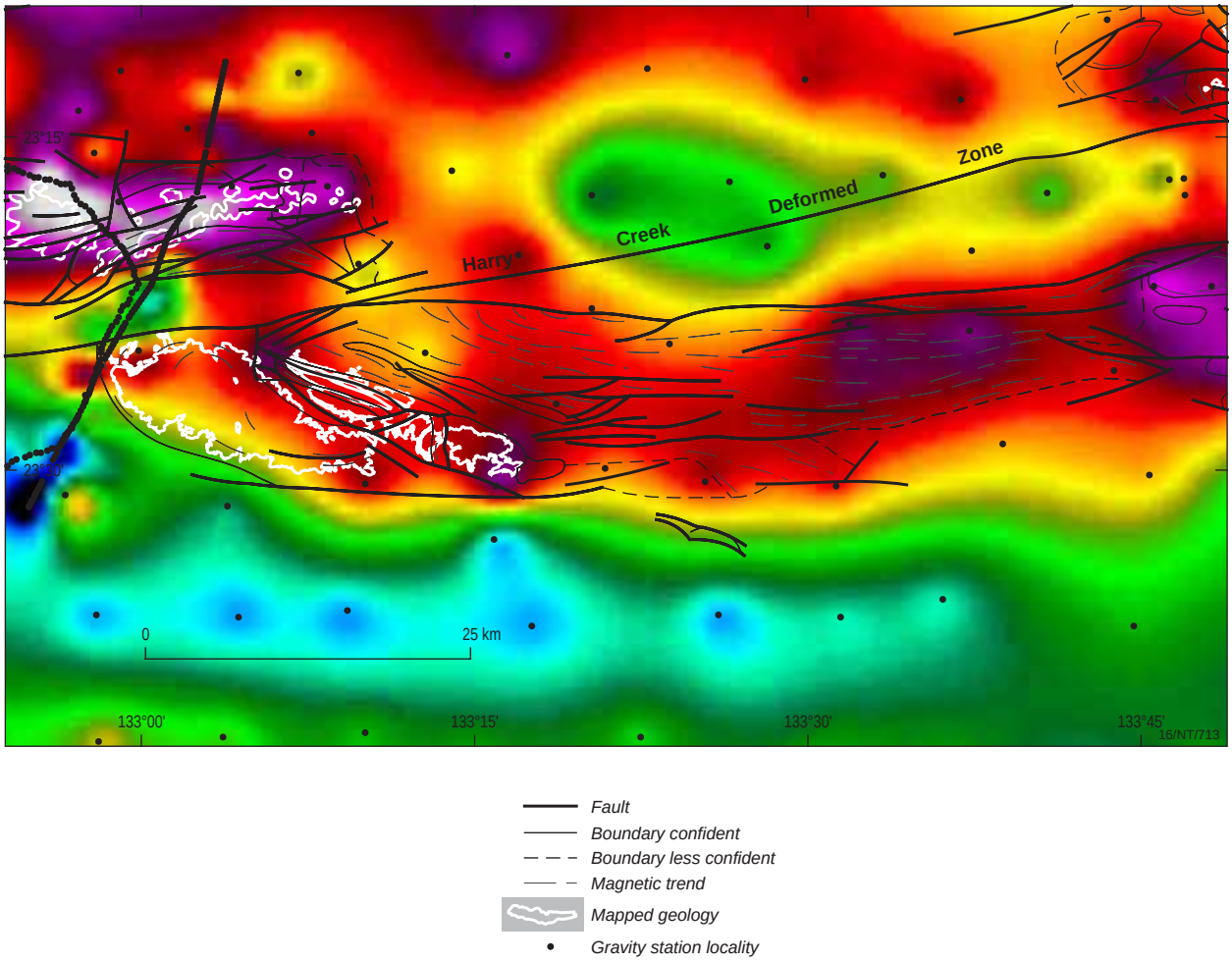

Figure 18c. Vertical gradient image of the Bouguer gravity field, including gravity station locations.

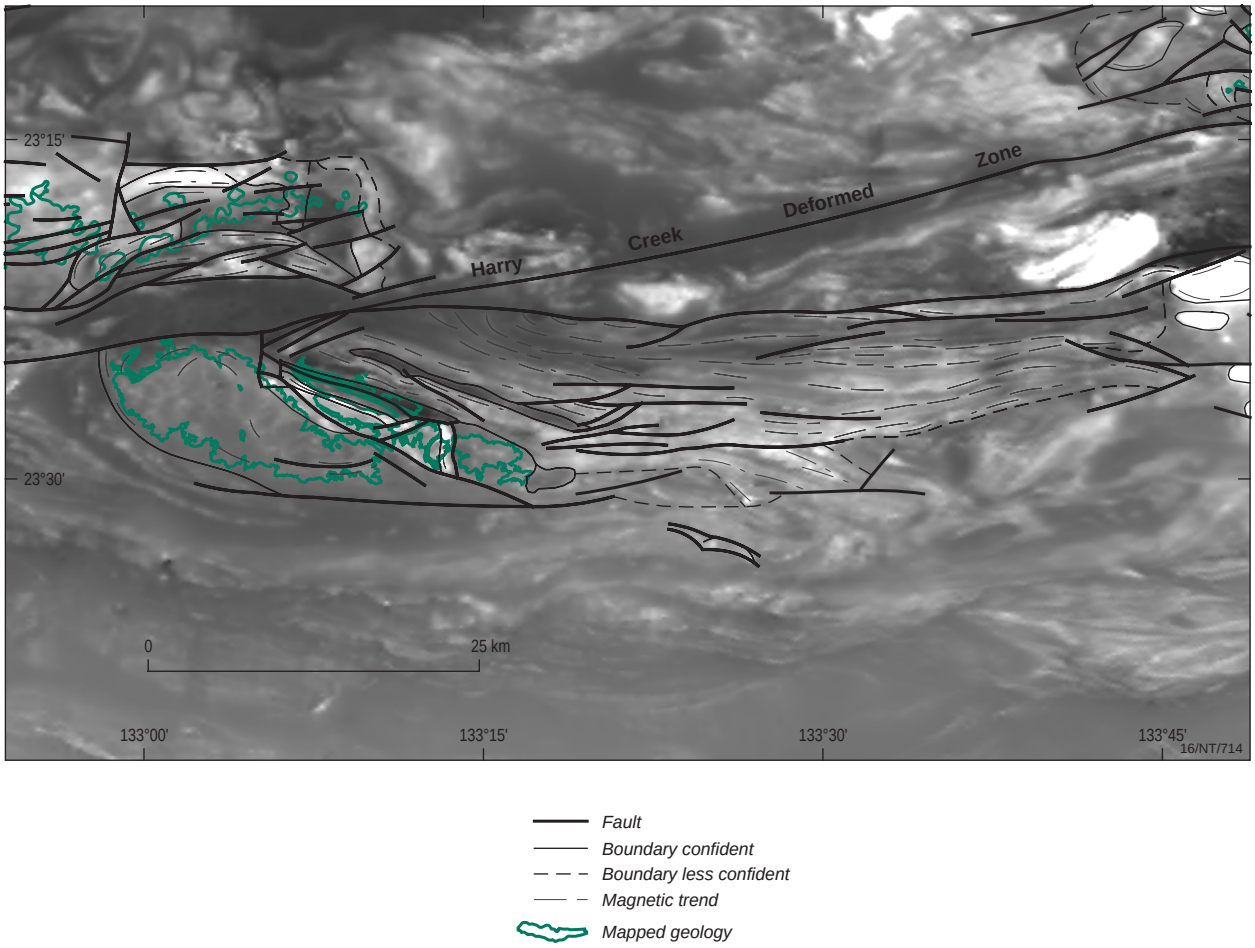

Figure 18d. Grey scale image of the total magnetic intensity - reduced to pole.

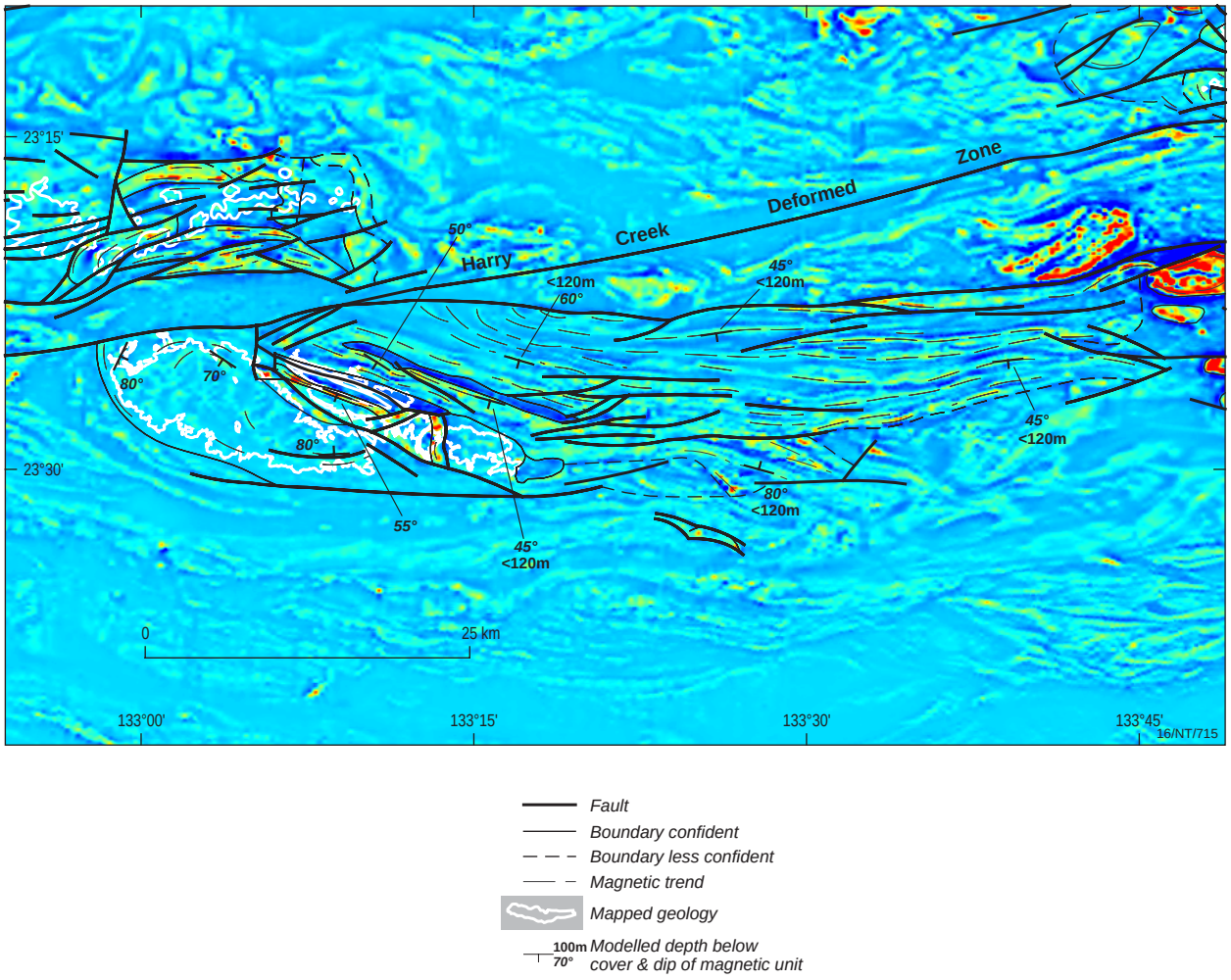

Figure 18e. Pseudo colour image of the vertical gradient applied to the total magnetic intensity (reduced to pole).

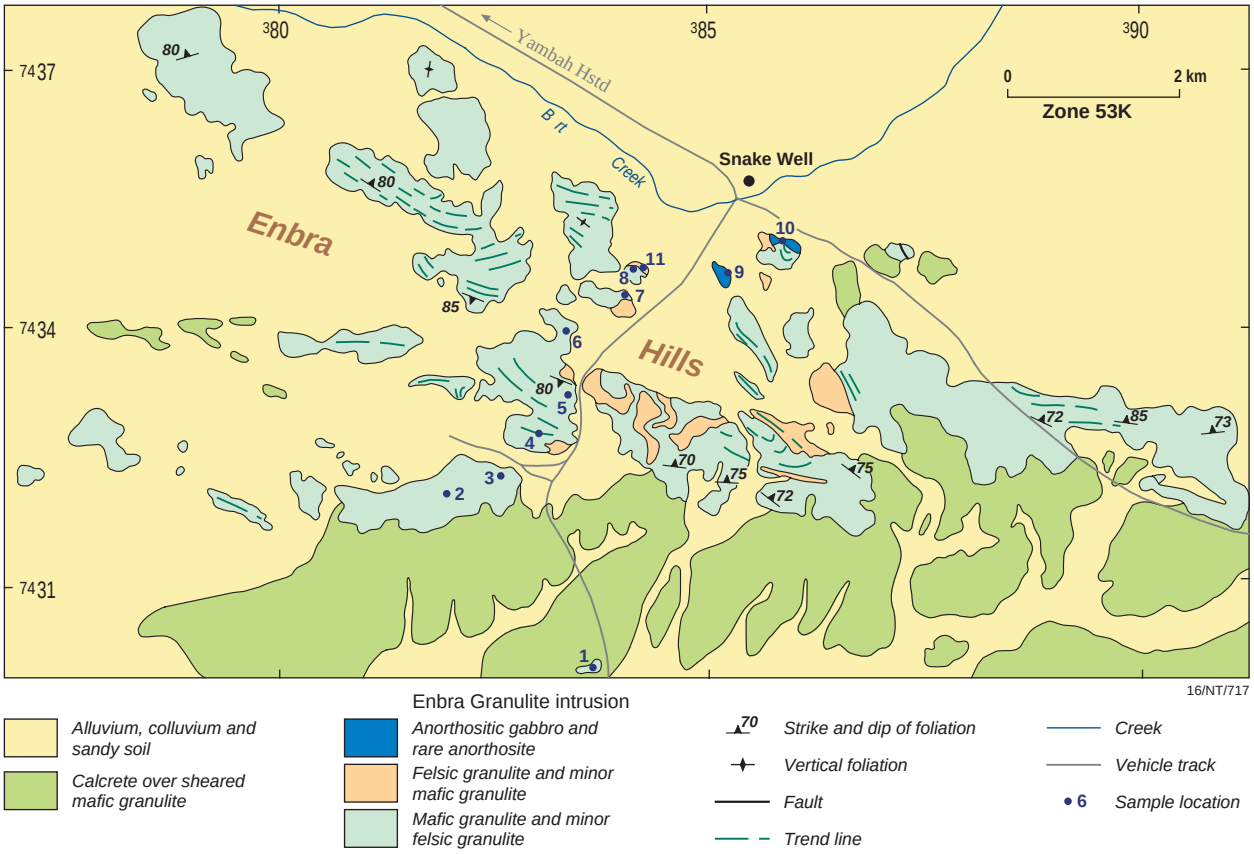

Figure 19a. Geological map of the Enbra Granulite intrusion (modified after Shaw et al., 1983).

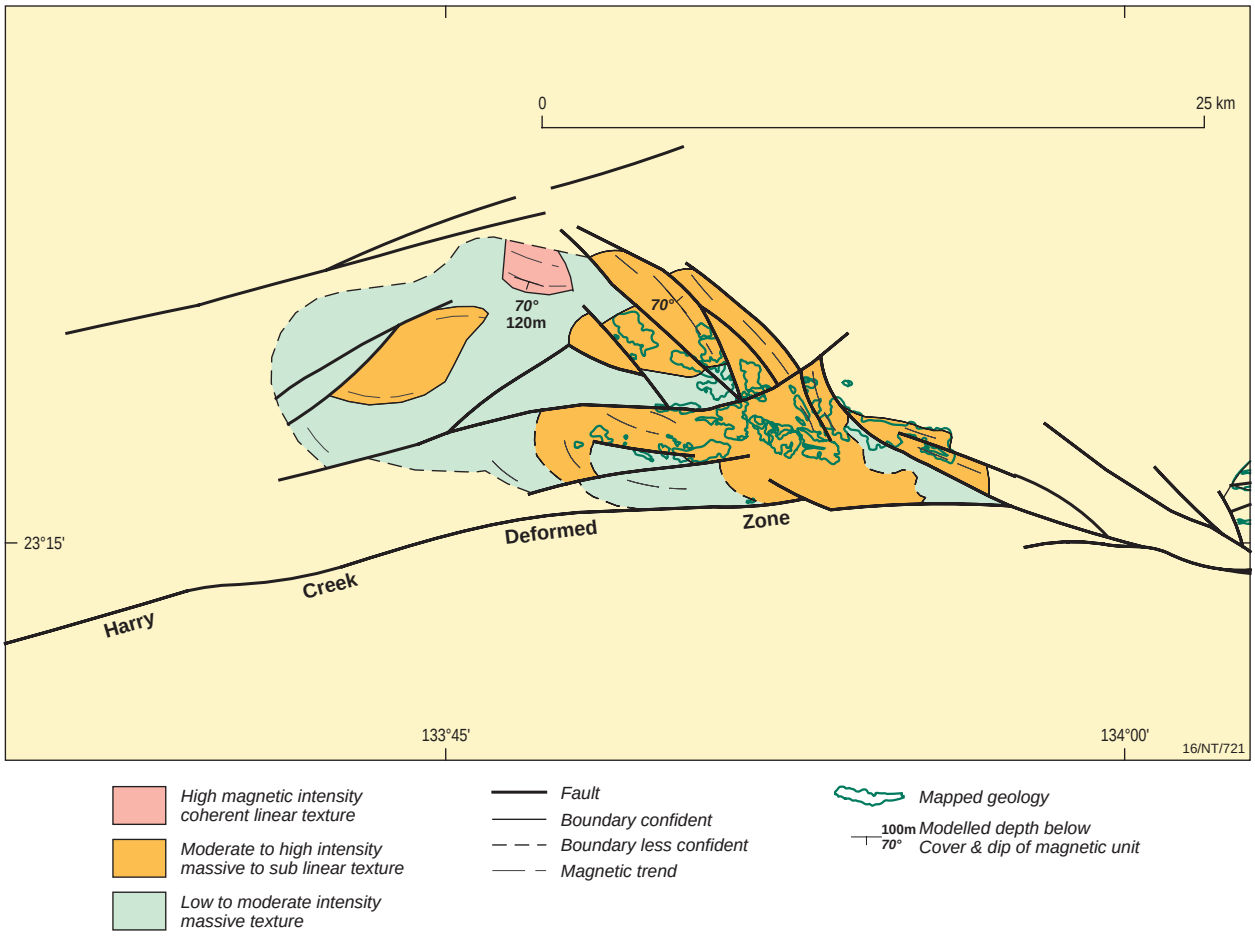

Figure 19b. Solid geology interpretation showing the full extent of the Enbra Granulite. The results of magnetic modelling defining depth of alluvial cover and dip and strike of macroscopic layering is also shown.

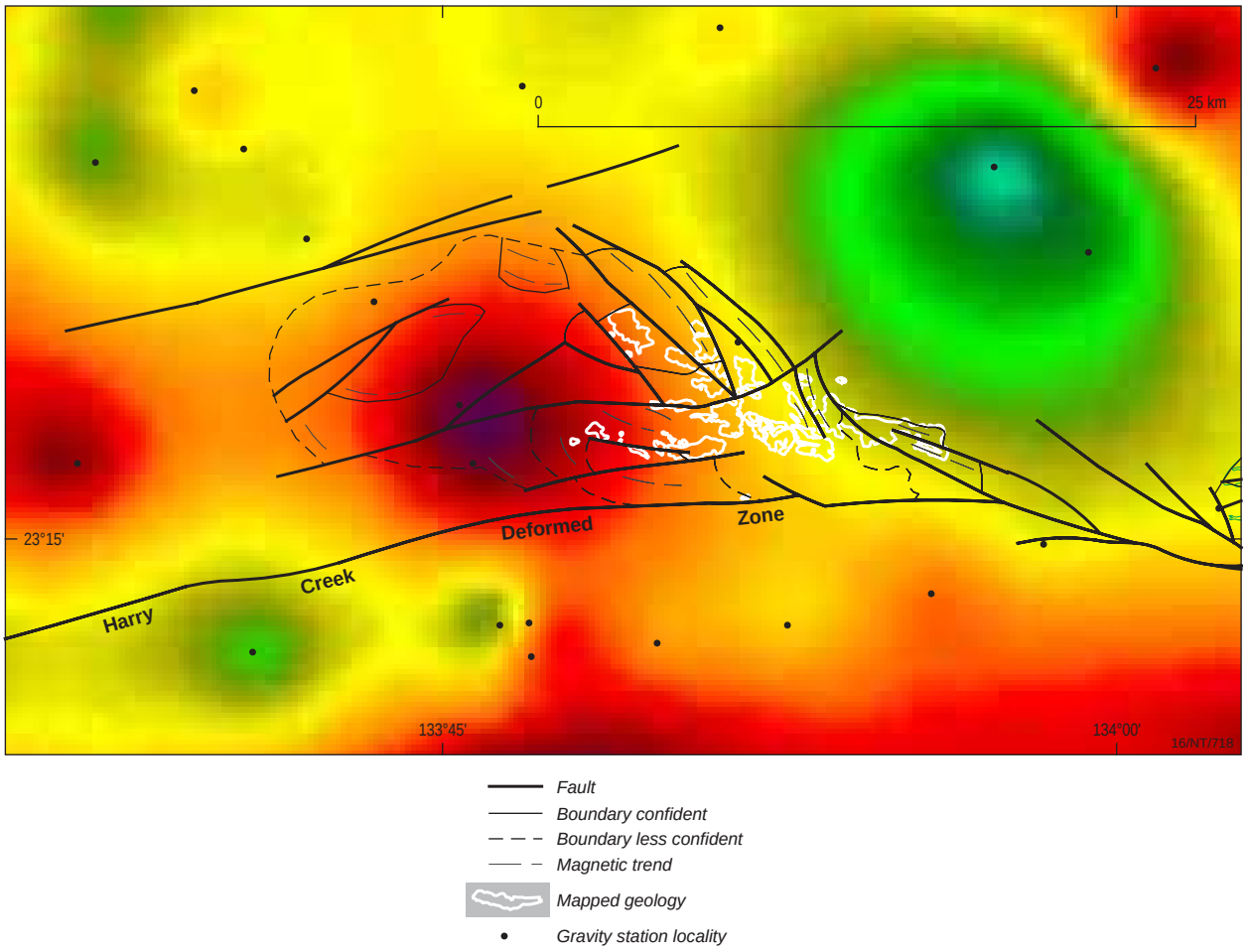

Figure 19c. Vertical gradient image of the Bouguer gravity field, including gravity station locations.

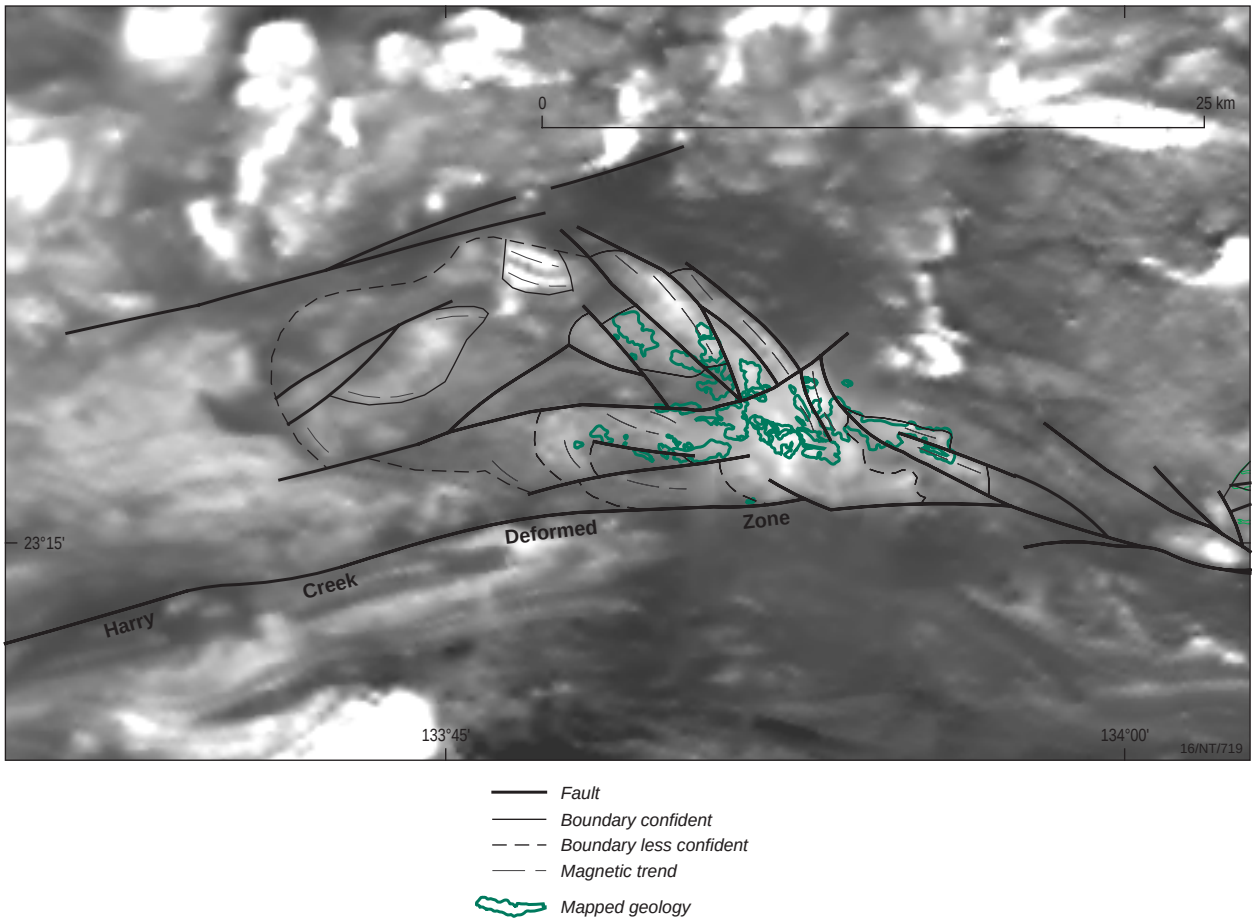

Figure 19d. Grey scale image of the total magnetic intensity - reduced to pole.

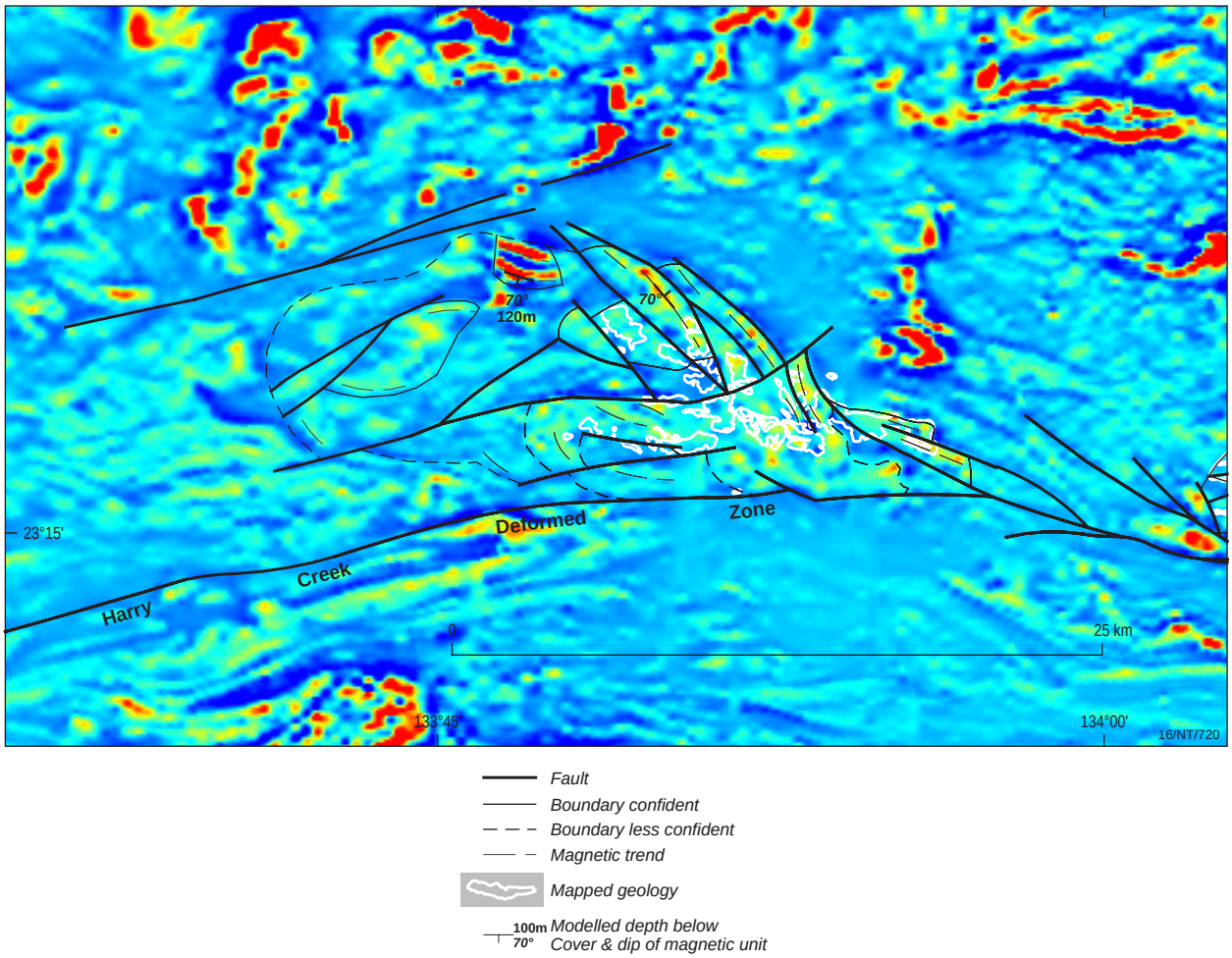

Figure 19e. Pseudo colour image of the vertical gradient applied to the total magnetic intensity (reduced to pole).

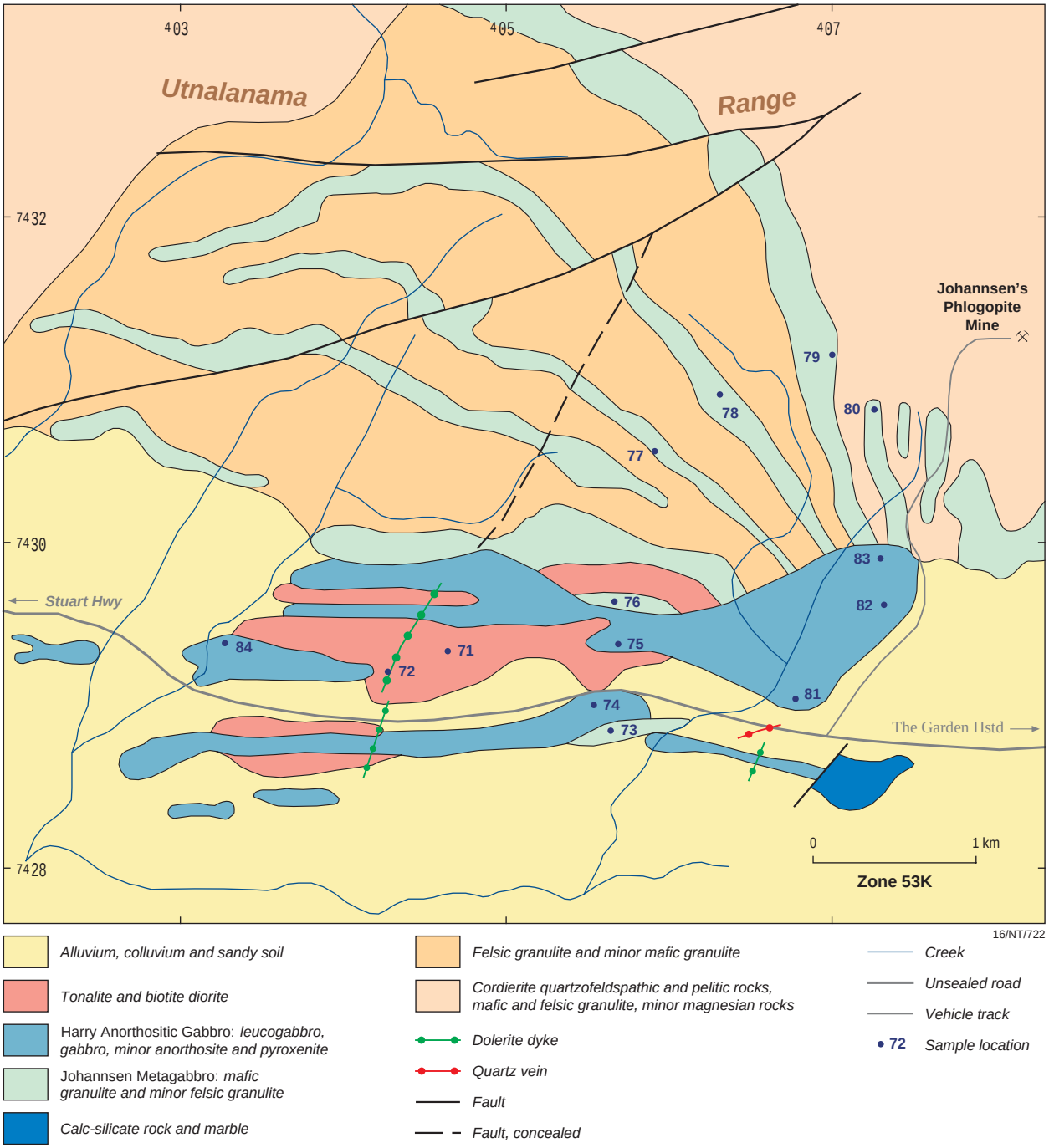

Figure 20a. Geological map of the Harry Anorthositic Gabbro and Johannsen Metagabbro intrusions (modified after Shaw et al., 1983).

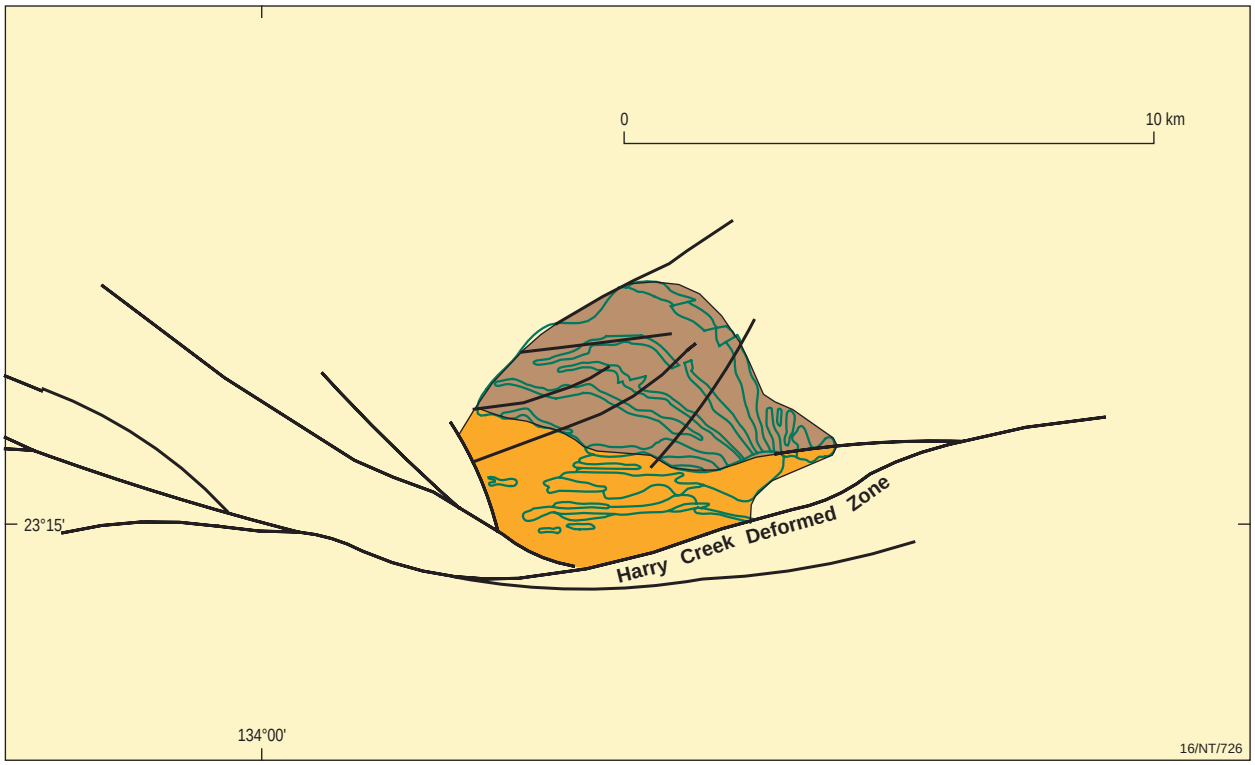

Figure 20b. Solid geology interpretation showing the full sub-cropping extent of the Harry Anorthositic Gabbro.

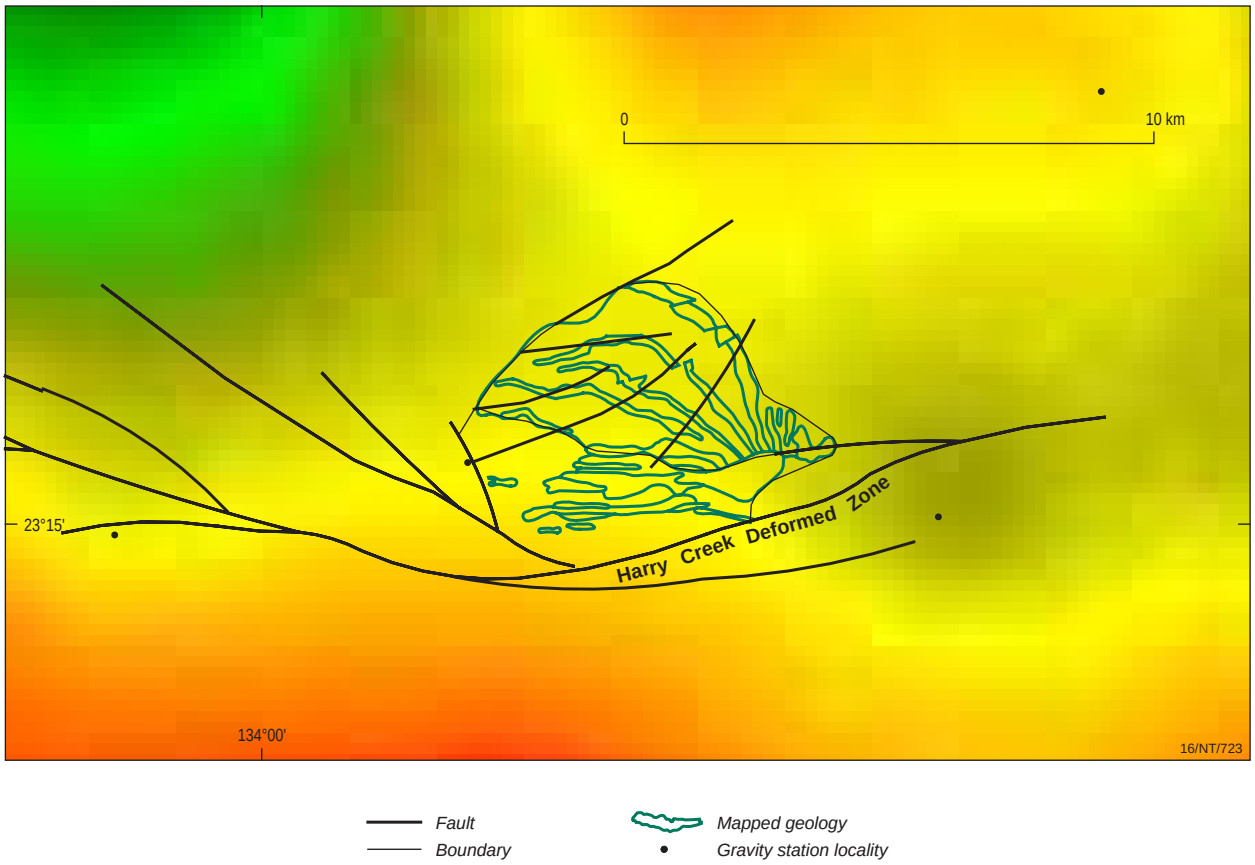

Figure 20c. Vertical gradient image of the Bouguer gravity field, including gravity station locations.

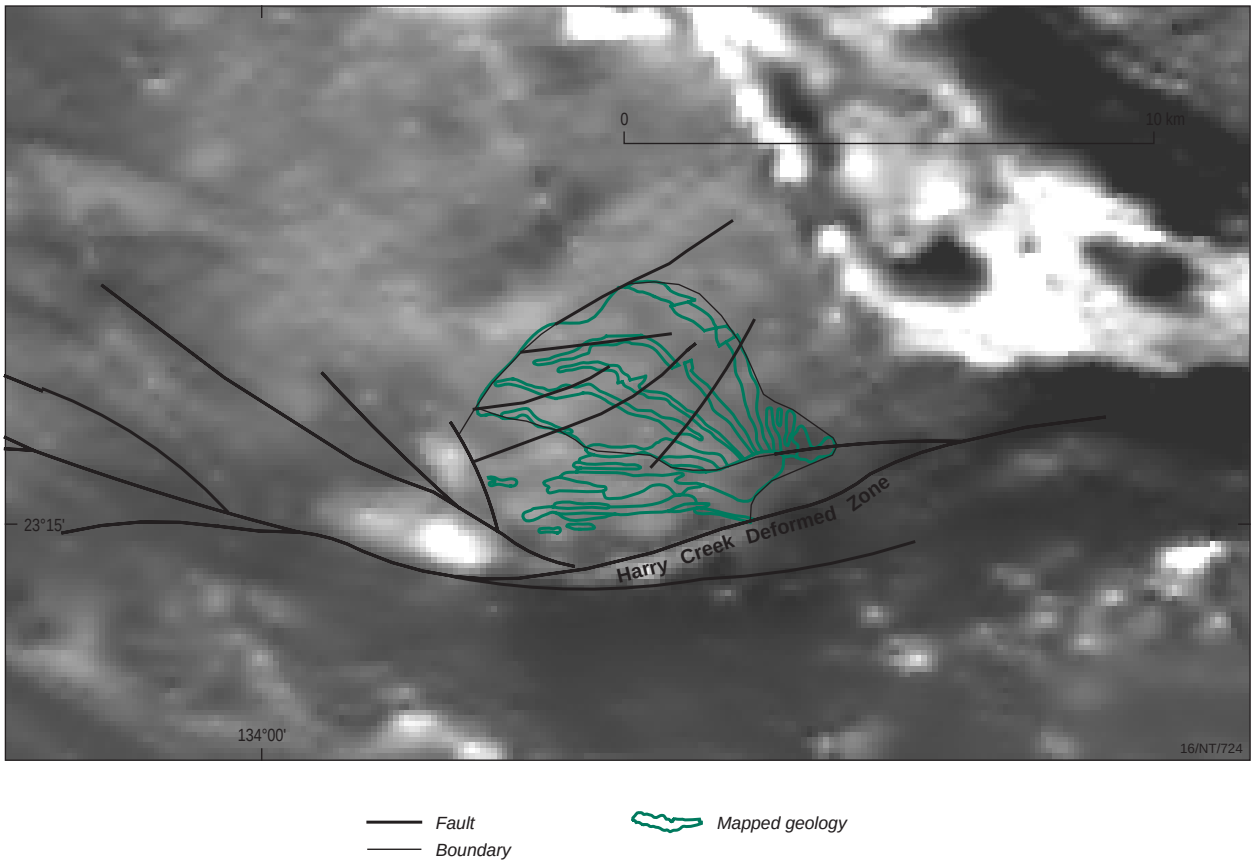

Figure 20d. Grey scale image of the total magnetic intensity - reduced to pole.

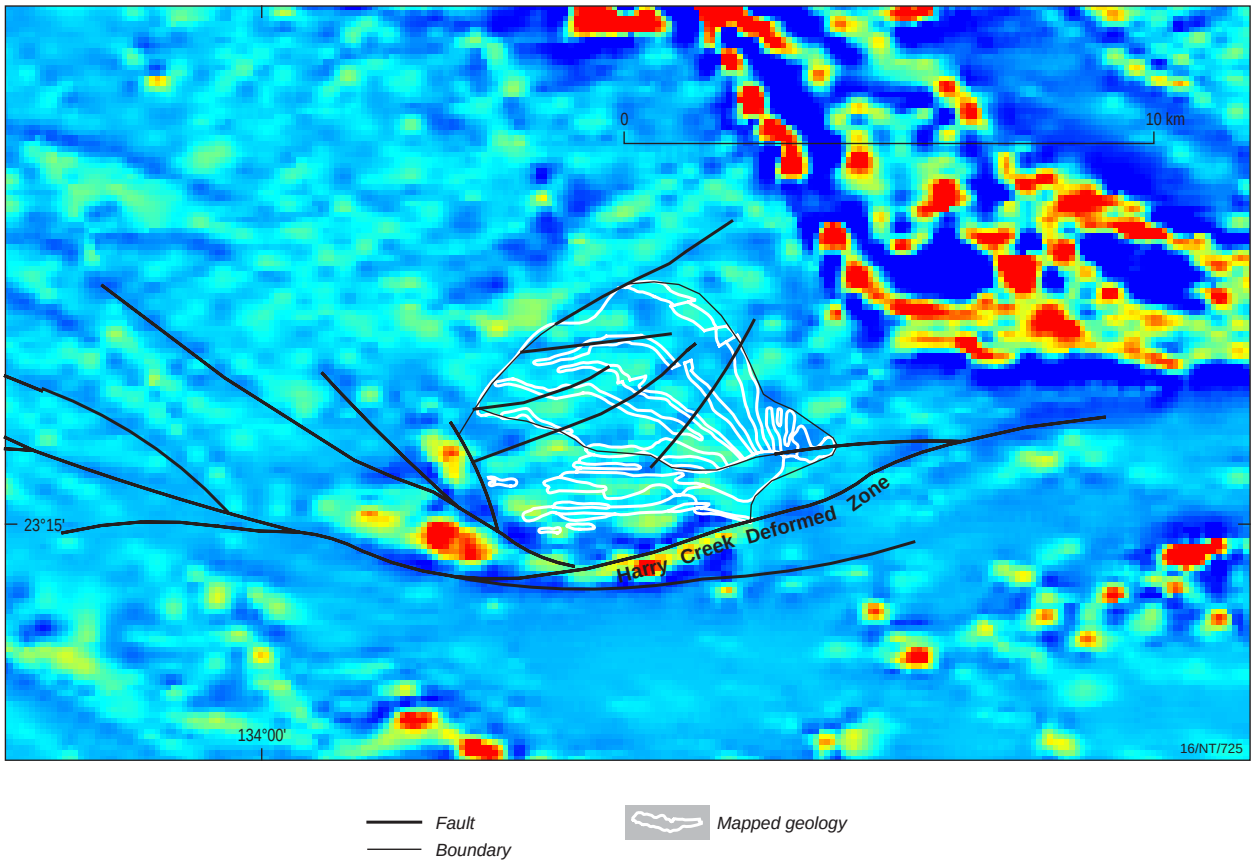

Figure 20e. Pseudo colour image of the vertical gradient applied to the total magnetic intensity (reduced to pole).

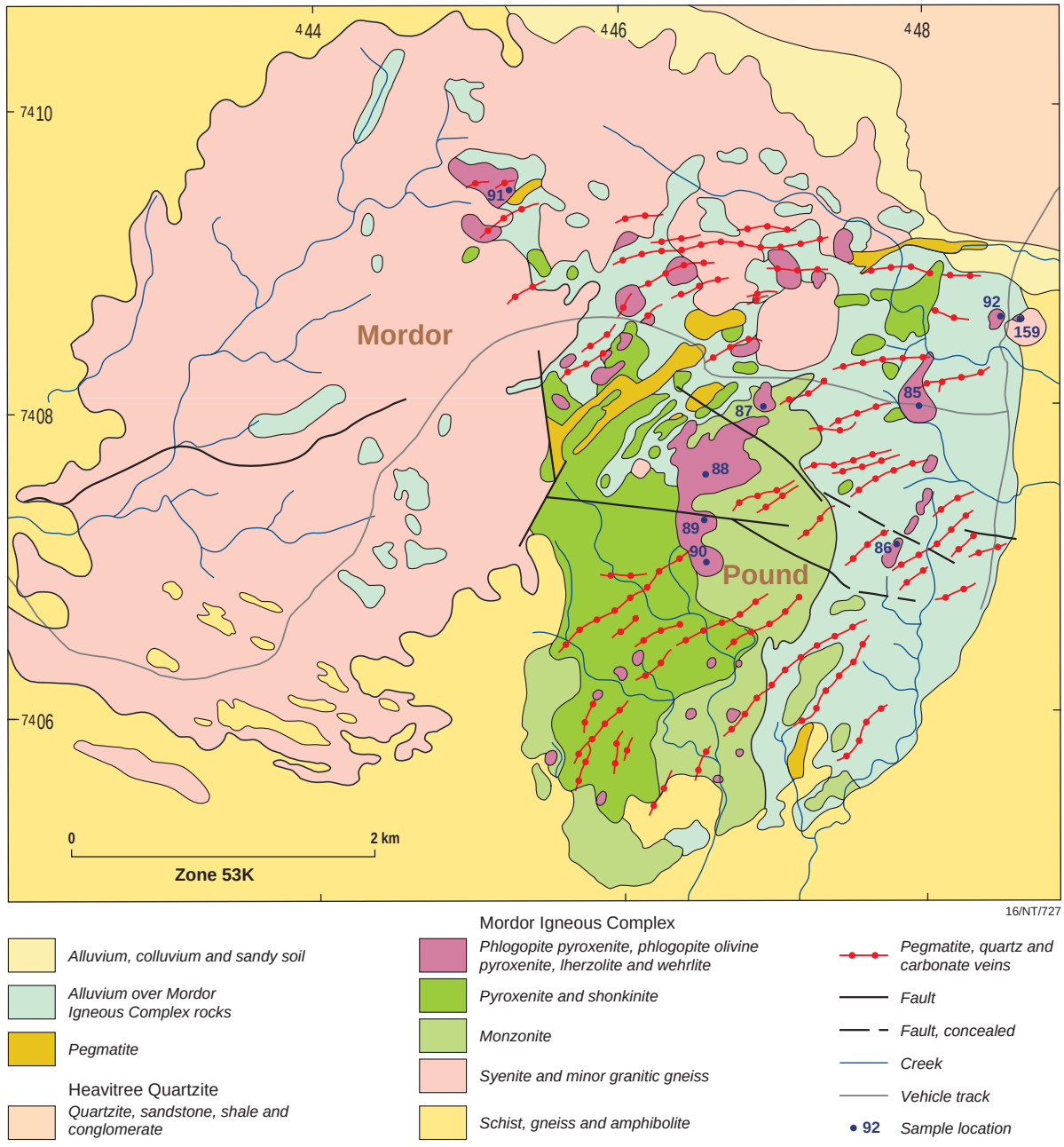

Figure 21a. Geological map of the Mordor Complex (modified after Langworthy & Black, 1978).

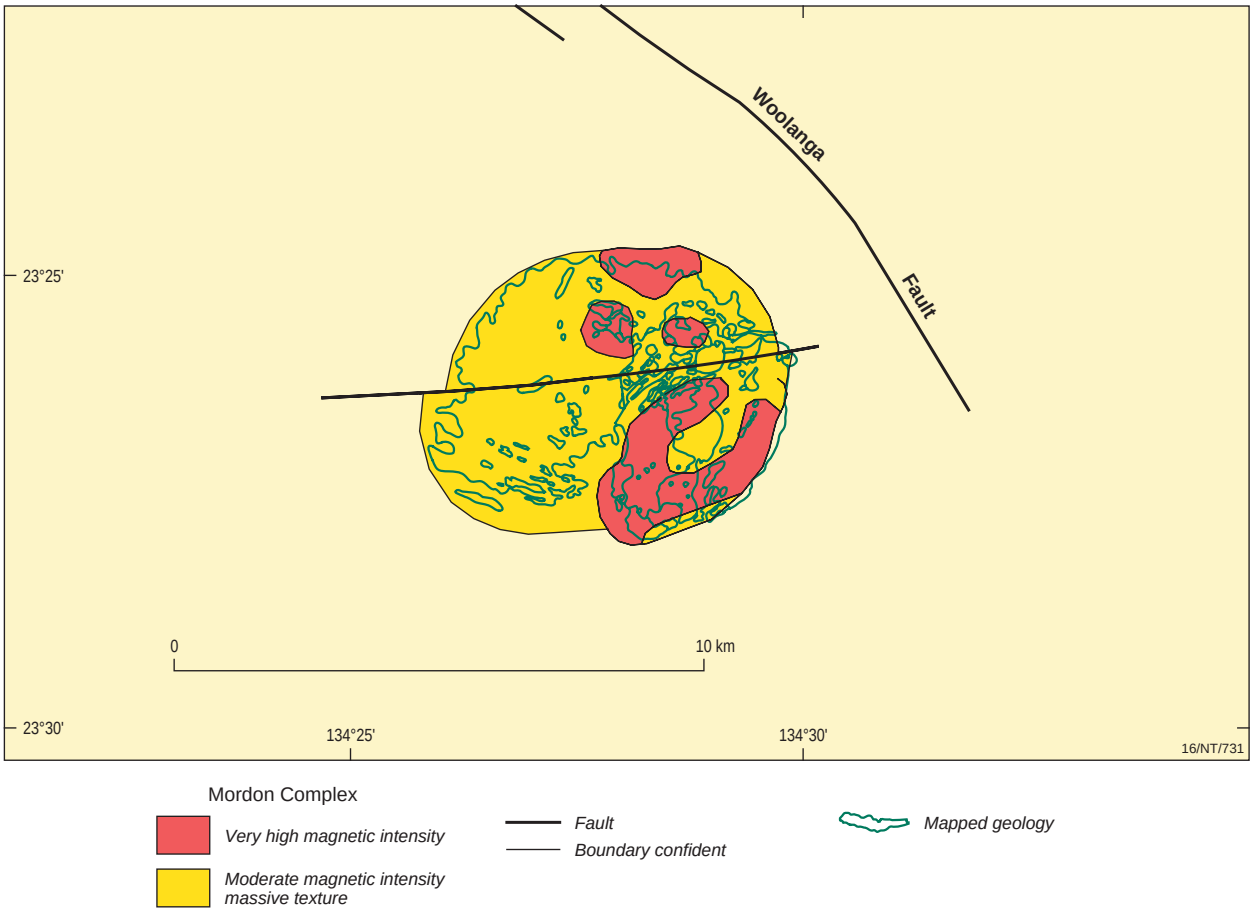

Figure 21b. Solid geology interpretation of the Mordor Complex.

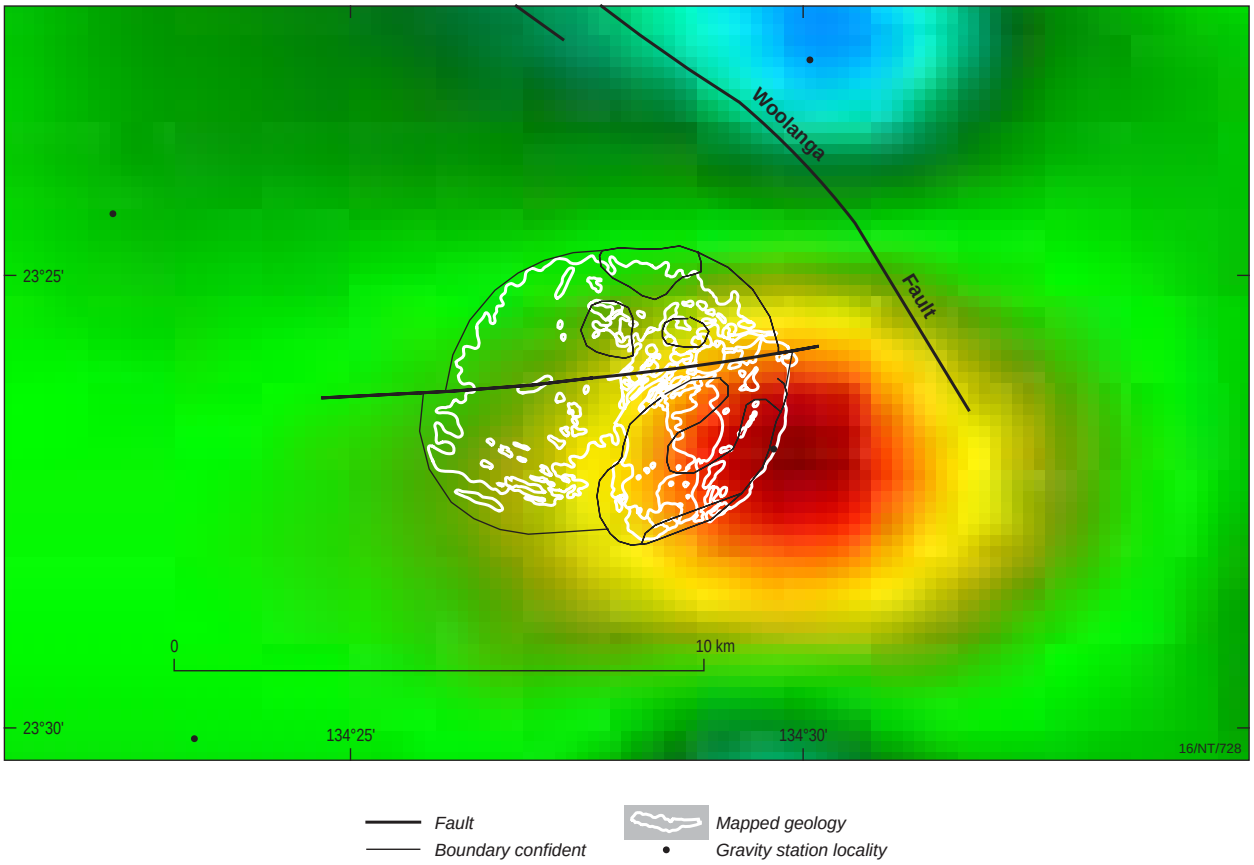

Figure 21c. Vertical gradient image of the Bouguer gravity field, including gravity station locations.

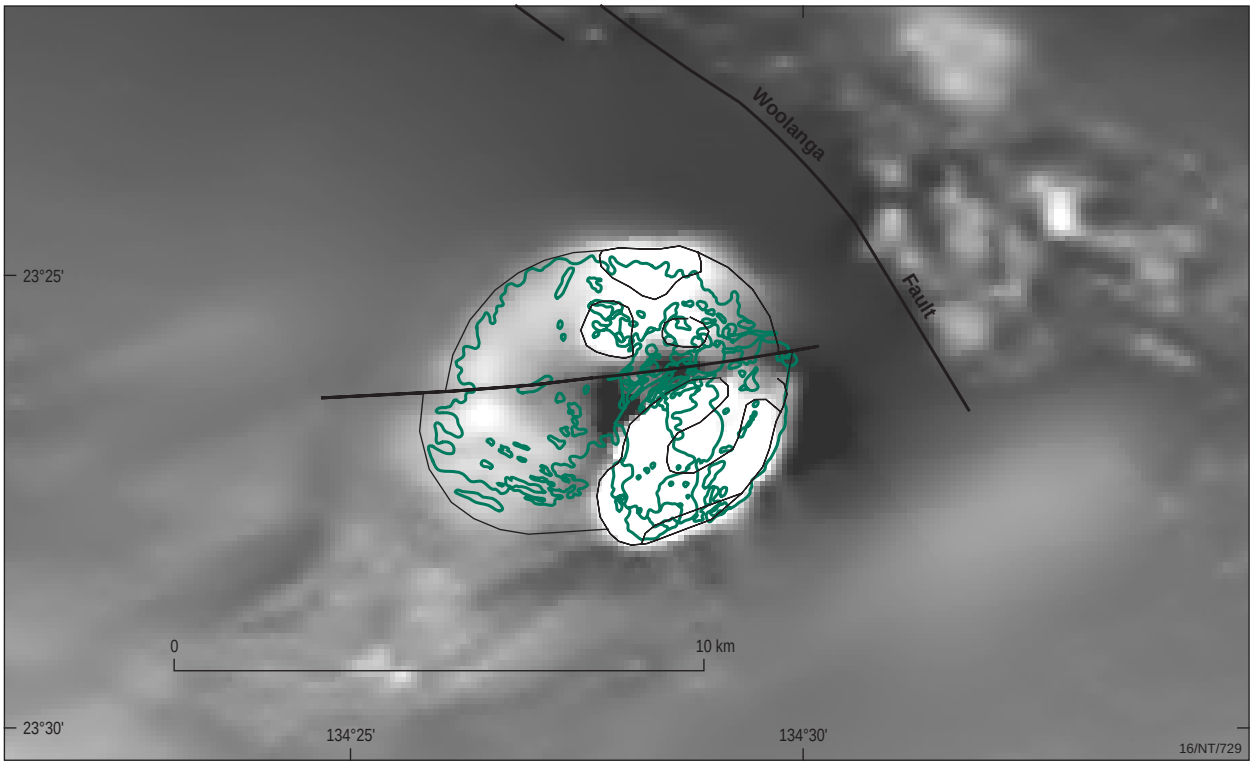

Figure 21d. Grey scale image of the total magnetic intensity - reduced to pole.

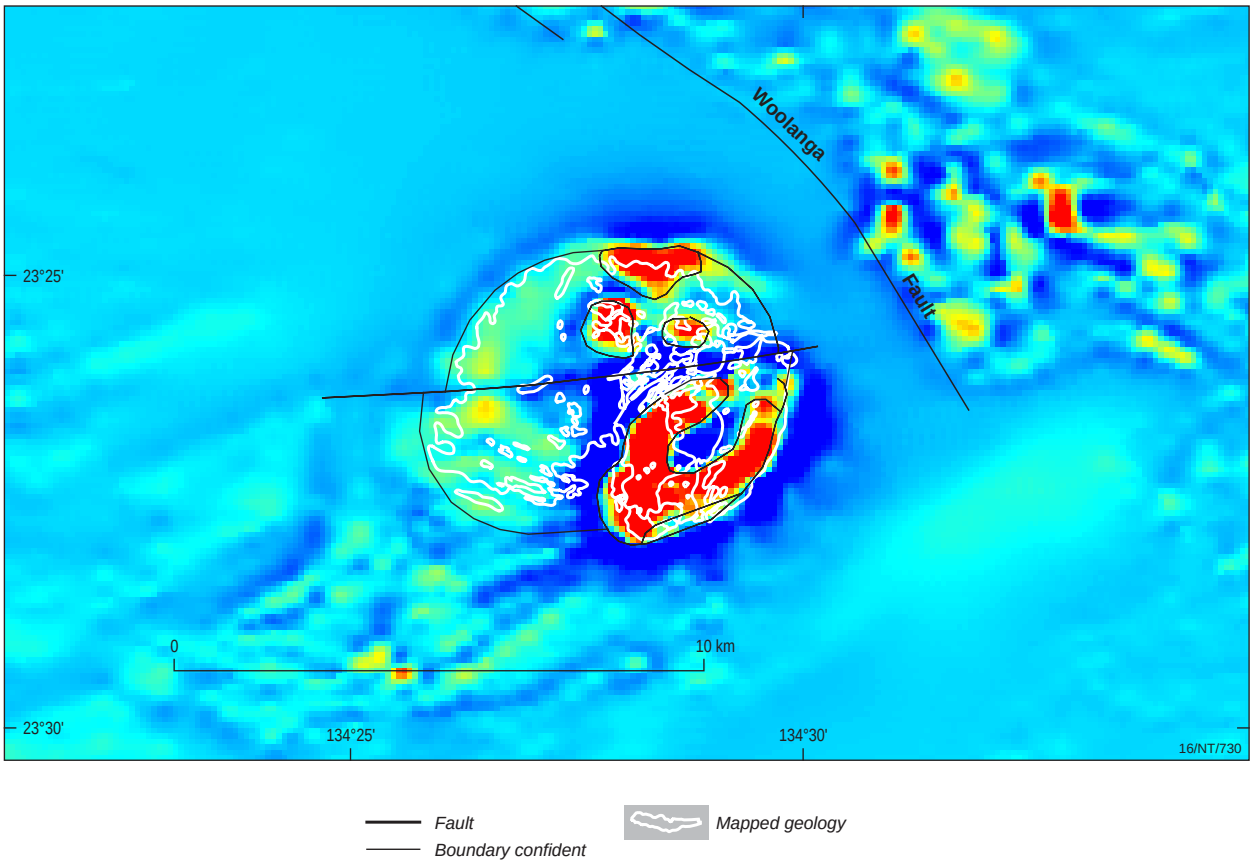

Figure 21e. Pseudo colour image of the vertical gradient applied to the total magnetic intensity (reduced to pole).

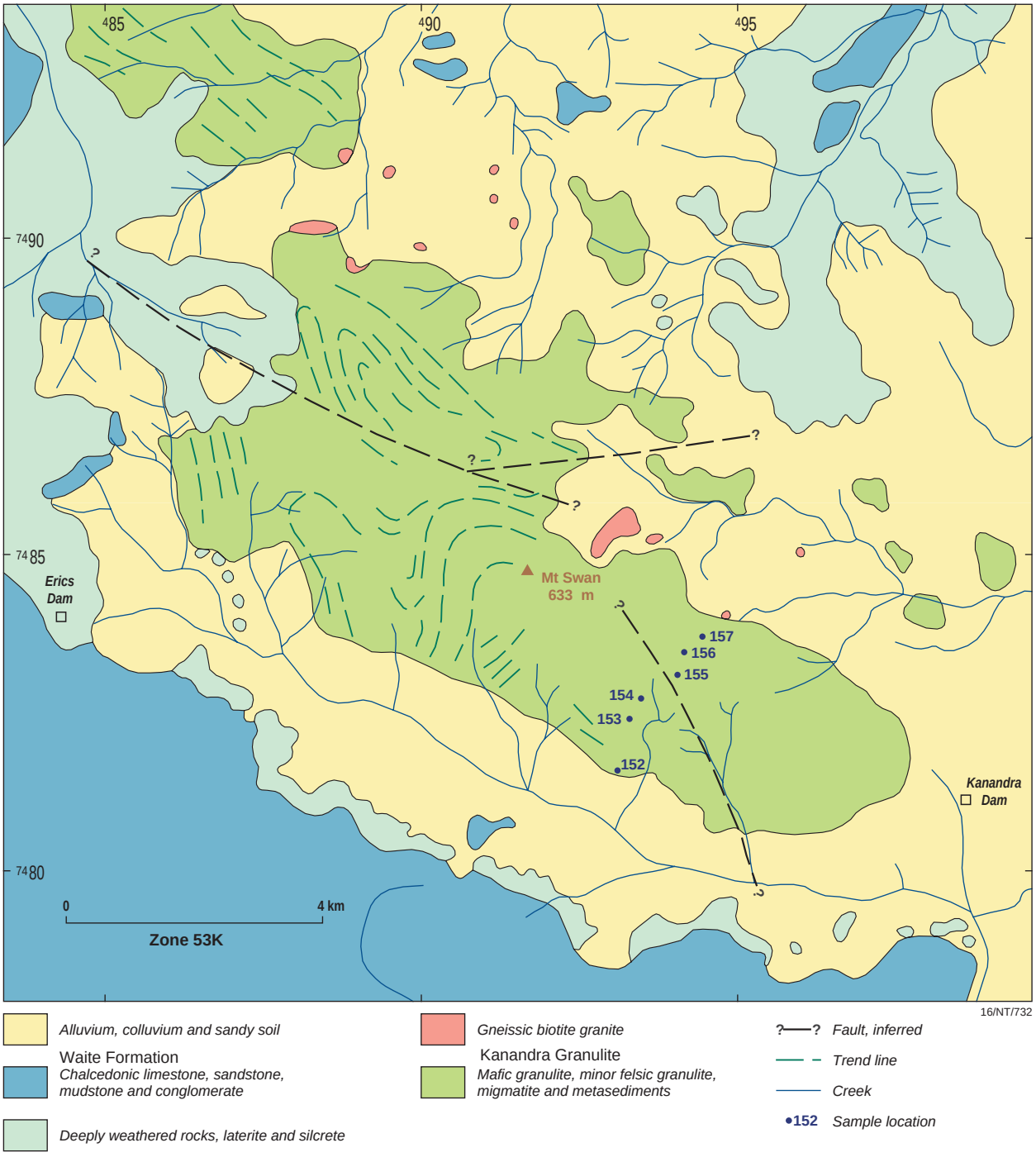

Figure 22a. Geological map of the Kanandra Granulite (modified after Shaw et al., 1975).

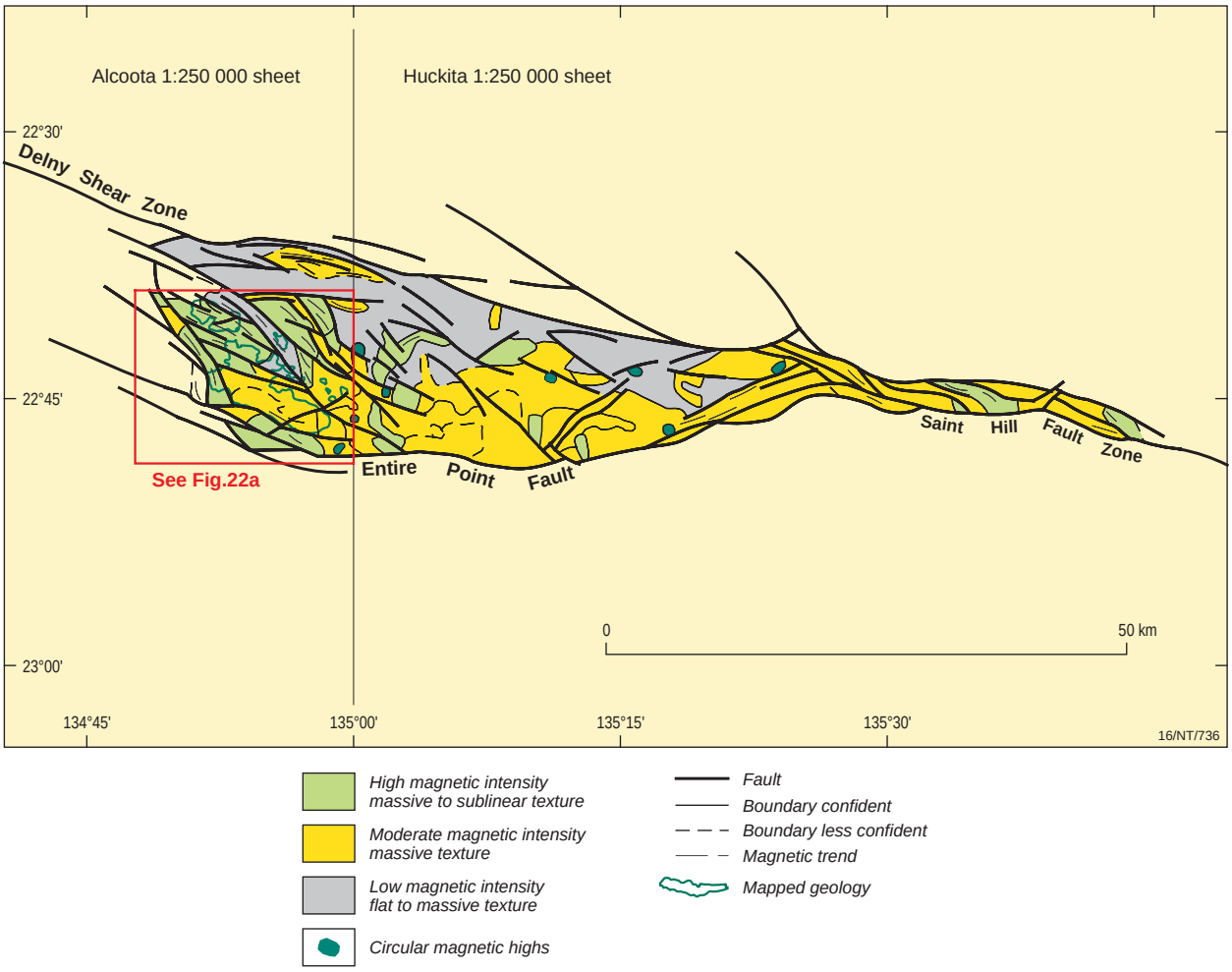

Figure 22b. Solid geology interpretation of the Kanandra Granulite showing the total interpreted sub-cropping extent. The region shown in the geological map (Fig.22a) is also displayed.

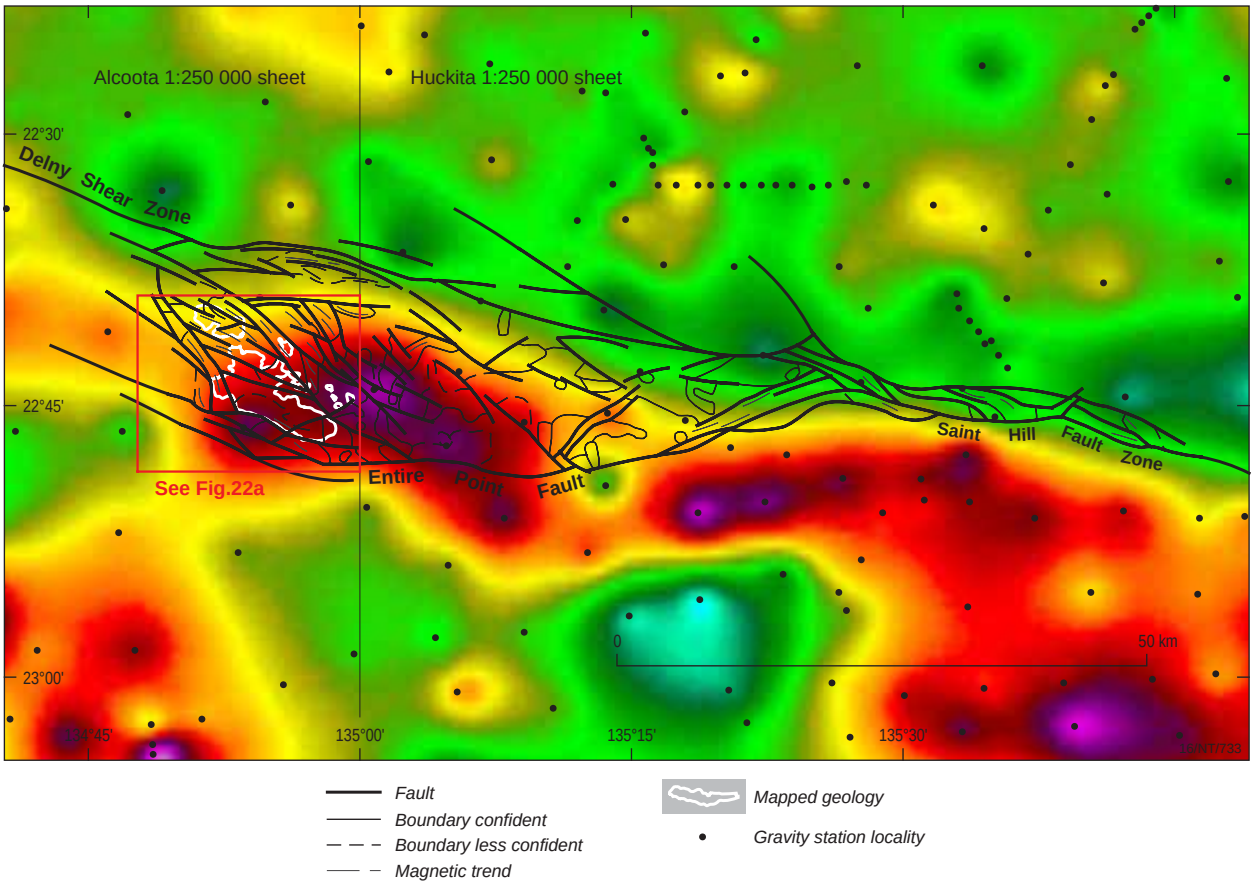

Figure 22c. Vertical gradient image of the Bouguer gravity field, including gravity station locations.

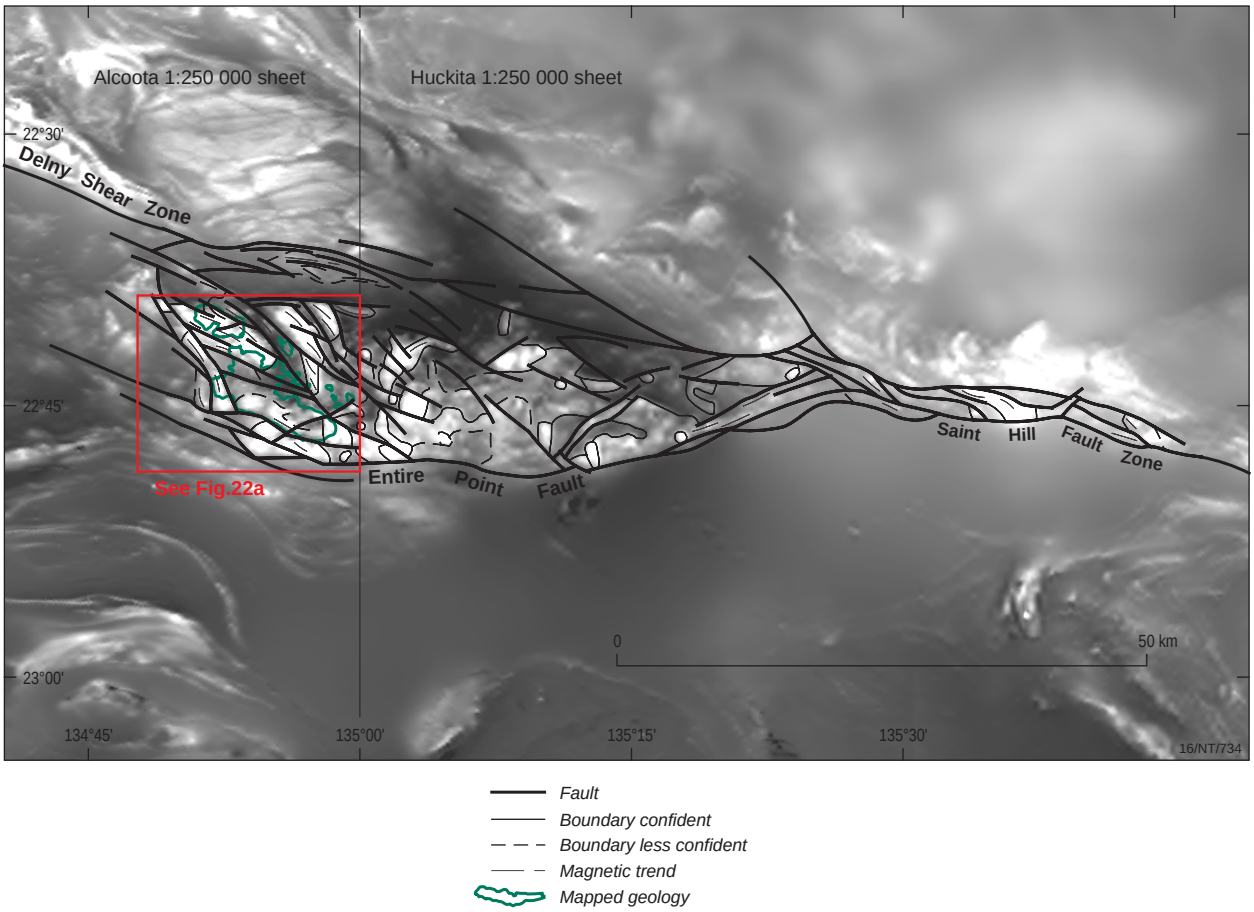

Figure 22d. Grey scale image of the total magnetic intensity - reduced to pole.

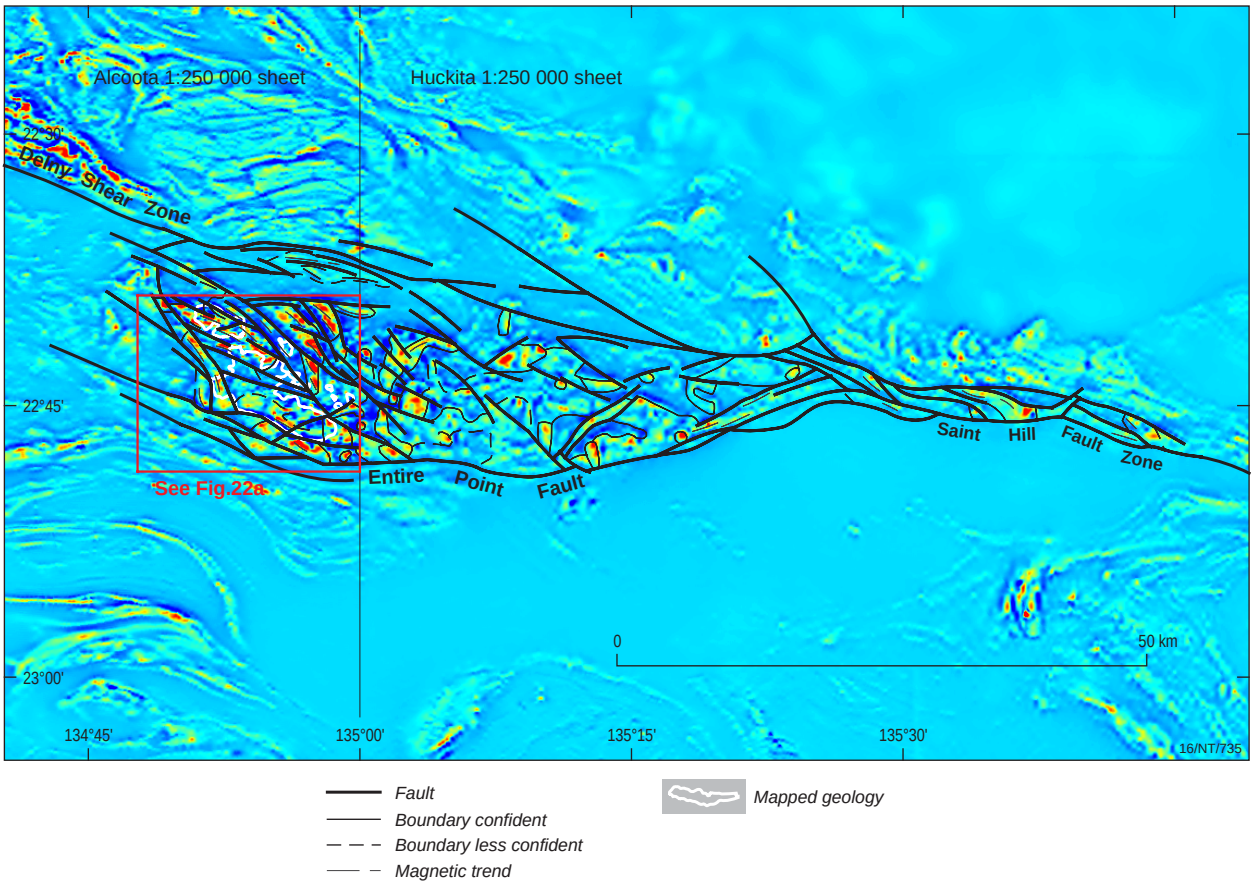

Figure 22e. Pseudo colour image of the vertical gradient applied to the total magnetic intensity (reduced to pole).

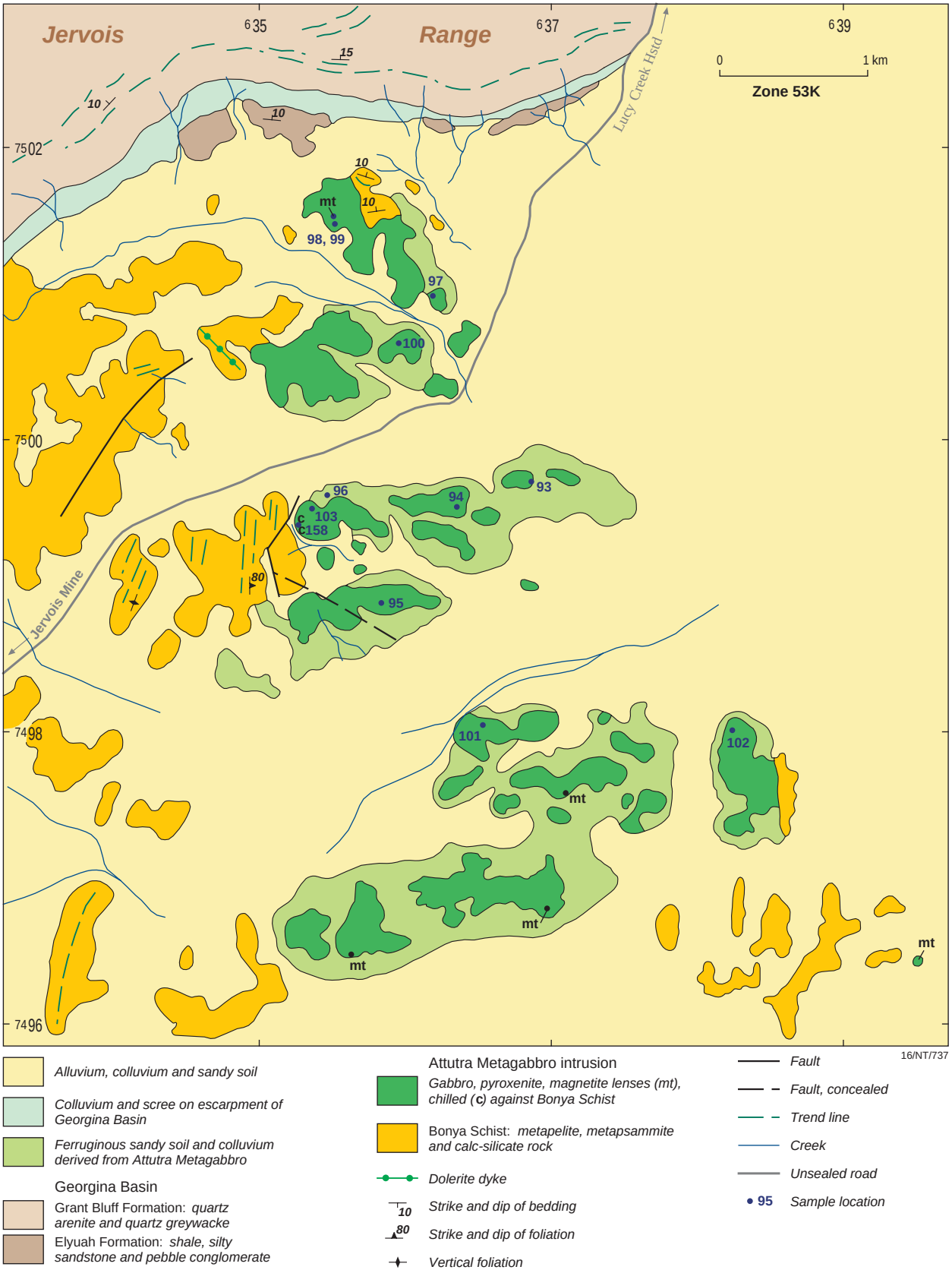

Figure 23a. Geological map of the Attutra Metagabbro (modified after Freeman, 1986).

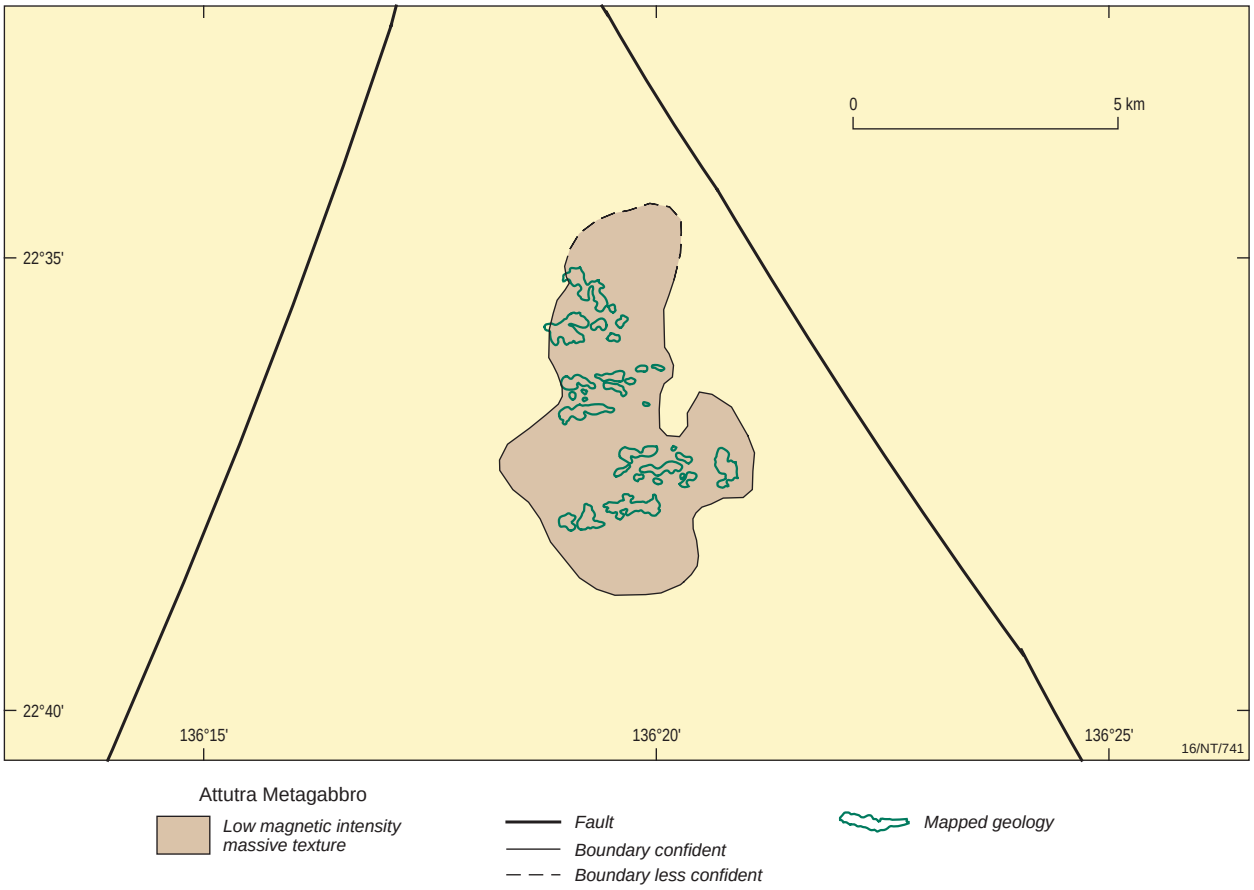

Figure 23b. Solid geology interpretation of the Attutra Metagabbro intrusion.

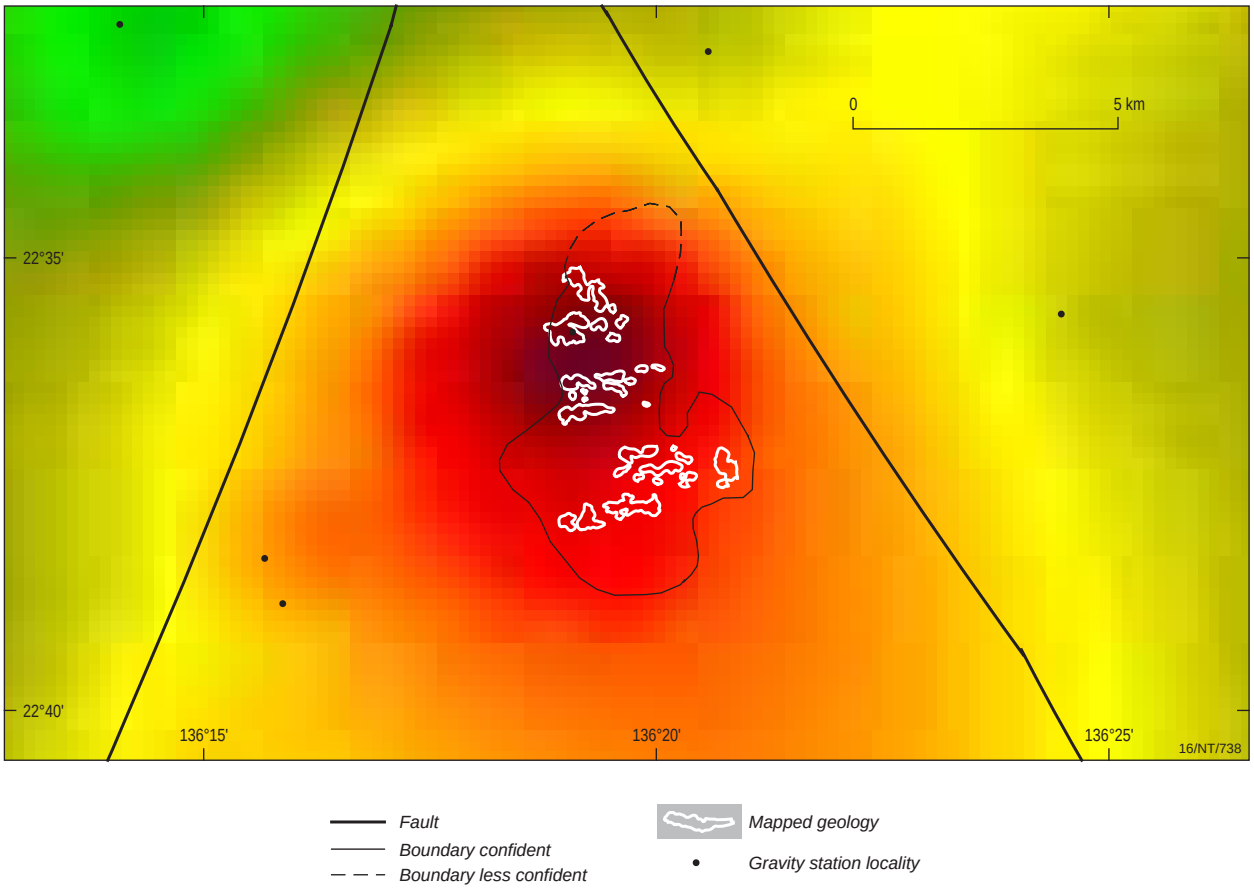

Figure 23c. Vertical gradient image of the Bouguer gravity field, including gravity station locations.

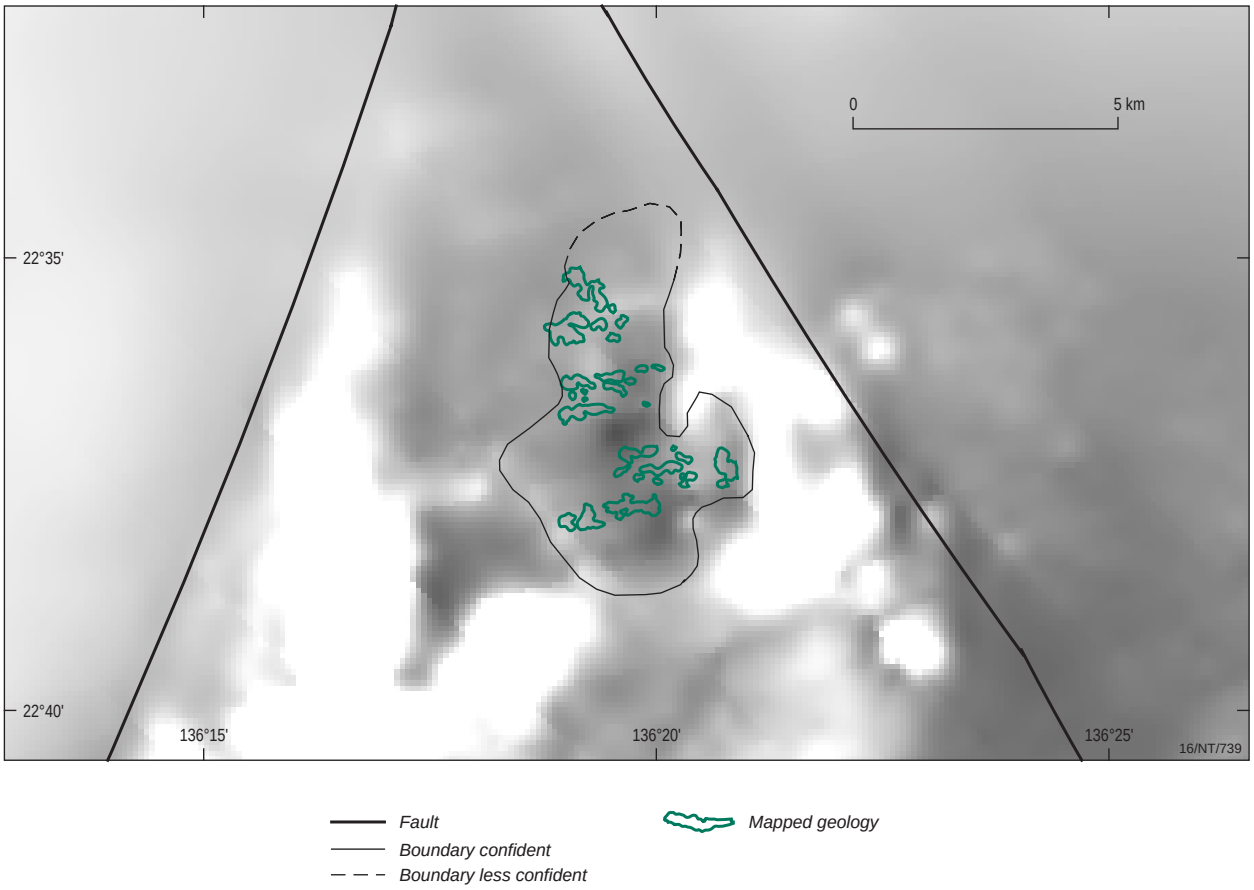

Figure 23d. Grey scale image of the total magnetic intensity - reduced to pole.

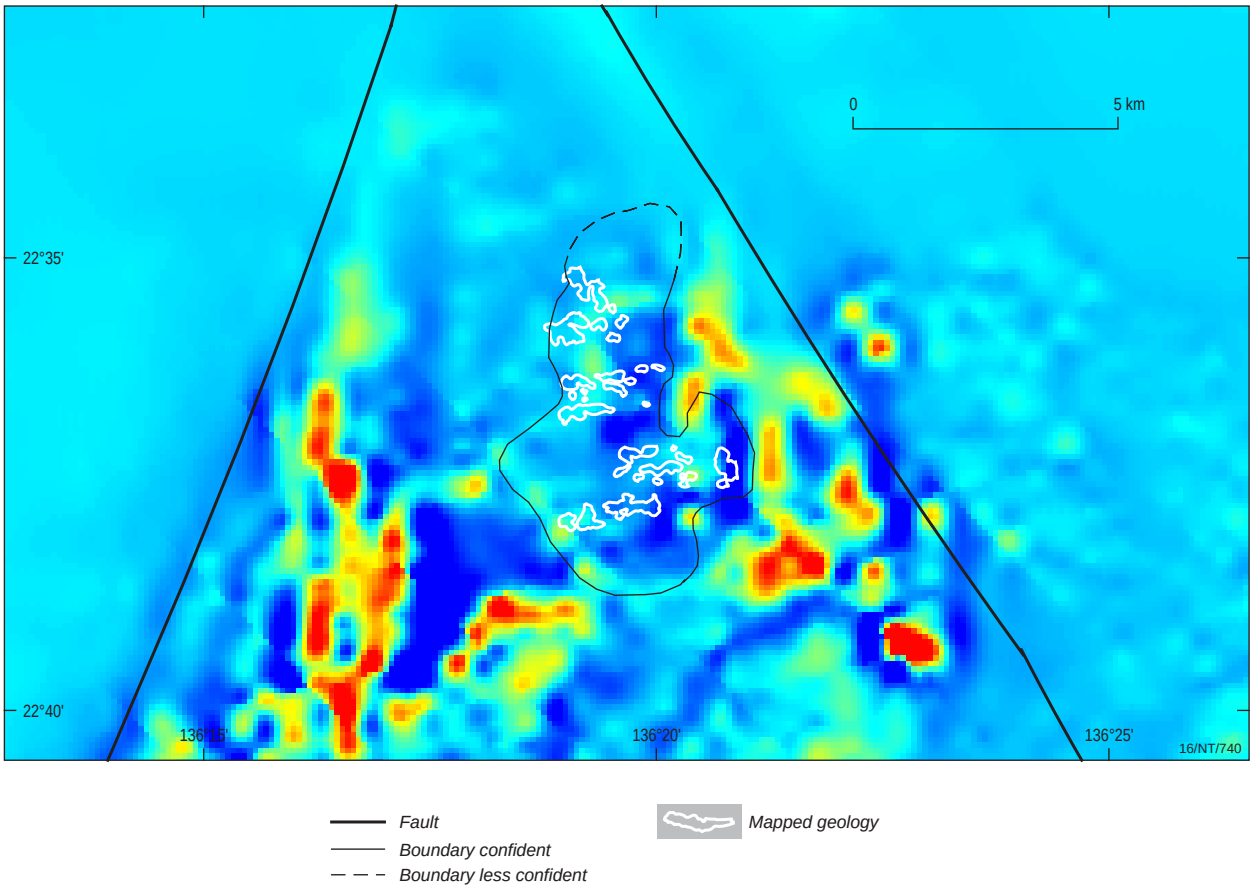

Figure 23e. Pseudo colour image of the vertical gradient applied to the total magnetic intensity (reduced to pole).

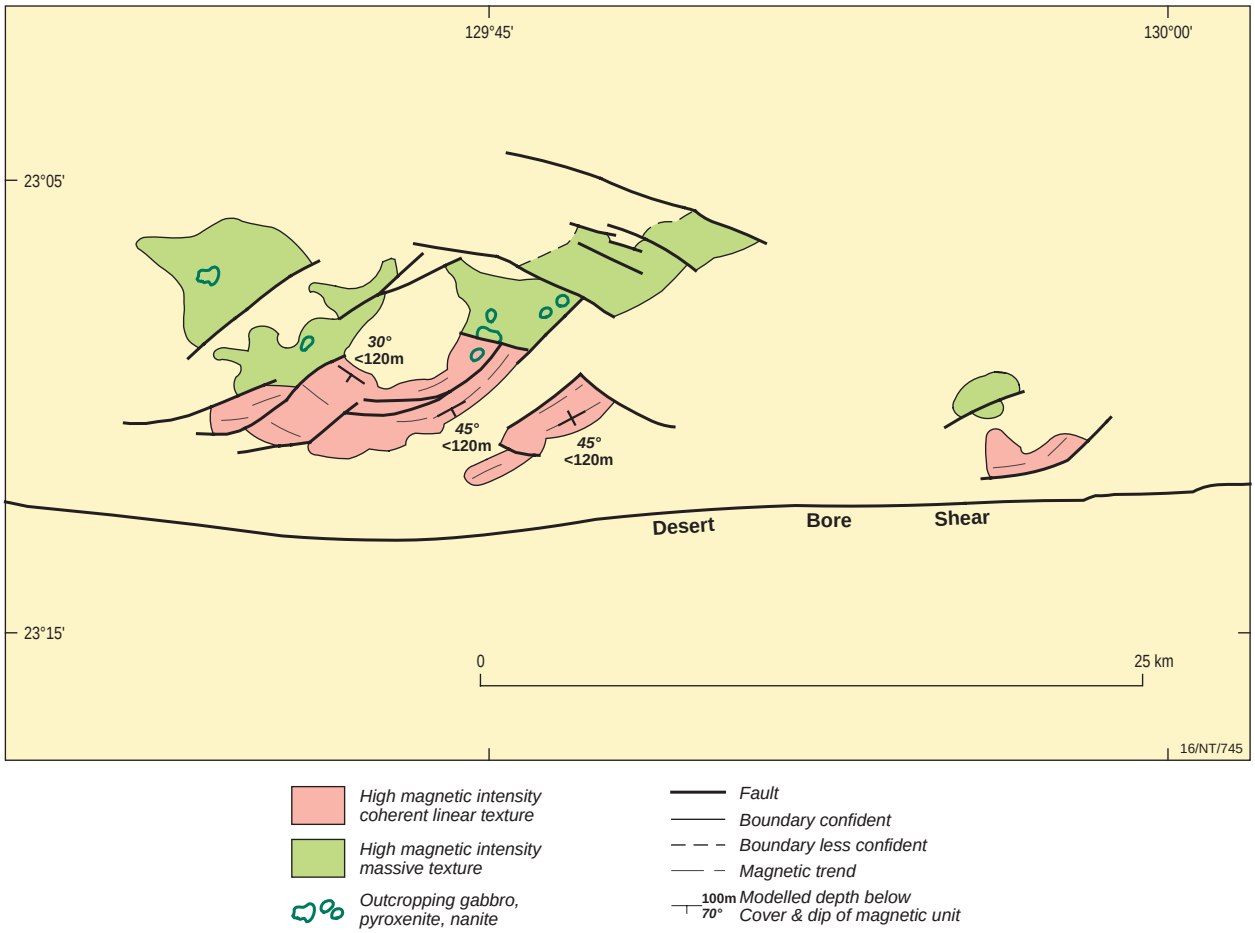

Figure 24a. Solid geology of the western mafic intrusions, showing total sub-cropping extent of the interpreted intrusions. The results of magnetic modelling defining depth of alluvial cover and dip and strike of macroscopic layering is also shown.

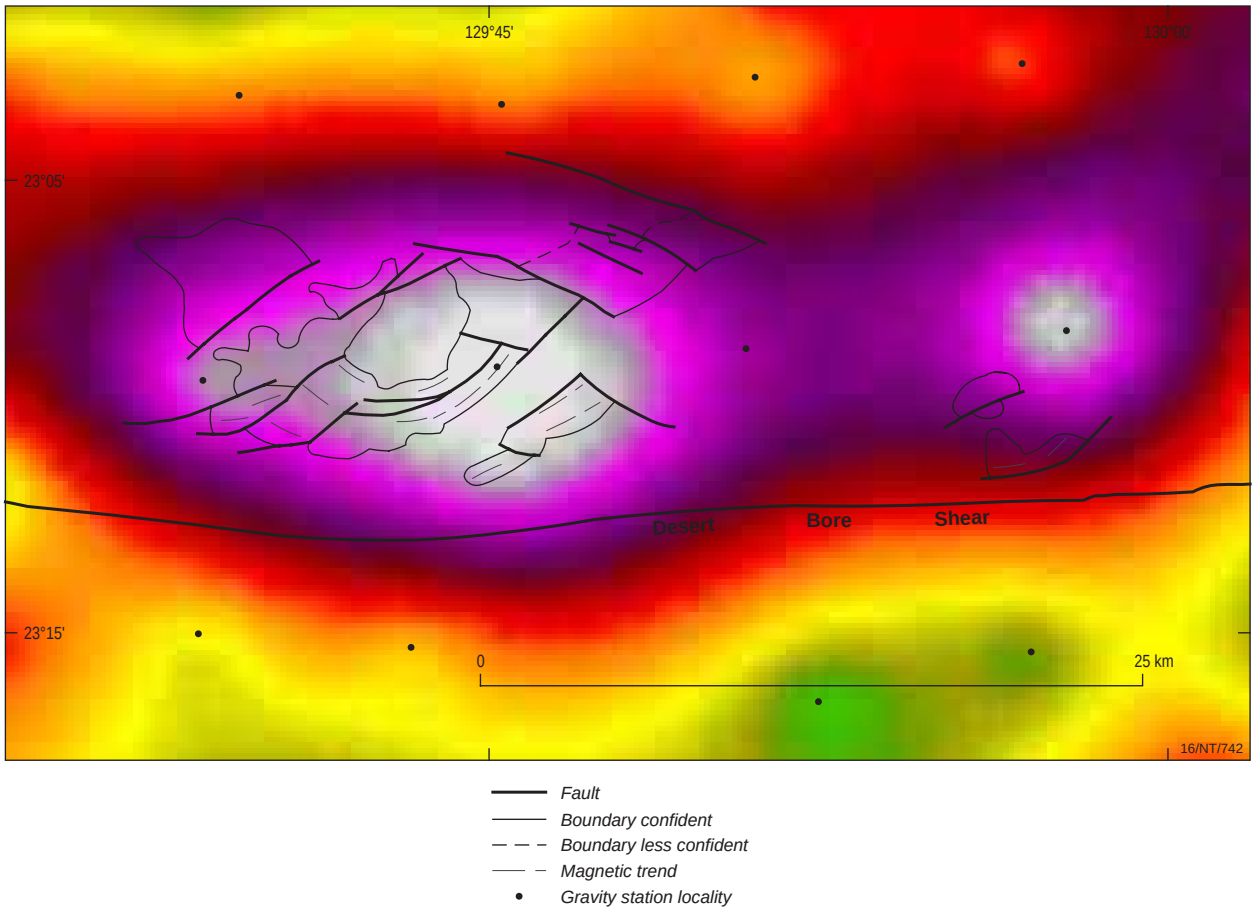

Figure 24b. Vertical gradient image of the Bouguer gravity field, including gravity station locations.

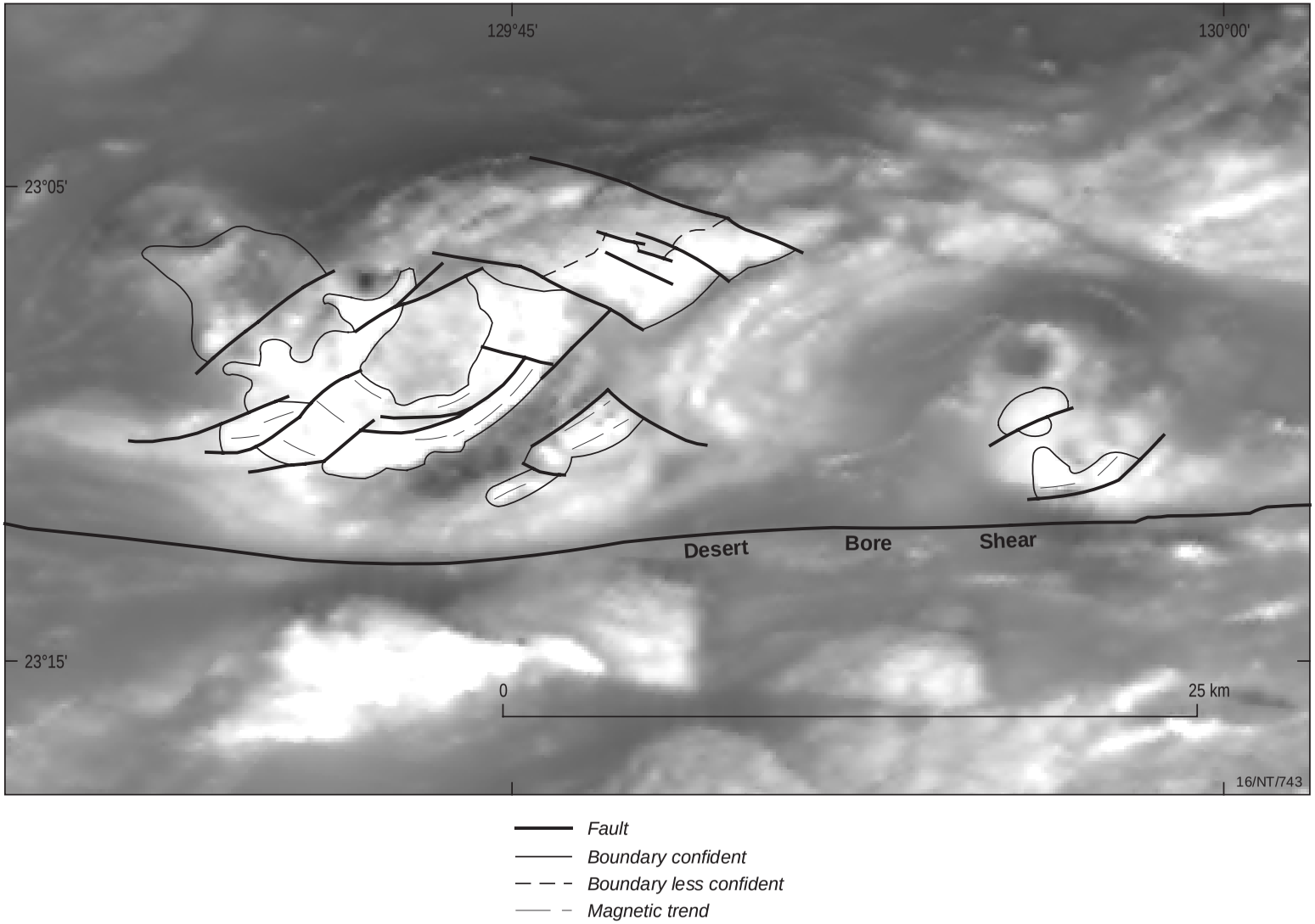

Figure 24c. Grey scale image of the total magnetic intensity - reduced to pole.

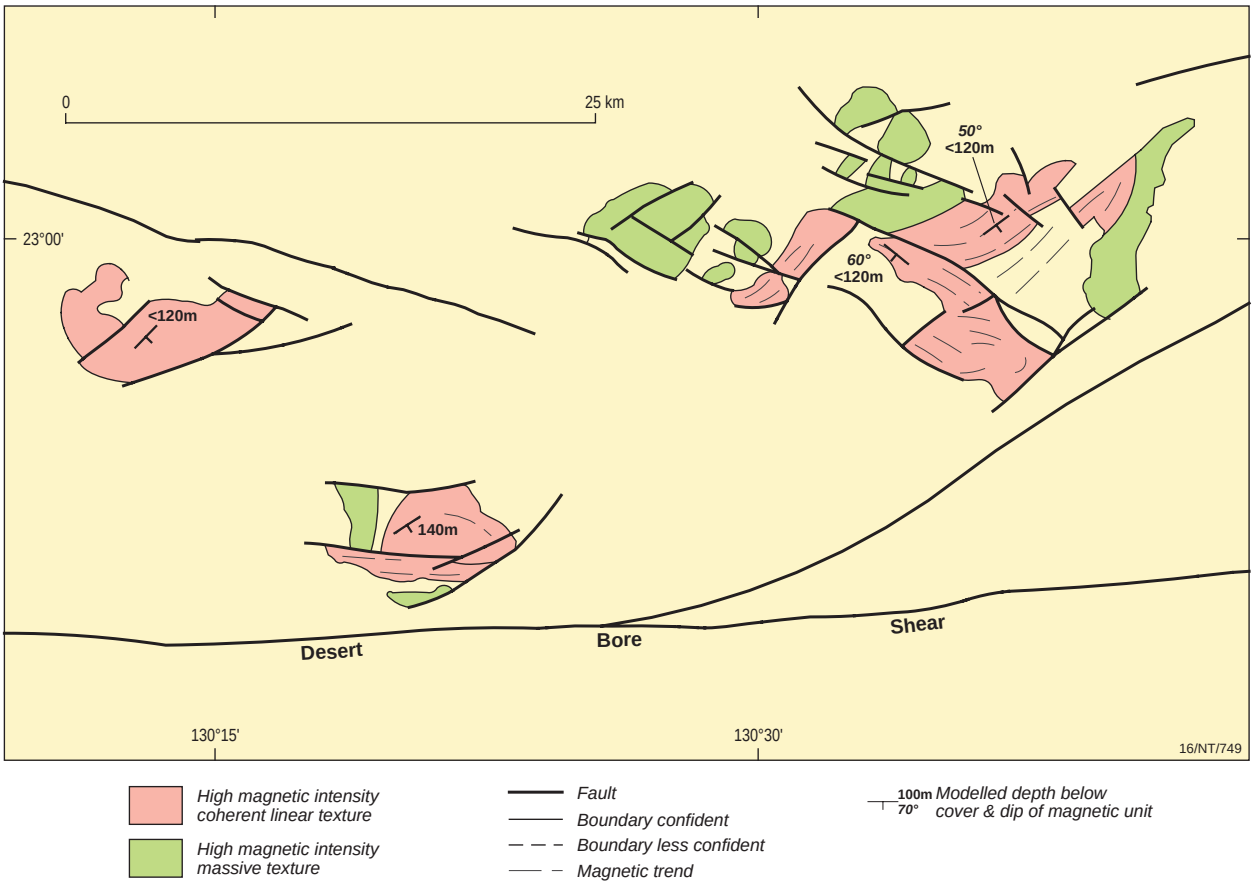

Figure 25a. Solid geology interpretation of the central mafic intrusions, showing total subcropping extent of the intrusions. The results of magnetic modelling, defining depth of alluvial cover and dip and strike of macroscopic layering is also shown.

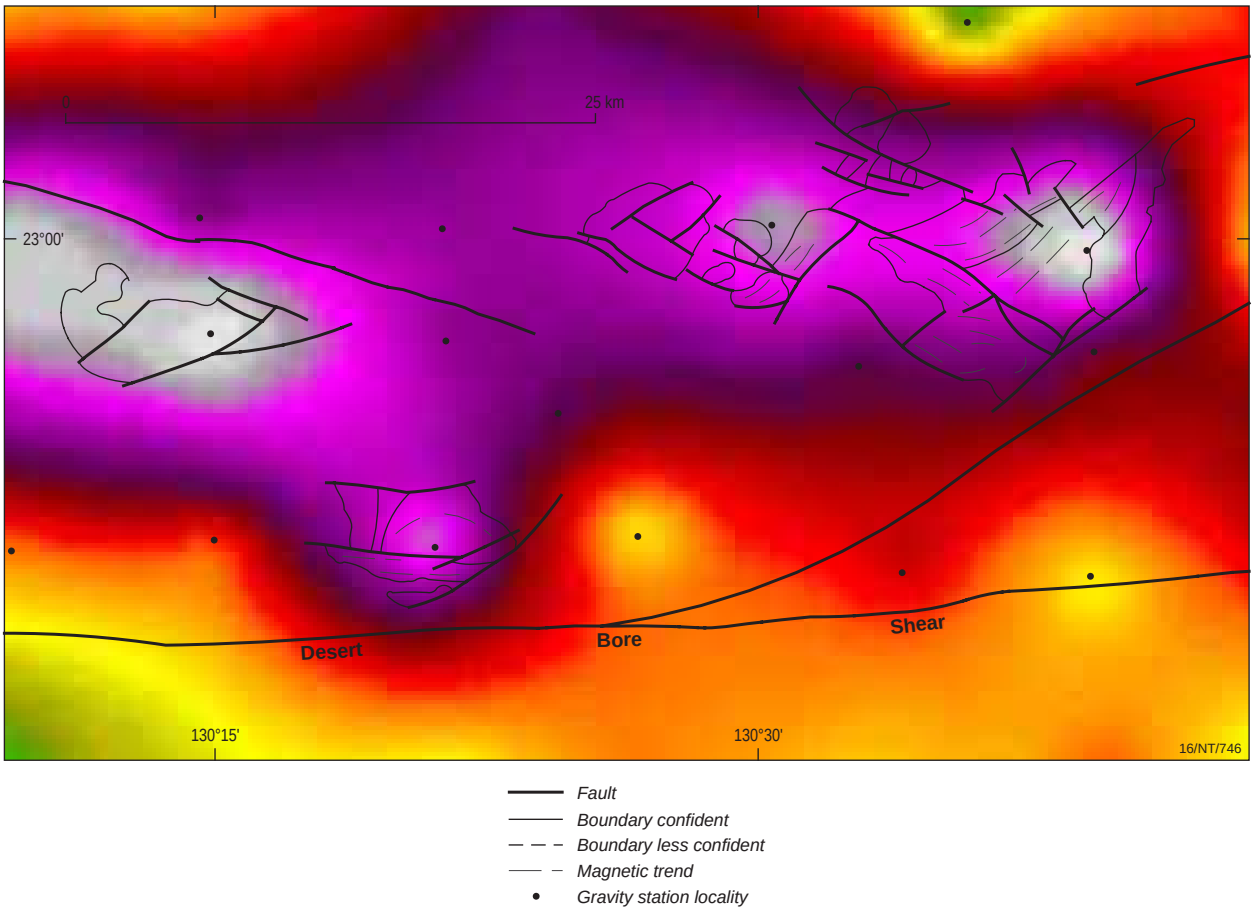

Figure 25b. Vertical gradient image of the Bouguer gravity field, including gravity station locations.

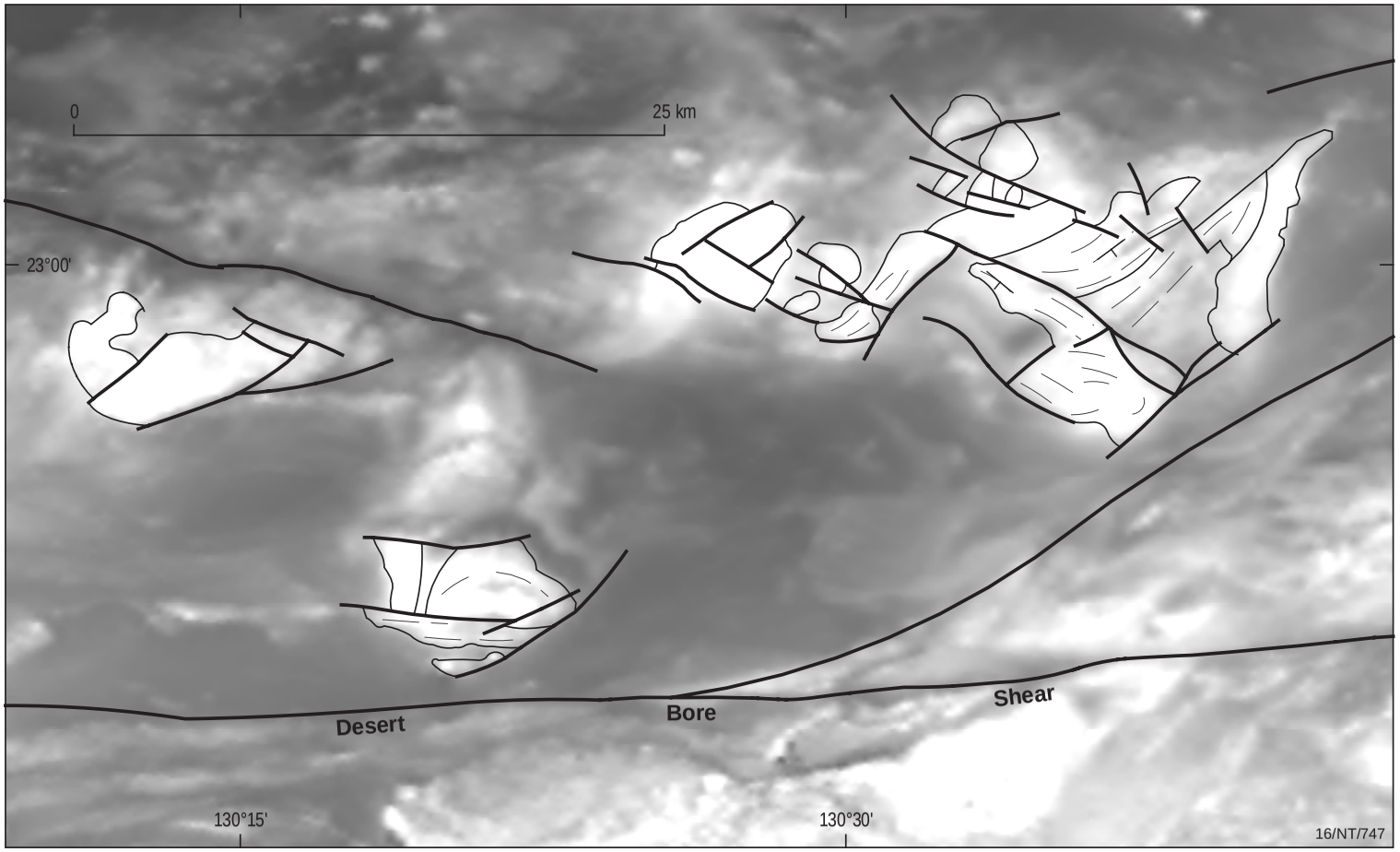

Figure 25c. Grey scale image of the total magnetic intensity - reduced to pole.

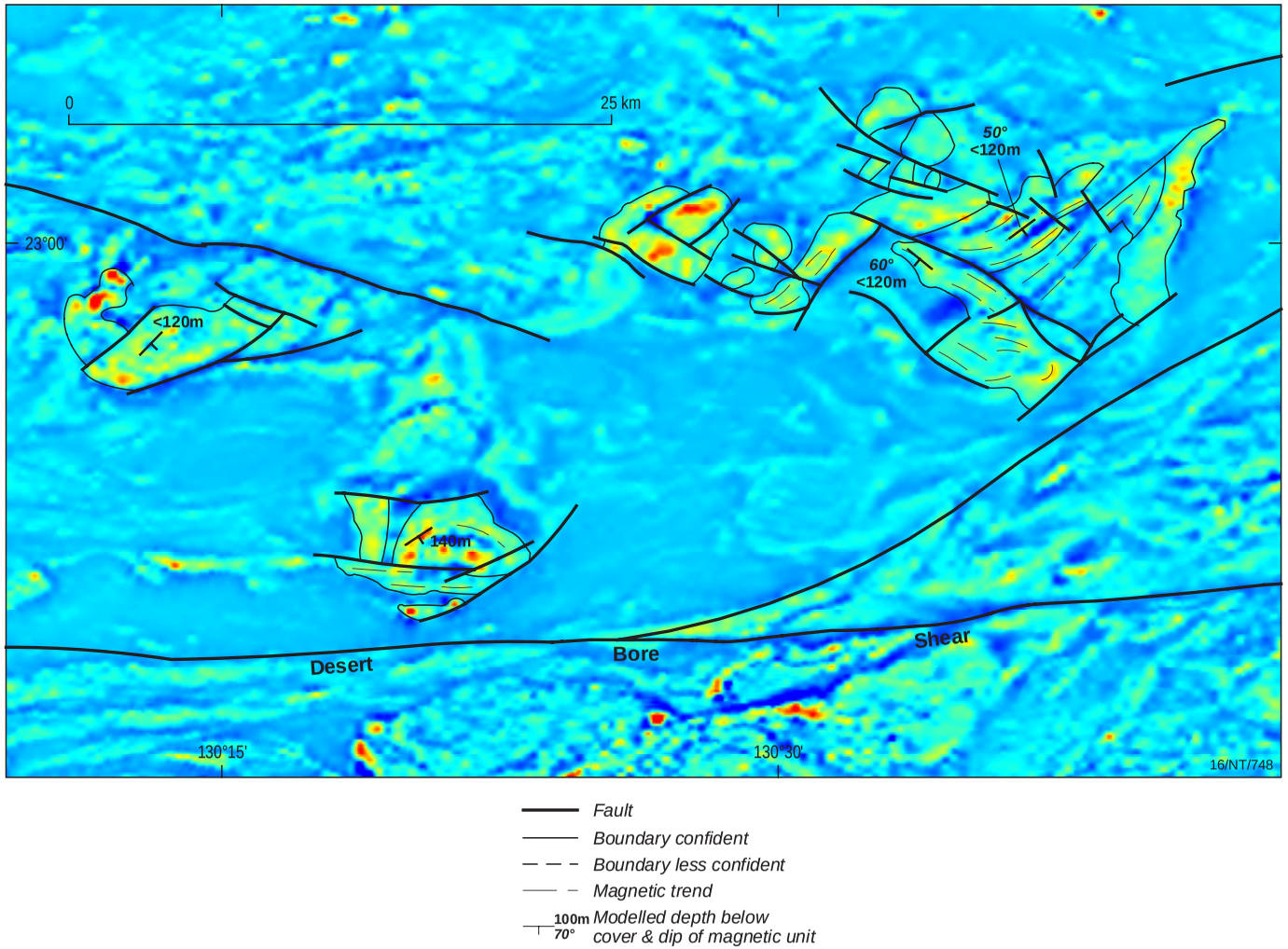

Figure 25d. Pseudo colour image of the vertical gradient applied to the total magnetic intensity (reduced to pole).

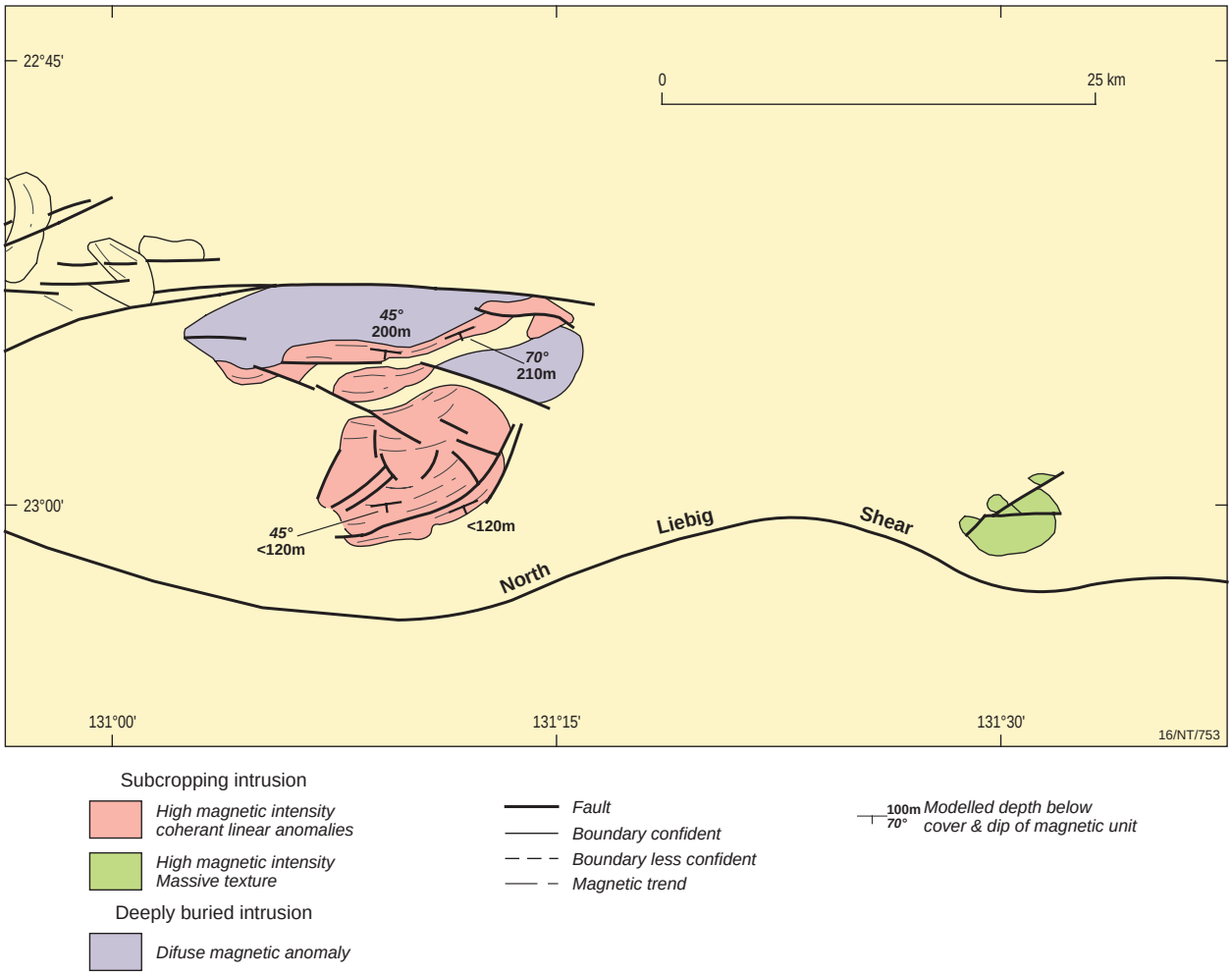

Figure 26a. Solid geology interpretation of the eastern mafic intrusions, showing the total subcropping extent and the location of deeply buried intrusions. The results of magnetic modelling defining depth of alluvial cover and dip and strike of macroscopic layering is also shown.

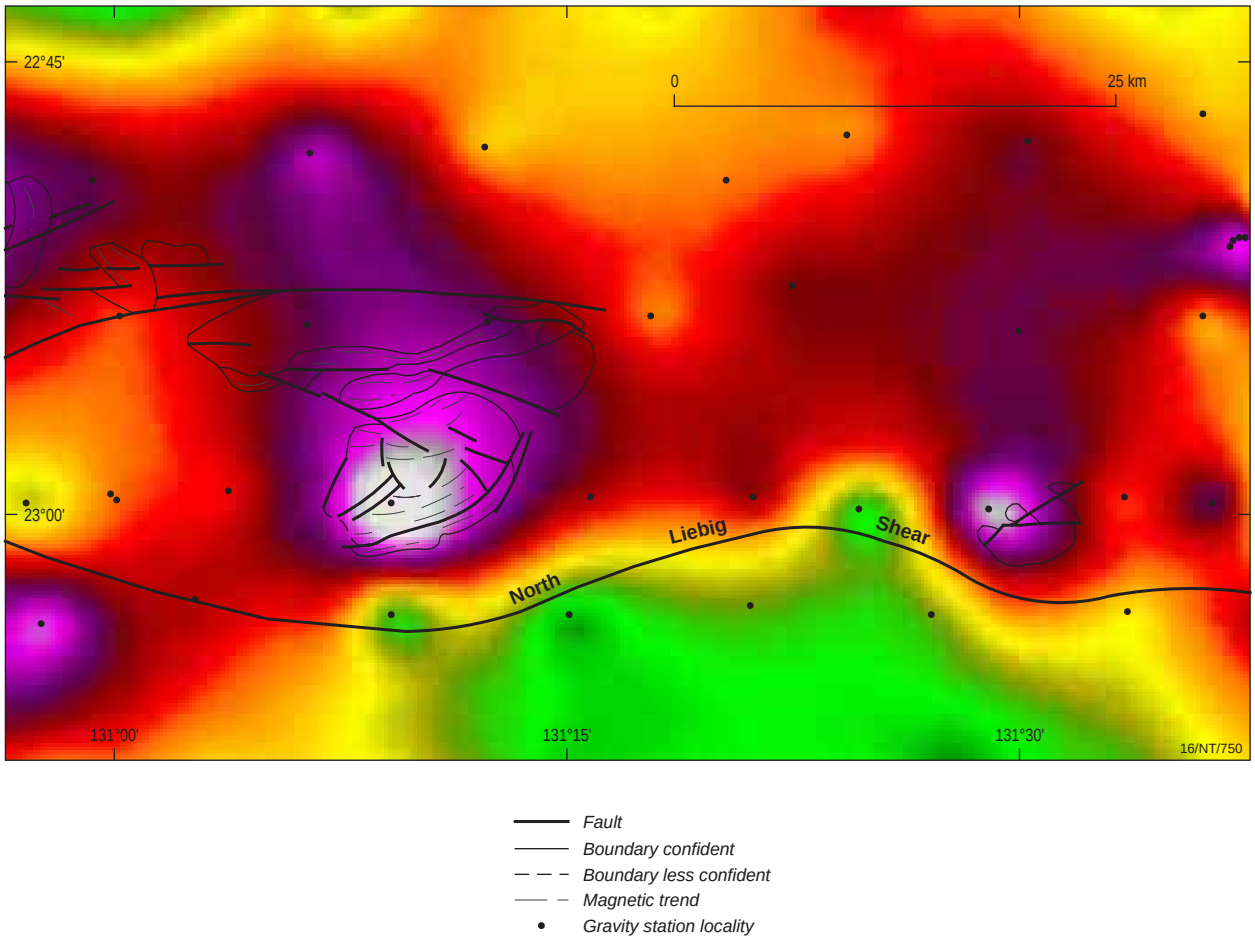

Figure 26b. Vertical gradient image of the Bouguer gravity field, including gravity station locations.

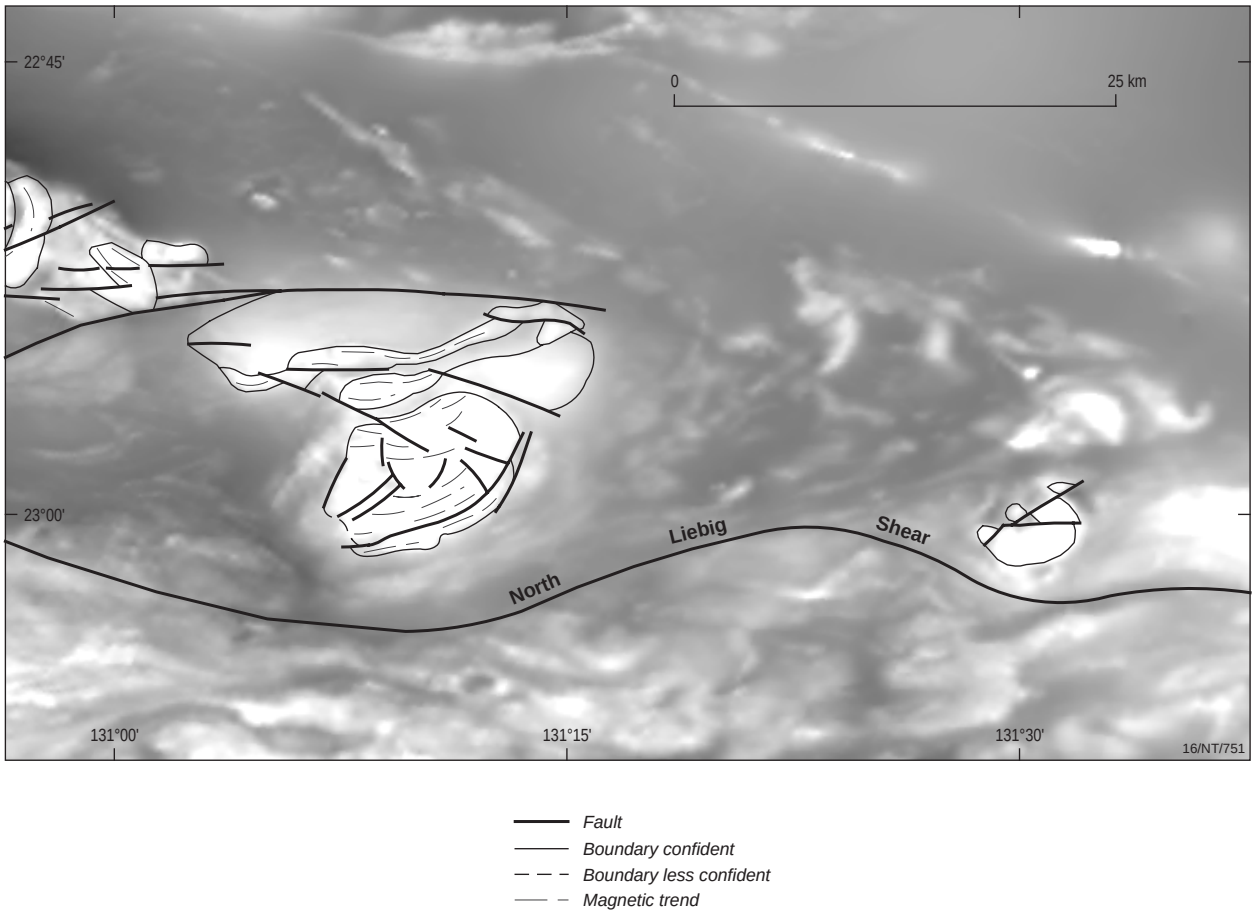

Figure 26c. Grey scale image of the total magnetic intensity - reduced to pole.

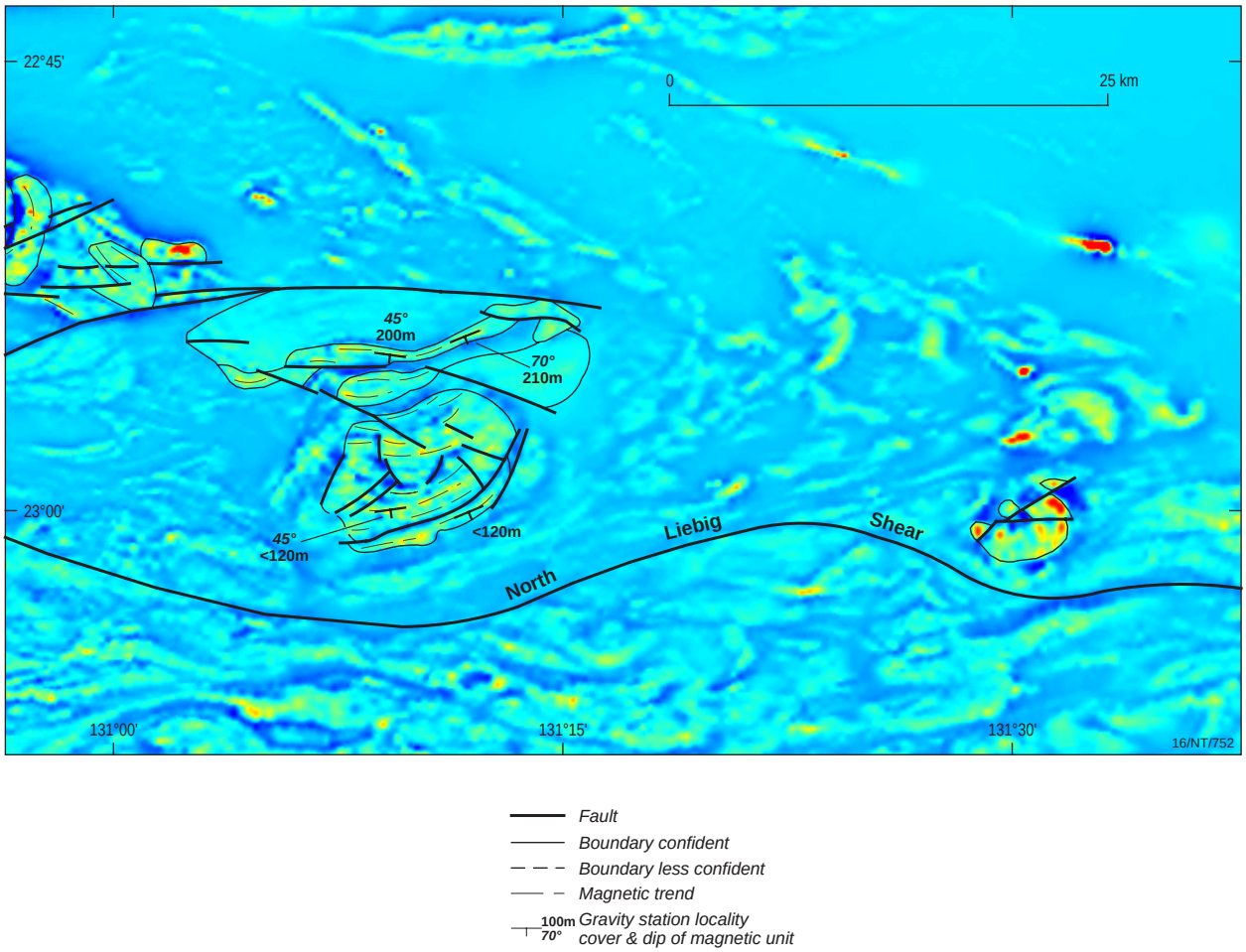

Figure 26d. Pseudo colour image of the vertical gradient applied to the total magnetic intensity (reduced to pole).

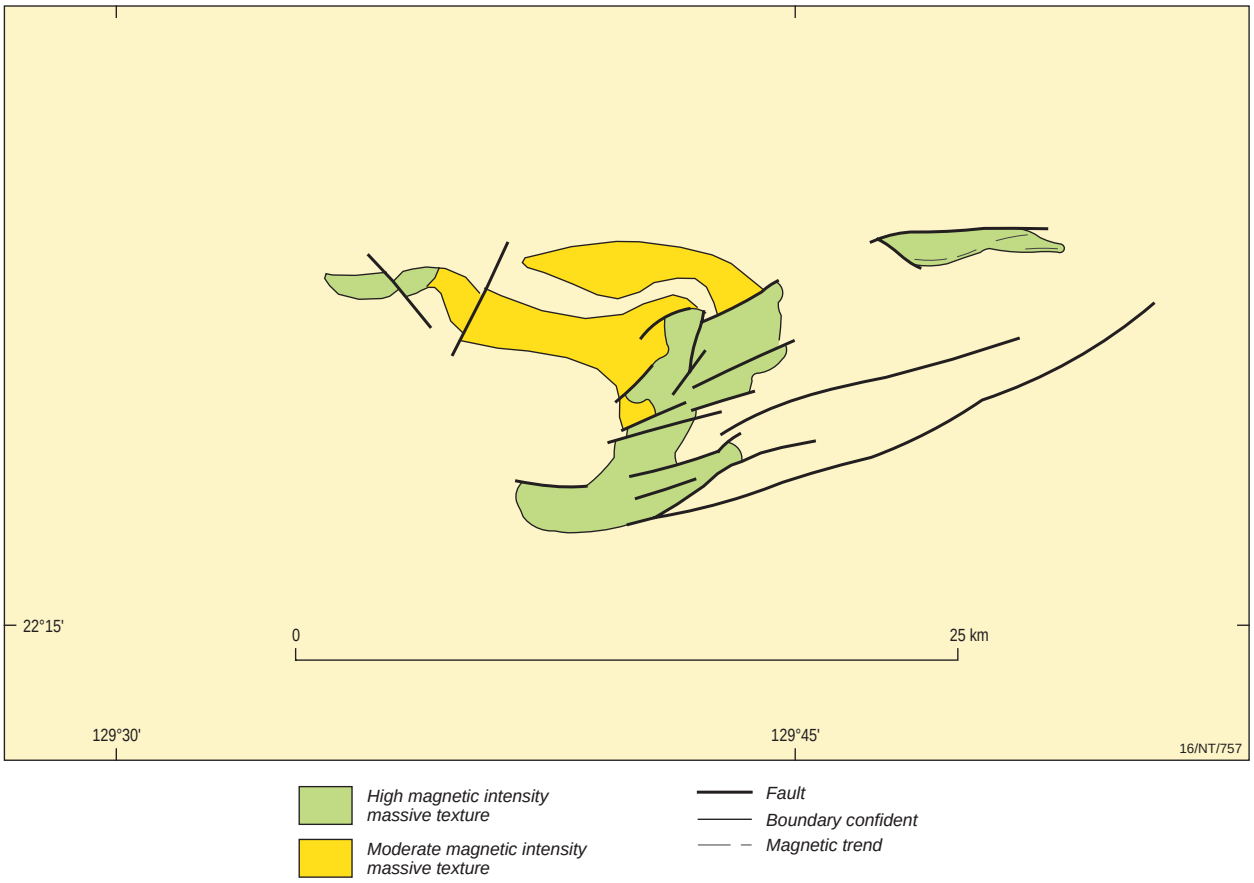

Figure 27a. Solid geology interpretationof the McEwin Hills mafic body, showing total sub-cropping extent of the intrusion.

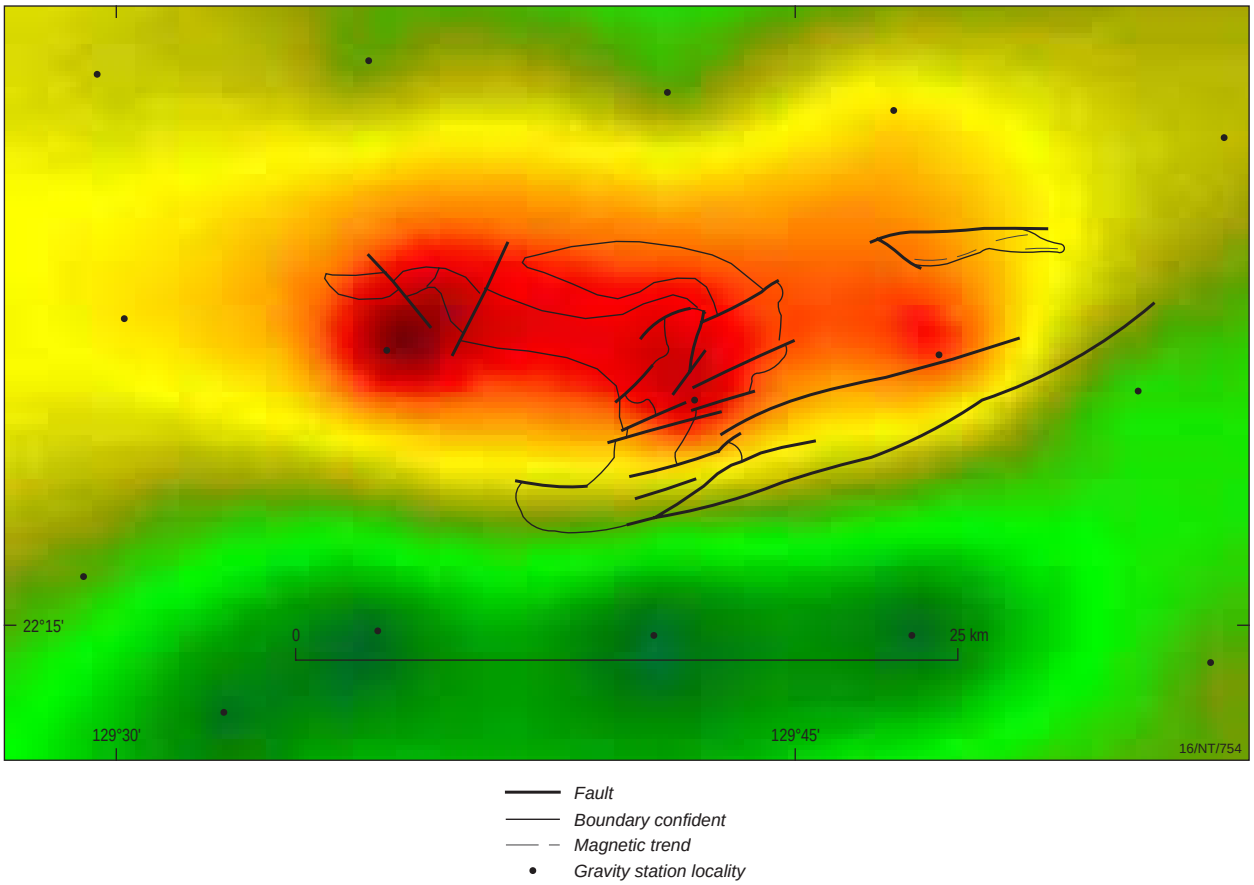

Figure 27b. Vertical gradient image of the Bouguer gravity field, including gravity station locations.

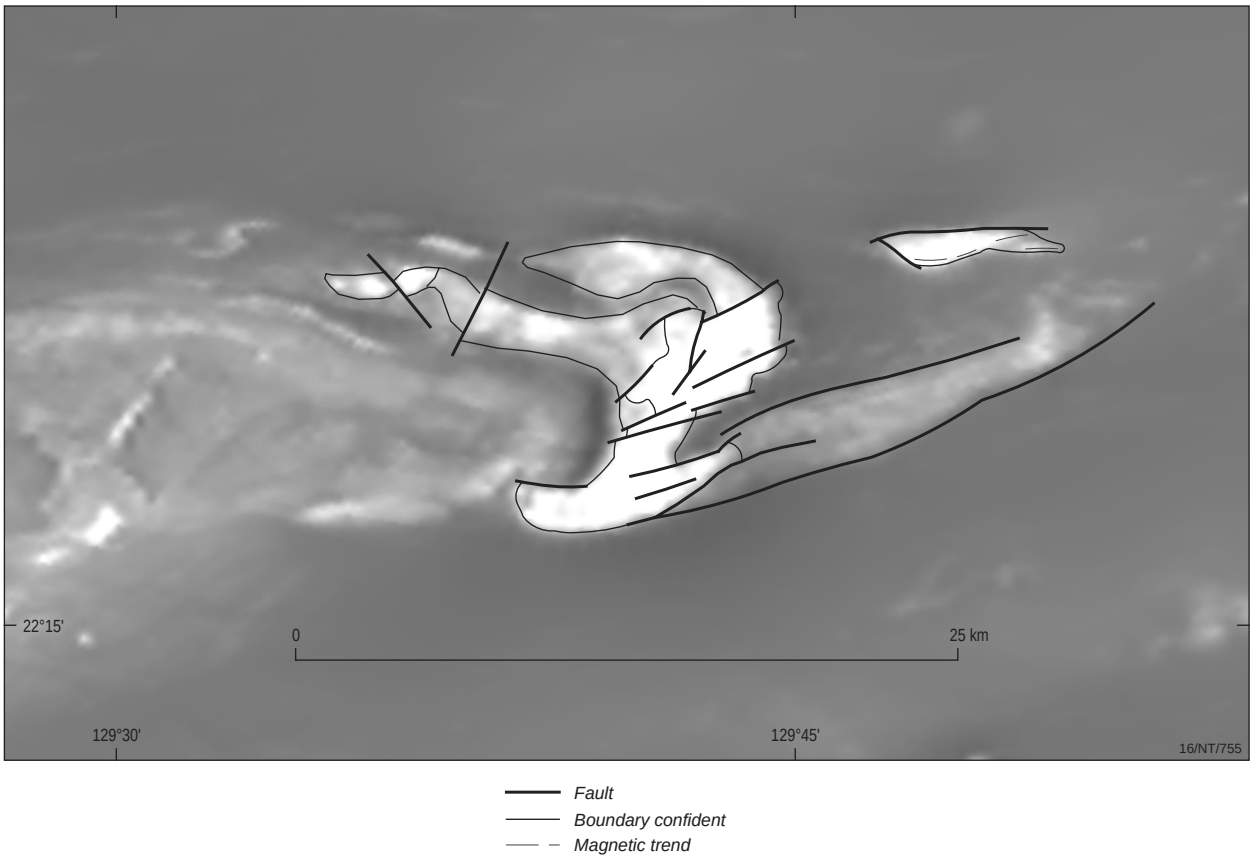

Figure 27c. Grey scale image of the total magnetic intensity - reduced to pole.

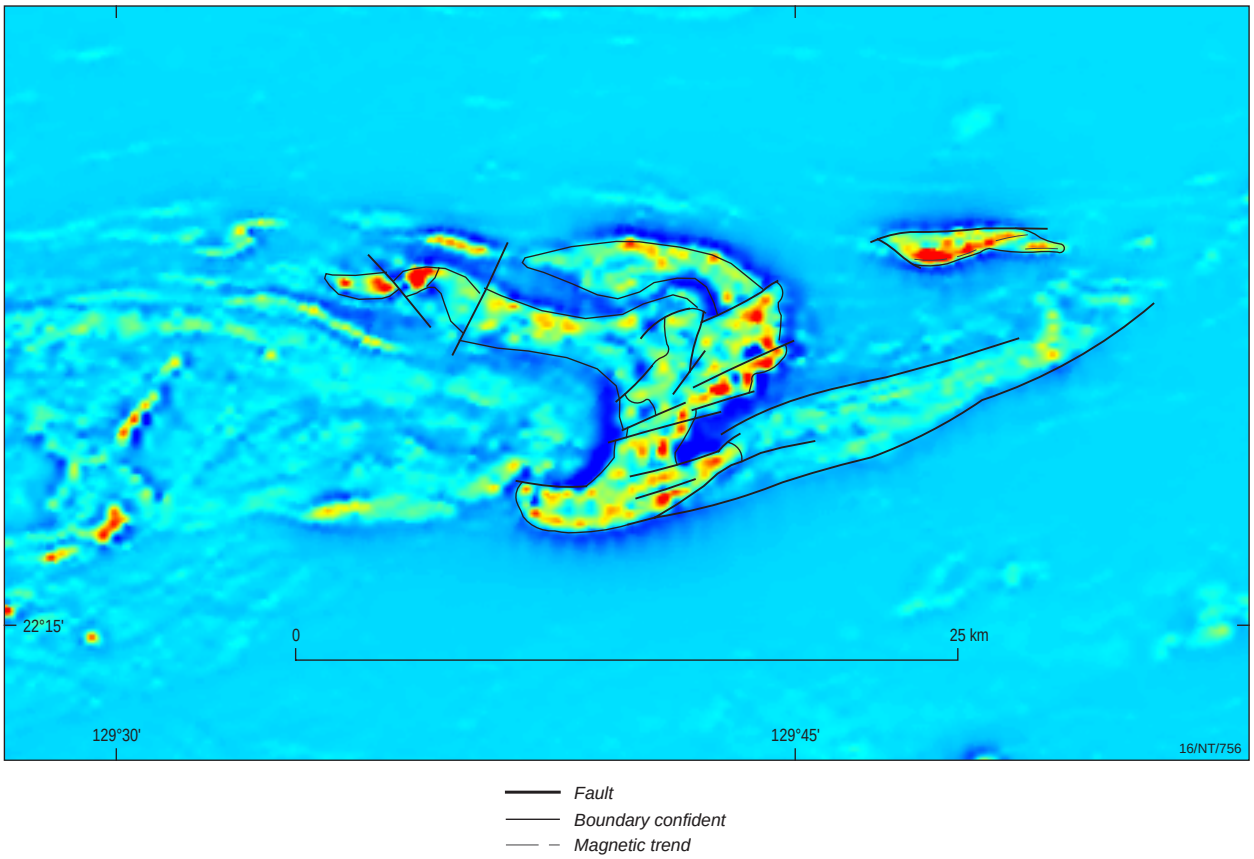

Figure 27d. Pseudo colour image of the vertical gradient applied to the total magnetic intensity (reduced to pole).

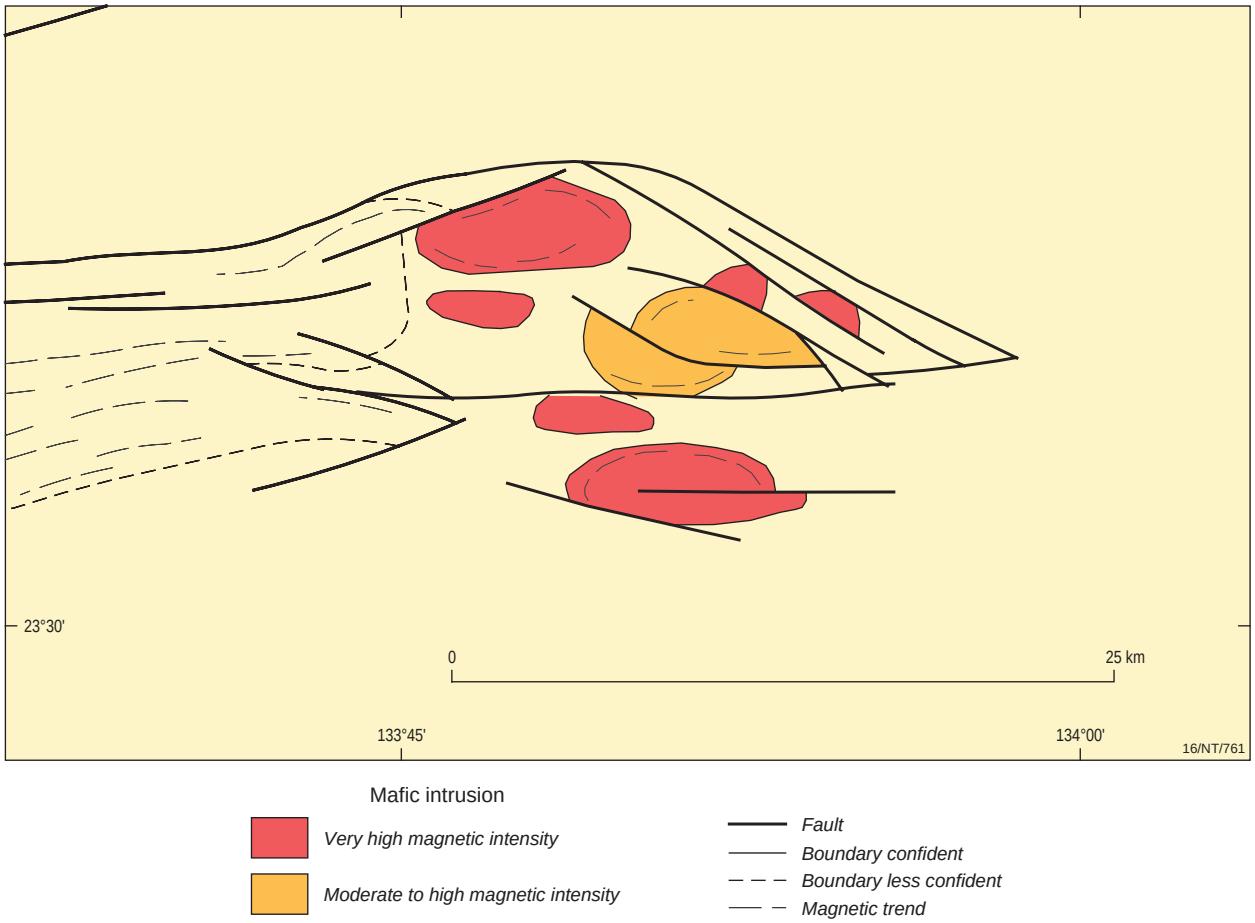

Figure 28a. Solid geology interpretationof the Joppita Bore mafic intrusions, showing the total sub-cropping extent of the intrusions.

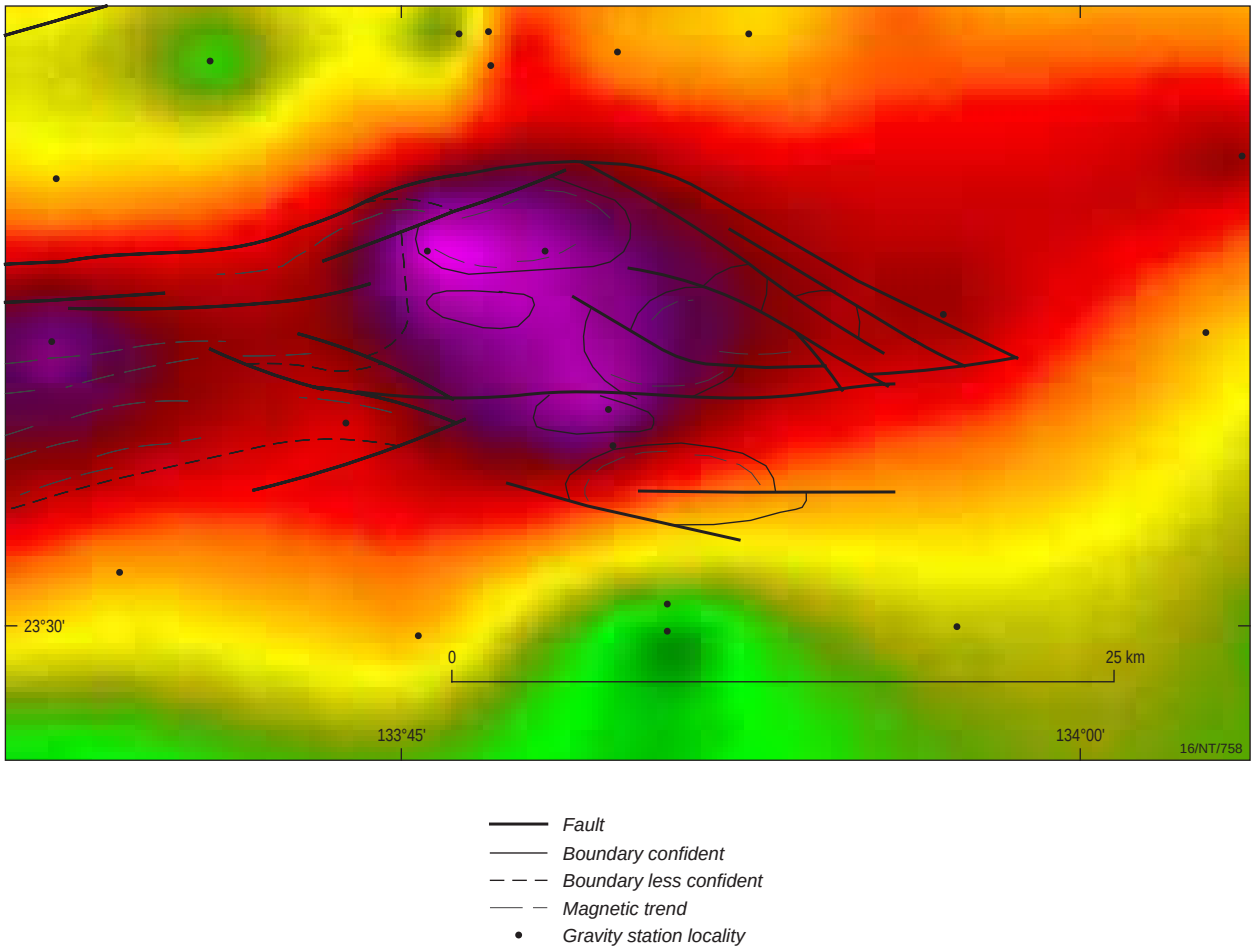

Figure 28b. Vertical gradient image of the Bouguer gravity field, including gravity station locations.

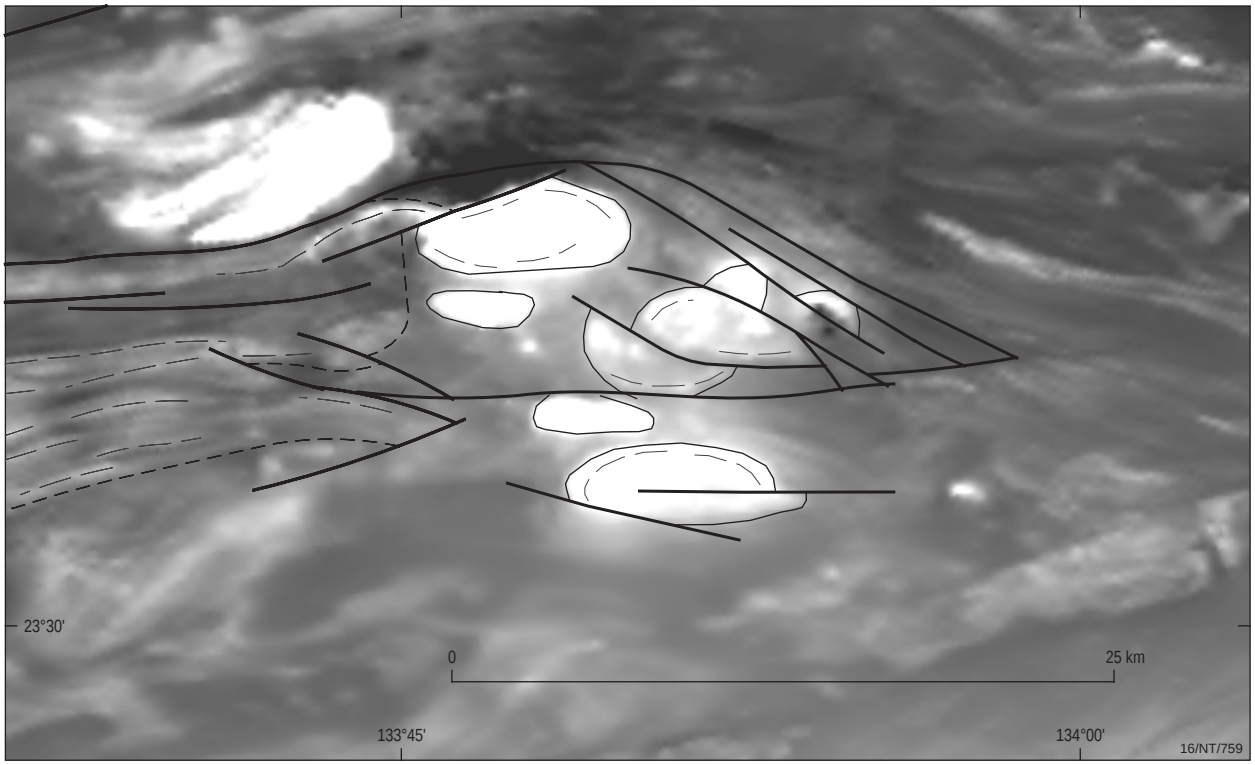

Fault
Boundary confident
Boundary less confident
Magnetic trend

Figure 28c. Grey scale image of the total magnetic intensity - reduced to pole.

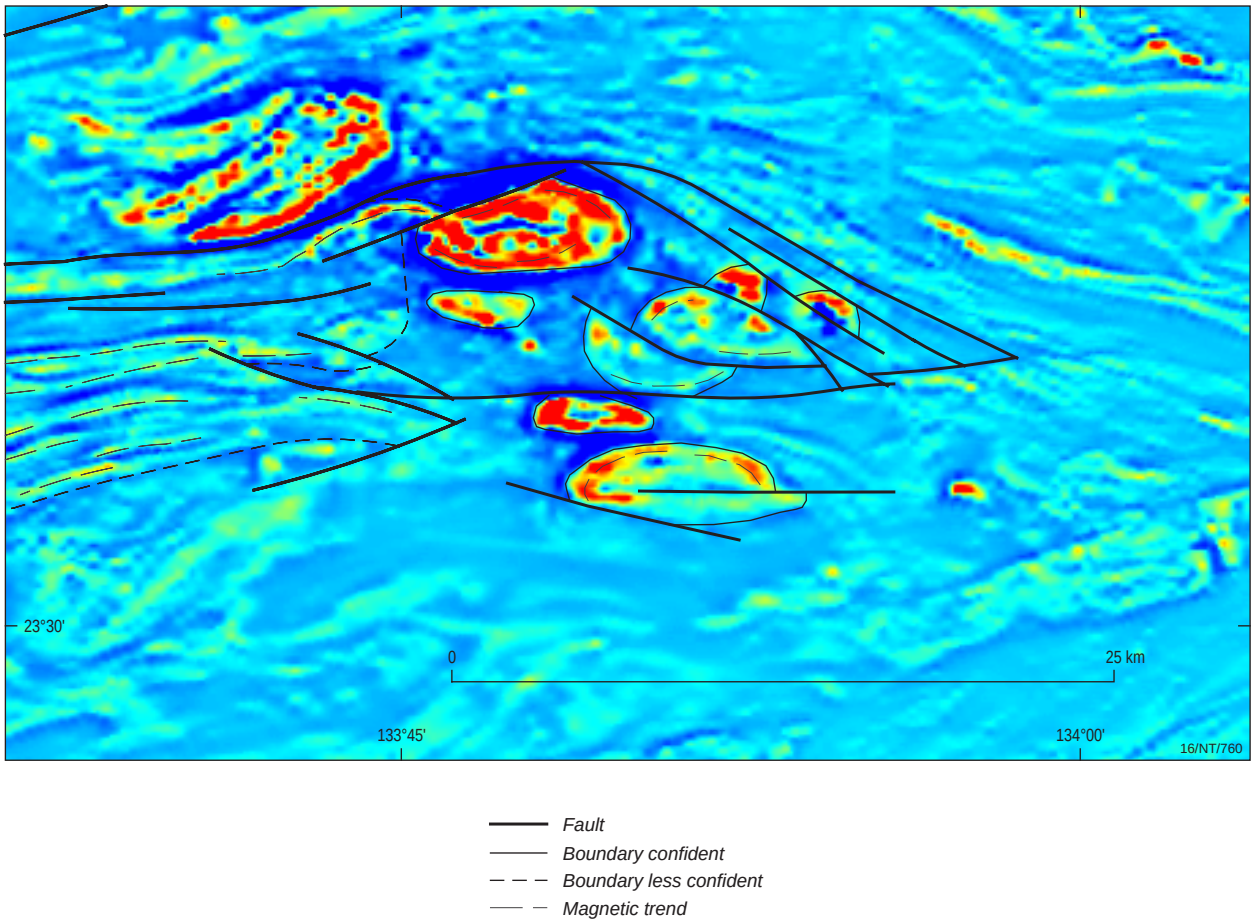

Figure 28d. Pseudo colour image of the vertical gradient applied to the total magnetic intensity (reduced to pole).